Article (refereed) - postprint

Atkin, Owen K.; Bloomfield, Keith J.; Reich, Peter B.; Tjoelker, Mark G.; Asner, Gregory P.; Bonal, Damien; Bönisch, Gerhard; Bradford, Matt G.; Cernusak, Lucas A.; Cosio, Eric G.; Creek, Danielle; Crous, Kristine Y.; Domingues, Tomas F.; Dukes, Jeffrey S.; Egerton, John J.G.; Evans, John R.; Farquhar, Graham D.; Fyllas, Nikolaos M.; Gauthier, Paul P.G.; Gloor, Emanuel; Gimeno, Teresa E.; Griffin, Kevin L.; Guerrieri, Rossella; Heskel, Mary A.; Huntingford, Chris; Ishida, Françoise Yoko; Kattge, Jens; Lambers, Hans; Liddell, Michael J.; Lloyd, Jon; Lusk, Christopher H.; Martin, Roberta E.; Maksimov, Ayal P.; Maximov, Trofim C.; Malhi, Yadvinder; Medlyn, Belinda E.; Meir, Patrick; Mercado, Lina M.; Mirotchnick, Nicholas; Ng, Desmond; Niinemets, Ülo; O'Sullivan, Odhran S.; Phillips, Oliver L.; Poorter, Lourens; Poot, Pieter; Prentice, I. Colin; Salinas, Norma; Rowland, Lucy M.; Ryan, Michael G.; Sitch, Stephen; Slot, Martijn; Smith, Nicholas G.; Turnbull, Matthew H.; Vanderwel, Mark C.; Valladares, Fernando; Veneklaas, Erik J.; Weerasinghe, Lasantha K.; Wirth, Christian; Wright, Ian J.; Wythers, Kirk R.; Xiang, Jen; Xiang, Shuang; Zaragoza-Castells, Joana. 2015. **Global variability in leaf respiration in relation to climate, plant functional types and leaf traits.** *New Phytologist*, 206 (2). 614-636. https://doi.org/10.1111/nph.13253

Revised submission to *New Phytologist*

Global variability in leaf respiration in relation to climate, plant functional types and leaf traits

Owen K. Atkin[1,2], Keith J. Bloomfield[2], Peter B. Reich[3,4], Mark G. Tjoelker[4], Gregory P. Asner[5], Damien Bonal[6], Gerhard Bönisch[7], Matt Bradford[8], Lucas A. Cernusak[9], Eric G. Cosio[10], Danielle Creek[2,4], Kristine Y. Crous[2,4], Tomas Domingues[11], Jeffery S. Dukes[12,13], John J. G. Egerton[2], John R. Evans[2], Graham D. Farquhar[2], Nikolaos M. Fyllas[14], Paul P.G. Gauthier[2,15], Emanuel Gloor[16], Teresa E. Gimeno[4], Kevin L. Griffin[17], Rossella Guerrieri[18,19], Mary A. Heskel[2], Chris Huntingford[20], Françoise Yoko Ishida[9], Jens Kattge[7], Hans Lambers[21], Michael J. Liddell[22], Jon Lloyd[9,32], Christopher H. Lusk[23], Roberta E. Martin[5], Ayal P. Maksimov[24], Trofim C. Maximov[24], Yadvinder Mahli[25], Belinda E. Medlyn[26], Patrick Meir[2,18], Lina M. Mercado[20,27], Nicholas Mirotchnick[28], Desmond Ng[2,29], Ülo Niinemets[30], Odhran S. O'Sullivan[2], Oliver L. Philips[16], Lourens Poorter[31], Pieter Poot[21], I. Colin Prentice[26,32], Norma Salinas[10,25], Lucy M. Rowland[18], Mike G. Ryan[33], Stephen Sitch[27], Martijn Slot[34,35], Nicholas G. Smith[13], Matthew H. Turnbull[36], Mark C. VanderWel[34,37], Fernando Valladares[38], Eric J. Veneklaas[21], Lasantha K. Weerasinghe[2,39], Christian Wirth[40], Ian J. Wright[26], Kirk Wythers[3], Jen Xiang[1,2], Shuang Xiang[2,41] and Joana Zaragoza-Castells[18,27]

[1]ARC Centre of Excellence in Plant Energy Biology, Research School of Biology, Building 134, The Australian National University, Canberra, ACT 0200, Australia; [2]Div Plant Sciences, Research School of Biology, Building 46, The Australian National University, Canberra, ACT 0200, Australia; [3]Dept of Forest Resources, University of Minnesota, 1530 Cleveland Avenue North, St. Paul, MN 55108, USA; [4]Hawkesbury Institute for the Environment, University of Western Sydney, Penrith, NSW 2751, Australia; [5]Dept of Global Ecology, Carnegie Institution for Science, Stanford, CA 94305; [6]INRA, UMR 1137 Ecologie et Ecophysiologie Forestières, Champenoux 54280, France; [7]Max-Planck-Institute for Biogeochemistry, P07745 Jena, Germany; [8]CSIRO Land and Water, Tropical Forest Research Centre, Atherton, Queensland, Australia; [9]School of Marine and Tropical Biology and Centre for Tropical Environmental and Sustainability Science, James Cook University, Cairns, Queensland, Australia; [10]Pontificia Universidad Católica del Perú, Seccion Quimica ,Av Universitaria 1801, San Miguel, Lima, Peru; [11]Universidade de São Paulo, Faculdade de Filosofia Ciências e Letras de Ribeirão Preto, Brazil; [12]Dept Forestry and Natural Resources, Purdue University, 715 West State Street, West Lafayette, IN 47907, USA; [13]Dept Biological Sciences, Purdue University, 915 West State Street, West Lafayette, IN 47907, USA; [14]Dept of Ecology and Systematics, Faculty of Biology, National and Kapodistrian University of Athens, Athens 15784, Greece; [15]Dept Geosciences, Princeton University, Guyot Hall, Princeton NJ 08544, USA; [16]School of Geography, University of Leeds, Woodhouse Lane, Leeds LS9 2JT, UK; [17]Dept Earth and Environmental Sciences, Lamont-Doherty Earth Observatory, Columbia University, Palisades, NY 10964-8000, USA; [18]School of Geosciences, University of Edinburgh, Edinburgh EH9 3JN, UK; [19]Earth Systems Research Center, University of New Hampshire, Morse Hall, 8 College Rd, Durham, NH 03824, USA; [20]Centre for Ecology and Hydrology, Wallingford OX10 8BB, UK; [21]School of Plant Biology, The University of

Western Australia, Crawley, Perth,WA 6009, Australia; [22]Discipline of Chemistry & Centre for Tropical Environmental and Sustainable Sciences, James Cook University, Cairns, Queensland, Australia; [23]Dept Biological Sciences, University of Waikato, Private Bag 3105, Hamilton, New Zealand; [24]Institute for Biological Problems of Cryolithozone Siberian Branch RAS (IBPC), Yakutsk, Russia; [25]Environmental Change Institute, School of Geography and the Environment, University of Oxford, South Parks Road, Oxford OX1 3QY, UK; [26]Dept Biological Sciences, Macquarie University, Sydney, NSW 2109, Australia; [27]Geography, College of Life and Environmental Sciences, Amory Building, University of Exeter, Exeter EX4 4RJ, UK; [28]Department of Ecology and Evolutionary Biology, University of Toronto, 25 Willcocks Street, Toronto, ON, M5S 3B2, Canada; [29]National Parks Board HQ, 1 Cluny Road, Singapore Botanic Gardens, 259569, Singapore; [30]Dept Plant Physiology, Estonian University of Life Sciences, Kreutzwaldi 1, 51014 Tartu, Estonia; [31]Forest Ecology and Forest Management Group, Wageningen University, PO Box 47, 6700AA Wageningen, Netherlands; [32]Dept Life Sciences, Imperial College London, Silwood Park Campus, SL5 7PY, UK; [33]Natural Resource Ecology Laboratory, Colorado State University, Fort Collins, CO 80523, USA; [34]Dept Biology, University of Florida, Gainesville, FL 32611, USA; [35]Smithsonian Tropical Research Institute, Apartado 0843-03092, Balboa, Republic of Panama; [36]School of Biological Sciences, University of Canterbury, Christchurch 8140, New Zealand; [37]Dept Biology, University of Regina, 3737 Wascana Pkwy, Regina, SK, S4S 3M4, Canada; [38]Laboratorio Internacional de Cambio Global (LINC-Global), Museo nacional de Ciencias Naturales, MNCN, CSIC, Serrano 115 dpdo, E-28006 Madrid, Spain; [39]Faculty of Agriculture, University of Peradeniya, Peradeniya 20400, Sri Lanka; [40]Institut für Spezielle Botanik und Funktionelle Biodiversität, Universität Leipzig, Johannisallee 21, 04103 Leipzig, Germany; [41]Chengdu Institute of Biology, Chinese Academy of Sciences, No. 9, Section 4, Renmin South Road, Chengdu, Sichuan 610041, China;

Author for correspondence: Owen Atkin, tel +61 (0)2 6125 5046, email: Owen.Atkin@anu.edu.au

Number of Figures: **7** (plus 9 in Supporting Information)
Number of Tables: **6** (plus 5 in Supporting Information)
Number of References: **159**
Number of Pages (text plus references**): 29**

Total Word count: **7991** (excluding abstract, references, figures and tables)
Abstract: **200** words
Introduction: **1517** words
Materials and Methods: **2010** words
Results: **1628** words
Discussion: **3062** words

Summary

- Leaf dark respiration (R_{dark}) is an important yet poorly quantified component of the global carbon-cycle. Given this, we analysed a new global database of R_{dark} and associated leaf traits.
- Data for 899 species were compiled from 100 sites (arctic-to-tropics). Several woody and non-woody plant functional types (PFTs) were represented. Mixed-effects models were used to disentangle sources of variation in R_{dark}.
- Area-based R_{dark} at the prevailing average-daily growth temperature (T) of each site increased only two-fold from the arctic-to-tropics, despite a 20°C increase in growing T (8 to 28°C). By contrast, R_{dark} at a standard T (25°C; R_{dark}^{25}) was three-fold higher in the arctic than tropics, and two-fold higher at arid than mesic sites. Species and PFTs at cold sites exhibited higher R_{dark}^{25} at a given photosynthetic capacity (V_{cmax}^{25}) or leaf nitrogen concentration ([N]) than species at warmer sites. R_{dark}^{25} values at any given V_{cmax}^{25} or [N] were higher in herbs than in woody plants.
- The results highlight variation in R_{dark} among species and across global gradients in T and aridity. In addition to their ecological significance, the results provide a framework for improving representation of R_{dark} in terrestrial biosphere models (TBMs) and associated land-surface components of Earth System Models (ESMs).

Keywords: Acclimation, aridity, climate models, leaf nitrogen, plant functional types, photosynthesis, respiration, temperature

Introduction

A challenge for the development of terrestrial biosphere models (TBMs) and associated land surface components of Earth System Models (ESMs) is improving representation of carbon exchange between terrestrial plants and the atmosphere, and incorporating biological variation arising from diversity in plant functional types (PFTs) and climate (Sitch *et al.*, 2008; Booth *et al.*, 2012; Prentice & Cowling, 2013; Fisher *et al.*, 2014). Accounting for patterns in leaf respiratory CO_2 release in darkness (R_{dark}) in TBMs and ESMs is crucial (King *et al.*, 2006; Huntingford *et al.*, 2013; Wythers *et al.*, 2013), since plant respiration – roughly half of which comes from leaves (Atkin *et al.*, 2007) - releases approximately 60 Pg C yr^{-1} (Prentice *et al.*, 2001; Canadell *et al.*, 2007; IPCC, 2013). Fractional changes in leaf R_{dark} as a consequence of climate change can, therefore, have large impacts on simulated net C-exchange and C-storage for individual ecosystems (Piao *et al.*, 2010) and, by influencing the CO_2 concentration of the atmosphere, potentially feedback so as to alter the extent of future global warming (Cox *et al.*, 2000; Huntingford *et al.*, 2013). There is growing acceptance, however, that leaf R_{dark} is not adequately represented in TBMs and ESMs (Huntingford *et al.*, 2013; Smith & Dukes, 2013), resulting in substantial uncertainty in future climate predictions (Leuzinger & Thomas, 2011); consequently, there is a need to improve representation of leaf R_{dark} in predictions of future vegetation-climate interactions for a range of possible fossil fuel burning scenarios (Atkin *et al.*, 2014). Achieving this requires: (1) an analysis of variation in leaf R_{dark} along global climate gradients and among taxa within ecosystems; and, (2) establishing whether relationships between leaf R_{dark} and associated leaf traits vary predictably among environments and plant functional types (PFTs) (Wright *et al.*, 2004; Reich *et al.*, 2006; Wright *et al.*, 2006; Atkin *et al.*, 2008). PFTs enable a balance to be struck between the computational requirements of TBMs to minimize the number of plant groups and availability of sufficient data to fully characterise functional types, versus the reality that plant species differ widely in trait values. Most TBMs contain at least five PFTs, with species being organized on the basis of canopy characteristics such as leaf size and life span, physiology, leaf mass-to-area ratio, canopy height and phenology (Fisher *et al.*, 2014). Although classifications that are directly trait-based are emerging (Kattge *et al.*, 2011), PFT classifications are still widely used in TBMs and land surface components of ESMs. As such, discerning the role of PFTs in modulating relationships between leaf R_{dark} and associated leaf traits will provide critical insights.

Although our understanding of global variation in leaf R_{dark} remains inadequate, it is known that in natural ecosystems rates vary markedly within and among species, and among PFTs. Surveys of leaf R_{dark} at a common temperature (T) of 25°C (R_{dark}^{25}) allow standardized comparisons of respiratory capacity (and associated investment in mitochondrial protein) to be made among contrasting sites and species. In a survey of 20 sites around the world, Wright *et al.* (2006) reported

a 16-fold variation in mass-based leaf R_{dark}^{25}. Importantly, much of the variation in rates of R_{dark}^{25} is present within sites among co-occurring species and PFTs, reflecting strong genetic (as opposed to environmental) control of respiratory flux, as demonstrated by inter-specific comparisons in controlled-environments (Reich *et al.*, 1998c; Loveys *et al.*, 2003; Xiang *et al.*, 2013) and field conditions (Bolstad *et al.*, 2003; Tjoelker *et al.*, 2005; Turnbull *et al.*, 2005; Slot *et al.*, 2013). Differences in demand for respiratory products (e.g. ATP, reducing equivalents and/or carbon skeletons) from metabolic processes (such as photosynthesis (*A*), phloem loading, N-assimilation and protein turnover) underpin genotype variations in leaf R_{dark} (Lambers, 1985; Bouma *et al.*, 1994; Bouma *et al.*, 1995; Noguchi & Yoshida, 2008). Consequently, inter-specific variations in leaf R_{dark} often scale with photosynthesis (Gifford, 2003; Wright *et al.*, 2004; Campbell *et al.*, 2007), and leaf nitrogen ([N]) (Ryan, 1995; Reich *et al.*, 1998b). Importantly, R_{dark}↔[N] relationships differ among PFTs, with R_{dark} at a given [N] being higher in forbs than in woody angiosperms and gymnosperms (Reich *et al.*, 2008).

Any analysis of global patterns of leaf R_{dark} must consider the impacts of the environment on respiratory metabolism; here, the impact of *T* on R_{dark} is of particular interest. Leaf R_{dark} is sensitive to short-term (scale of minutes) changes in *T* (Wager, 1941; Atkin & Tjoelker, 2003; Kruse *et al.*, 2011), with the sensitivity declining as leaf *T* increases (Tjoelker *et al.*, 2001). With sustained changes in the prevailing ambient growth *T*, leaf R_{dark} often acclimates to the new conditions (Tjoelker *et al.*, 2009; Ow *et al.*, 2010; Dillaway & Kruger, 2011; Slot *et al.*, 2014a), resulting in higher rates of R_{dark}^{25} in cold-acclimated plants (Larigauderie & Körner, 1995; Atkin & Tjoelker, 2003). Such acclimation can occur as quickly as within one to a few days (Atkin *et al.*, 2000) and can result in leaf R_{dark} measured at the prevailing ambient *T* (R_{dark}^{amb}) being nearly identical (i.e. near-homeostatic) in thermally contrasting environments (Zaragoza-Castells *et al.*, 2008). Another factor that can influence leaf R_{dark} is drought, with rates declining following the onset of drought (Flexas *et al.*, 2005; Ayub *et al.*, 2011; Crous *et al.*, 2011). However, the response to drought can vary, with other studies reporting no change (Gimeno *et al.*, 2010) or an increase in R_{dark}^{25} with increasing drought (Bartoli *et al.*, 2005; Slot *et al.*, 2008; Metcalfe *et al.*, 2010). Thus, while exposure to hot growth conditions is invariably associated with a decline in R_{dark}^{25}, there is as yet no clear consensus on how differences in water availability across sites impact on R_{dark}^{25}.

As noted above, an overview of global variations in R_{dark} is needed to provide benchmarking data to constrain and test alternative representations of autotrophic respiratory CO_2 release in TBMs and the land surface components of ESMs. The data reported by Wright *et al.* (2006) represent the largest compilation to date, having compared mass-based rates of leaf R_{dark} in 208 woody and 60 herb/grass species from 20 contrasting sites, mostly in temperate regions. However, no data were available for plants growing in upland tropical or arctic ecosystems. Nevertheless, several

interesting phenomena were identified, including that rates of R_{dark}^{25} (and R_{dark}^{25}↔[N] relationships) were similar at sites that differ in growth *T*; a similar result was reported in an earlier analysis by Reich *et al.* (1998b). This observation contrasts with earlier studies that reported higher R_{dark} at a standard measurement *T* in plants growing at colder sites (Stocker, 1935; Wager, 1941; Semikhatova *et al.*, 2007), consistent with thermal acclimation responses of respiratory metabolism (Atkin & Tjoelker, 2003). A new global database not only requires rates of R_{dark}^{25} and R_{dark}^{amb}, but also values of other leaf traits currently used in TBMs to predict respiration.

While there is no single approach to estimating leaf R_{dark} in TBMs – Schwalm *et al.* (2010) reported 15 unique approaches from 21 TBMs – it is common for R_{dark} to be related to gross primary productivity (GPP), either directly as a fraction of GPP, or indirectly as a fraction of maximum carboxylation capacity, with GPP estimated from enzyme kinetic or stomatal conductance models. Other models estimate leaf R_{dark} from other traits, including [N] [e.g. Biome-BGC; Thornton *et al.* (2002)] and/or vegetation carbon [Lund-Postdam-Jena model (*LPJ*); Sitch *et al.* (2003)]. In the UK Hadley Centre model *JULES* [Joint UK Land Environment Simulator (Clark *et al.*, 2011)], R_{dark}^{25} is assumed to be proportional to photosynthetic carboxylation capacity at 25°C (V_{cmax}^{25}), with V_{cmax}^{25} predicted from PFT-dependent values of leaf [N] according to a single V_{cmax}^{25}↔[N] relationship (Schulze *et al.*, 1994; Cox *et al.*, 1998); *JULES* also provides the opportunity to link terrestrial carbon cycling to climate prediction. However, as with other models linking R_{dark}^{25} to GPP, *JULES* does not account for climate or PFT-dependent variations in R_{dark}^{25}↔V_{cmax}^{25}↔[N] relationships. A new global database will enable assessment of R_{dark}^{25}↔V_{cmax}^{25}↔[N] (and phosphorous concentrations [P]) relationships, both among PFTs and along climate gradients.

Here, using published and unpublished data (Supporting Information, Tables S1 and S2), we report on a newly compiled global leaf R_{dark} and associated traits (*GlobResp*) database. The *GlobResp* database increases biogeographical and phylogenetic coverage compared to earlier data sets, and contains information on leaf R_{dark} and associated leaf traits for 899 species from 100 sites. We used the *GlobResp* database to address the following questions. First, do rates of R_{dark} at prevailing ambient *T* (R_{dark}^{amb}) and at a standardized reference *T* of 25°C (R_{dark}^{25}) vary with climate across sites in relation to *T* (i.e. thermal environment) and aridity. Second, are the observed patterns consistent with hypotheses concerning thermal acclimation and adaptation (i.e. evolutionary response resulting from genetic changes in populations and taxa) of R_{dark}. And third, does scaling between leaf R_{dark} and associated leaf traits vary among environments and PFTs? Finally, a key aim of our study was to predict global variability in R_{dark}^{25} from a group of independent input variables, using data on corresponding leaf traits, climate or a combination of traits and climate; here our aim was to provide equations that would facilitate improved representation of leaf R_{dark} in TBMs and associated land surface components of ESMs.

Materials and Methods

Compilation of a global database

To create a global leaf respiration and associated leaf traits (*GlobResp*) database, we combined data from recent field campaigns (Supporting Information, Table S1) with previously published data (Table S2). Data were obtained from recent publications (Atkin *et al.*, 2013; Slot *et al.*, 2013; Slot *et al.*, 2014b; Weerasinghe *et al.*, 2014) and the *TRY* trait database (Kattge *et al.*, 2011) that included published studies (Mooney *et al.*, 1983; Oberbauer & Strain, 1985; Oberbauer & Strain, 1986; Chazdon & Kaufmann, 1993; Kamaluddin & Grace, 1993; Kloeppel *et al.*, 1993; García-Núñez *et al.*, 1995; Kloeppel & Abrams, 1995; Zotz & Winter, 1996; Grueters, 1998; Miyazawa *et al.*, 1998; Reich *et al.*, 1998b; Bolstad *et al.*, 1999; Craine *et al.*, 1999; Mitchell *et al.*, 1999; Niinemets, 1999; Wright *et al.*, 2001; Meir *et al.*, 2002; Wright & Westoby, 2002; Veneklaas & Poot, 2003; Wright *et al.*, 2004; Tjoelker *et al.*, 2005; Machado & Reich, 2006; Poorter & Bongers, 2006; Wright *et al.*, 2006; Meir *et al.*, 2007; Swaine, 2007; Sendall & Reich, 2013). The combined database contains data from 100 thermally contrasting sites (899 species representing 136 families, and *c.* 1200 species-site combinations) from biomes ranging from 69ºN to 43ºS and from sea-level to 3450 m asl (Fig. 1a; Tables 1, 2).

A wide range of terrestrial biomes is represented in the new combined *GlobResp* database (Table 1) along with most of the plant functional types (PFTs) categorised in *JULES* - a land surface component of an Earth System Model (ESM) frameworks (Clark *et al.*, 2011); and in *LPJ* - representing a model with a greater diversity of PFTs from the wider TBM community (Sitch *et al.*, 2003)] (Table 2). Users who would like to use *GlobResp* (to be available via the *TRY* trait database) will also be provided with species classified according to other PFT schemes [including the Sheffield DGVM (Woodward *et al.*, 1998)]. Several PFTs, however, remain poorly represented in *GlobResp*: plants that use the C_4 photosynthetic pathway, boreal deciduous needle-leaved trees (BorDcNl) and tropical herbs/grasses (TrpH – which in the database includes a mixture of species that use either C_3 or C_4 pathways of photosynthesis). Lianas are not yet included in PFT classifications of global TBMs, and are also absent from *GlobResp* , although some data are now emerging for a limited number of sites (Slot *et al.*, 2013). The *GlobResp* database was limited to field-collected data from sites where climate data could be attributed. We excluded data from controlled-environment experiments (e.g. growth cabinets and glasshouses), as well as experiments where atmospheric CO_2, temperature, irradiance, nutrient supply and/or water supply were manipulated. For each site, long-term climate data were obtained from the *WorldClim* climate database for years 1960–1990, at a resolution of 30 arc seconds, or 1 km at the equator (Hijmans *et al.*, 2005). Aridity indices [AI, ratio of mean annual

precipitation (MAP) to potential evapo-transpiration (PET), and hence a lower value of AI indicates more arid conditions] at each site were estimated according to Zomer *et al.* (2008) using the CGIAR-CSI Global-PET database (http://www.cgiar-csi.org).

Mean temperature of the warmest quarter (i.e. warmest three-month period per year; TWQ) and measuring month (MMT - mean temperature of the month when respiration data were recorded) were used to characterise the growth T at each site. Records of the actual measuring month, required to estimate MMT, were only available for half the sites. Consequently, we used TWQ as a measure of the growth T, as most temperate and arctic sites were sampled in summer which corresponded with the warmest quarter. For tropical sites we also used TWQ, although seasonal T variation is comparatively low in tropical regions (Archibold, 1995).

Data were collected using similar protocols described herein (Supporting Information Methods S1) and in published works (Table S2). Outer canopy leaves were sampled early-mid morning, kept in moist, dark conditions, with R_{dark} measured using infra-red gas analysers following a period of dark-adjustment – typically 30-45 mins (Azcón-Bieto *et al.*, 1983; Atkin *et al.*, 1998). Only data from mature, fully expanded leaves were included; as such, R_{dark} did not reflect the metabolic demands of biosynthesis associated with localized cell division/expansions processes. Rather, the measured rates of R_{dark} likely reflected demands for respiratory products associated with cellular maintenance, and potentially phloem loading (Amthor, 2000). We note that the daytime measured rates of R_{dark} may have differed from equivalent fluxes at night (when compared at an equivalent T), reflecting the potential for diel differences in substrate availability and the extent of sucrose loading.

The *GlobResp* database contains R_{dark} expressed per unit leaf dry mass and per unit leaf area. Where available, the database includes values of light-saturated photosynthesis (A_{sat}) and associated values of internal CO_2 concentration (C_i) and stomatal conductance (g_s), leaf mass per area (M_a), leaf nitrogen concentration ([N]) and leaf phosphorus concentration ([P]).

Temperature normalisation of respiration rates

Leaf measurement temperatures (T) ranged from 6 to 40ºC among sites, with most measured between 16 and 33°C (T_1 in Eqn 1). To enable comparisons of leaf R_{dark}, we calculated area- and mass-based rates both for a common temperature (25°C) and at the growth T at each site (TWQ and MMT) – see Methods S2 in Supporting Information for further details. To estimate rates of R_{dark} (R_2) at a given T (T_2), we calculated rates of R_{dark} at 25ºC (R_{dark}^{25}), TWQ (R_{dark}^{TWQ}) and MMT (R_{dark}^{MMT}) using a temperature-dependent Q_{10} (Tjoelker *et al.*, 2001) based on a known rate (R_1) at experimental T (T_1) using the equation:

$$R_2 = R_1(3.09 - 0.043\left[\frac{(T_2+T_1)}{2}\right])^{\left[\frac{T_2-T_1}{10}\right]} \qquad \text{Eqn 1}$$

Calculations of R_{dark} at the abover temperatures yielded similar rates, irrespective of whether a *T*-dependent Q_{10} or fixed Q_{10} was used (Supporting Information, Fig. S1).

Calculation of photosynthetic capacity

Given our objective to assess relationships between R_{dark} and the carboxylation capacity of Rubisco (V_{cmax}), we calculated the V_{cmax} for C_3 species (i.e. excluding C_4 species) for all observations where A_{sat} and C_i values were available (Farquhar *et al.*, 1980; Niinemets, 1999; von Caemmerer, 2000); this included all of the previously unpublished data (Table S1) and much of the previously published data (Table S2). V_{cmax} values were calculated according to:

$$V_{\text{cmax}} = \left(A_{\text{sat}} + R_{\text{light}}\right)\frac{C_i+K_c[1+O/K_O]}{C_i-\Gamma_*} \qquad \text{Eqn 2}$$

where $\Gamma*$ is the CO_2-compensation point in the absence of non-photorespiratory mitochondrial CO_2 release (36.9 µbar at 25ºC), *O* is the partial pressure of oxygen, C_i is the inter-cellular CO_2 partial pressure, R_{light} is the rate of non-photorespiratory mitochondrial CO_2 release (here assumed to be equal to R_{dark}), and K_c and K_o are the Michaelis-Menten constants (K_m) of Rubisco for CO_2 and O_2, respectively (von Caemmerer *et al.*, 1994). While the assumption that $R_{light} = R_{dark}$ is unlikely to be correct in many situations (Hurry *et al.*, 2005; Tcherkez *et al.*, 2012), estimates of V_{cmax} are largely insensitive to this assumption. We assumed K_c and K_o at 25ºC to be 404 µbar and 248 mbar, respectively (Evans *et al.*, 1994; von Caemmerer *et al.*, 1994) and that K_c and K_o at the measurement *T* could be calculated assuming activation energies (E_a) of K_c and K_o of 59.4 and 36 kJ mol^{-1}, respectively (Farquhar *et al.*, 1980). Next, we standardised V_{cmax} to 25ºC (V_{cmax}^{25}) assuming E_a = 64.8 kJ mol^{-1} (Badger & Collatz, 1977) according to:

$$V_{\text{cmax}^{25}} = \frac{V_{\text{cmax}}}{exp^{\left[(T-25)E_a/(298*rT)\right]}} \qquad \text{Eqn 3}$$

where *T* is the leaf temperature at which A_{sat} was measured/reported (and thus V_{cmax} initially estimated), and *r* is the gas constant (8.314 $J K^{-1} mol^{-1}$). Estimates were made for C_3 species only, since representation of C_4 plants in our database was minimal (Table 2).

For data from unpublished field campaigns (Table S1), leaf area and mass values were determined as outlined in Supporting Information (Methods S1); for sites where leaf [N] and [P] were both reported, analyses were made using Kjeldahl acid digests (Allen, 1974). For sites where only [N] was measured, leaf samples were analyzed by mass spectrometry for total N concentration (Loveys *et al.*, 2003); see Table S1 for further details. Details of the N and P analysis procedures

used for previously published data can be found in the citations listed in Table S2. Collectively, the *GlobResp* database contains *c.* 1050 species:site mean values of mass- ($[N]_m$) and area-based leaf nitrogen concentrations ($[N]_a$), and *c.* 735 species:site mean values of $[P]_m$ and $[P]_a$.

Data analysis

Prior to analyses, *GlobResp* data were filtered for statistical outliers. Outlying values were identified as those falling beyond a central tendency band of twice the interquartile range. Three filters were applied in sequence to each PFT class separately (using *LPJ* groupings to enable separation of evergreen and deciduous life histories, and because there were broadly similar numbers of observations within each *LPJ* PFT category compared to that of *JULES*, where the majority of observations were within the broadleaved tree (BlT) category). Three filters were applied in the sequence: (1) mass-based respiration at 25ºC ($R_{dark,m}^{25}$); (2) area-based respiration at 25ºC ($R_{dark,a}^{25}$); and, (3) C_i (impacting on the calculation of V_{cmax}). Whenever an outlier was identified, the entire observational row was removed from the *GlobResp* database. Application of the above filters resulted in removal of *c.* 3% of the rows from the initial database. Where leaf traits followed an approximate log-normal distribution, such values were log_{10}-transformed before screening for outliers and subsequent analysis. Analyses were then conducted using: (1) trait averages for unique site:species combinations; and, where noted, (2), individual rows of data.

Bivariate regression was used to explore relationships between area- and mass-based R_{dark} and latitude, TWQ (mean temperature of the warmest quarter, calculated using all data), MMT (mean T of the month when R_{dark} was recorded) and/or AI (ratio of MAP to PET). In addition, backwards-stepwise regression was used to select the best fitting equation from a starting set of input leaf traits, climate or the combination of traits plus climate variables; parameters were chosen that exhibited variance inflation factors (VIF) less than 2.0 (i.e. minimal co-linearity); F-to-remove criterion was used to identify best-fit parameters. Multiple regression analyses were then conducted to estimate predictive equations for the chosen variables. The PRESS statistic (predicted residual error sum of squares) was used to provide a measure of how well each regression model predicted observed R_{dark} values. Relative contributions of leaf trait and climate variables to each regression were gauged from their standardised partial regression coefficients.

Standardised major axis (SMA) analysis was used to determine the best-fit lines ($\alpha = 0.05$) for the key relationships involving R_{dark}^{25} both on an area- and mass-basis (Falster *et al.*, 2006; Warton *et al.*, 2006; Warton *et al.*, 2012) We tested for differences among PFT classes (*JULES*) and site-based temperature bands (5ºC TWQ); to facilitate visual comparison of PFTs, we chose to use the four PFTs within the *JULES* framework, rather than the larger number of PFTs contained in the *LPJ* model. Using the *JULES* PFTs also provided an opportunity to assess how changes in growth

temperature impacted on bivariate relationships within a PFT [broad leaved trees (BlT)] for which there was a large number of observations and widespread distribution. We used a mixed-effects linear model to account for variability in R_{dark}^{25} on both area- and mass-bases. Given the hierarchical nature of the database, the linear mixed-effects model combined fixed and random components (Zuur *et al.*, 2009). The available fixed effect variables included: PFT, leaf traits (R_{dark}^{25}, V_{cmax}^{25}, leaf mass per unit area (M_a), [N], [P]) and climate variables (TWQ and AI). Models were run using PFT classifications from *JULES* and *LPJ*.

All continuous explanatory leaf variables were centred on their mean values prior to inclusion. Co-linearity among leaf variables was tested using VIFs. Model specification and validation was based on the protocols outlined in Zuur *et al*. (2009) and fitted using the *nlme* package (R package ver. 3.1–105, R Foundation for Statistical Computing, Vienna, Austria, R Development Core Team 2011). Due to the global nature of the database, species, family and site identifiers were treated as random rather than fixed effects, placing our focus on the variation contained within these terms, rather than mean values for each phylogeny/site level. Model comparisons and the significance of fixed-effects terms were assessed using Akaike's information criterion (AIC).

Stepwise and associated multiple linear regressions were conducted using Sigmaplot Statistics v12 (Systat Software Inc., San Jose, CA, USA). All other statistical analyses and modelling were conducted using the open-sourced statistical environment 'R' (R Development Core Team, 2011).

Results

Comparison of traits among plant functional types

Across the *GlobResp* database, leaf mass per unit projected leaf area (M_a) varied 40-fold (from 19 to 780 g m^{-2}), $[N]_a$ varied 70-fold (from 0.13 to 9.13 g m^{-2}) and $[P]_a$ varied 125-fold, from 10 to 1260 mg m^{-2}. In four out of the five *JULES* PFTs (i.e. needle-leaved trees, broad-leaved trees, shrubs and C_3-herbs/grasses), ranges of each of M_a, $[N]_a$ and $[P]_a$ values were relatively similar (Figs 2 and S2). C_4 plants were poorly represented (Table 2), and were generally omitted from subsequent analyses. On average, shrubs and needle-leaved trees exhibited greater leaf mass per unit area (M_a) values than their broad-leaved tree and C_3 herb/grass counterparts. By contrast, $[N]_a$ values were relatively similar among the four PFTs (excluding C_4 plants) (Figs 2 and S2). While $[P]_a$ values were similar among broad-leaved trees, C_3 herbs/grasses and shrubs, levels were higher in needle-leaved trees.

Area- and mass-based V_{cmax}^{25} varied markedly within the four PFTs; needle-leaved trees exhibited a narrower range of V_{cmax}^{25} values compared with the others (Fig. 3a,c). Overall, the average values of V_{cmax}^{25} were relatively similar among the four PFTs. By contrast, average rates of R_{dark}^{25}

384 differed relatively more among PFTs, being highest in C_3 herbs/grasses, both on an area and mass
385 basis (Fig. 3b,d).
386

Relationships between leaf traits and climate

To test whether R_{dark}^{25} was related to growth temperature or water availability, we plotted R_{dark}^{25} against absolute latitude, TWQ and AI (Figs 4a-c and 4g-i). Against latitude (considering northern and southern hemispheres separately), area-based R_{dark}^{25} ($R_{dark,a}^{25}$) exhibited a significant, positive relationship (Table 3), being three-fold faster in arctic than at the equator (Fig. 4a), suggesting, as expected, that factors other than latitude *per se* play the key roles in determining variations in $R_{dark,m}^{25}$. A similar pattern in the northern (but not southern) hemisphere was observed for mass-based R_{dark}^{25} (Fig. 4g; Table 3). Against TWQ, variations in $R_{dark,a}^{25}$ and $R_{dark,m}^{25}$ followed trends consistent with the latitudinal patterns, with rates being fastest at the coldest sites (Figs 4b,h). Negative relationships were found between both area- and mass-based R_{dark}^{25} and AI (Figs 4c,i; Table 3) – recalling that AI is lowest at the driest sites - with $R_{dark,a}^{25} \leftrightarrow$AI markedly steeper when data from the wet cool temperate rainforest site in New Zealand were excluded (Supporting Information, Fig. S2). Collectively, these results suggest that rates of leaf R_{dark} at 25ºC are lowest at warm/moist sites near the equator, and fastest at cold/drier sites at high latitudes.

We now consider global patterns of leaf R_{dark} at the long-term average ambient growth T at each site (R_{dark}^{amb}), with R_{dark}^{amb} estimated using calculations of R_{dark} at TWQ (R_{dark}^{TWQ}) (Figs 4d-f, j-l). In the northern hemisphere, both area- and mass-based R_{dark}^{TWQ} decreased with increasing latitude (Figs 4d,j; Table 3). A similar pattern was observed in the southern hemisphere for mass-based but not area-based R_{dark}^{TWQ} (Fig. 4d). Both $R_{dark,a}^{TWQ}$ and $R_{dark,m}^{TWQ}$ increased with increasing TWQ (Fig. 4e,k; Table 3), indicating that rates of R_{dark}^{amb} are likely faster at the warmest sites. Similarly, the negative $R_{dark}^{TWQ} \leftrightarrow$AI association was significant (both on an area and mass-basis; Fig. 4f,l; Table 3). However, exclusion of mass-based data from the unusually wet site in New Zealand resulted in there being no significant $R_{dark,m}^{TWQ} \leftrightarrow$AI association (Fig. S3). Collectively, R_{dark}^{amb} (both on an area and mass-basis) was faster at the hottest sites in the tropics and mid-latitude regions. These patterns were consistent whether TWQ or MMT were used as estimates of site-specific ambient growth T (Fig. S4).

A focus of our study was determining the best function to predict area- and mass-based R_{dark}^{25} around the globe from a group of independent input variables. Regression analysis (Table 4) shows that, based solely on leaf traits (i.e. ignoring climate), 17% and 31% of the variance in $R_{dark,a}^{25}$ and $R_{dark,m}^{25}$, respectively, was accounted for using regression equations that included leaf [N] and area:mass metrics (i.e. M_a or SLA). Adding leaf [P] did little to improve the proportion of variance in R_{dark}^{25} accounted for by regression; however, [P] replaced [N] in the resultant selected equations (Table 4). By contrast, addition of V_{cmax}^{25} to the available range of leaf traits improved the r^2 of the resultant regressions (i.e. accounting for 22% and 41% of the variance in $R_{dark,a}^{25}$ and $R_{dark,m}^{25}$, respectively; Table 4). Climate parameters alone (TWQ, PWQ and/or AI) accounted for only 9-17%

of variance in R_{dark}. However, combining climate with leaf traits accounted for 35% and 50% of the variance in $R_{dark,a}^{25}$ and $R_{dark,m}^{25}$, respectively (Table 4), with M_a, TWQ, V_{cmax}^{25}, rainfall/aridity and leaf [P] contributing to variance in R_{dark}, largely in that order. Replacing [P] with [N] had little effect on the r^2 of the resultant linear regressions. Thus, analysis using multiple linear regression strongly suggests that variations in leaf R_{dark} are tied to related variations in leaf structure, chemistry, and photosynthetic capacity, the thermal environment in the period during which R_{dark} measurements were made, and the average water availability.

Relationships among plant functional types

For the $R_{dark,a}^{25} \leftrightarrow V_{cmax,a}^{25}$ association, tests for common slopes revealed no significant differences among the four *JULES* PFTs, nor did the elevations of those common slopes differ, except for C_3 herbs/grasses, which exhibited faster rates of $R_{dark,a}^{25}$ at a given $V_{cmax,a}^{25}$ compared with the other PFTs (Fig. 5a). Among TWQ classes, there were also no significant differences in slopes, but the elevation (i.e. *y*-axis intercept) of the relationships differed systematically when considering all PFTs collectively (Fig. 5b), and broad-leaved trees alone (Fig. 5c). With respect to the effect of TWQ on $R_{dark,a}^{25} \leftrightarrow V_{cmax,a}^{25}$ relationships, the elevation was similar for the three highest TWQ classes (15-20, 20-25 and >25ºC), whereas $R_{dark,a}^{25}$ at any given $V_{cmax,a}^{25}$ was significantly faster at the two lowest TWQ classes (Fig. 5b; Table S3). A similar pattern emerged when assessing a single widely-distributed PFT (broad-leaved trees; Fig. 5c). Thus, in addition to area-based rates of R_{dark}^{25} at any given photosynthetic capacity being fastest in C_3 herbs, $R_{dark,a}^{25}$ was also faster in plants growing in cold environments.

Analysed on a mass-basis, tests for common slopes among $R_{dark,m}^{25} \leftrightarrow V_{cmax,m}^{25}$ relationships revealed significant differences among PFTs and TWQ classes. Among PFTs, the slope of the $R_{dark,m}^{25} \leftrightarrow V_{cmax,m}^{25}$ relationship was greatest in C_3 herbs/grasses and smallest in needle-leaved trees (Fig. 5d; Table S3); thus, variation in mass-based photosynthetic capacity was matched by greater variation in leaf $R_{dark,m}^{25}$ in herbs/grasses than in needled-leaved trees. Although the effect of TWQ on $R_{dark,m}^{25} \leftrightarrow V_{cmax,m}^{25}$ was not as consistent as for area-based relationships, in general the pattern was for $R_{dark,m}^{25}$ at any given $V_{cmax,m}^{25}$ to be fastest in plants growing in the coldest habitats, particularly when considering species that exhibit rapid metabolic rates (Fig. 5e,f).

Figure 6 shows PFT- and TWQ-dependent variation in $R_{dark}^{25} \leftrightarrow$[N]. Assessed on a leaf-area basis, tests for common slopes revealed no significant differences among PFTs (Fig. 6a) or TWQ classes (Fig. 6b). The elevation of the relationships differed such that at any given leaf $[N]_a$, rates of $R_{dark,a}^{25}$ were ranked in order of C_3 herbs/grasses > shrubs > broad-leaved trees = needle-leaved trees (Table S3). Considering all PFTs collectively, rates of $R_{dark,a}^{25}$ at any given $[N]_a$ were fastest in the

coldest-grown plants, with the overall pattern being one of decreasing $R_{dark,a}^{25}$ with increasing TWQ (Fig. 6b). Within broadleaved trees, slopes of $R_{dark,a}^{25} \leftrightarrow [N]_a$ relationships differed significantly, being greater at sites with TWQ values of 15-20ºC compared with the two remaining warmer TWQ categories (Table S3). Hence, for broadleaved tree species with high $[N]_a$, $R_{dark,a}^{25}$ was faster in cold habitats than in their warmer counterparts, at least when considering TWQ classes >15ºC. Analysing $R_{dark}^{25} \leftrightarrow [N]$ on a mass-basis revealed significant slope differences among PFTs (Fig. 6d) and TWQ classes (Fig. 6e,f). For the latter, the overall pattern was one of increasing $R_{dark,m}^{25} \leftrightarrow [N]_m$ slope in plants growing at the colder sites.

Mixed effects model analyses

Fitting linear mixed-effects models confirmed that the assigned *JULES* PFTs accounted (in conjunction with assigned random effects) for much of the variation in area-based R_{dark}^{25} present in the *GlobResp* database. For example, a 'null' model where fixed effects were limited to four PFT classes (with species, families and sites treated as random effects) explained 48% of variation in the $R_{dark,a}^{25}$ response (i.e. $r^2 = 0.48$; Table 5a); for an equivalent model that did not include any random effects, inclusion of the four PFT classes alone as fixed terms explained 27% of the variation in $R_{dark,a}^{25}$. Inclusion of additional fixed terms resulted in an increase in the explanatory power of the 'best' predictive model, such that 70% of variation in $R_{dark,a}^{25}$ was accounted for via inclusion of $[N]_a$, $[P]_a$, $V_{cmax,a}^{25}$ and TWQ (Fig. 7a, Fig. S3-S5). The variance components of the preferred model, as defined by the random term (Table 5), indicated that while species and family (Fig. S6) only accounted for *c.* 8% of the unexplained variance (i.e. the response variance not accounted for by the fixed terms), *c.* 23% was related to site differences (Fig. S7; Table 5a). Importantly, the linear mixed-effects model confirmed that $R_{dark,a}^{25}$ decreased with increasing growth *T* (TWQ; Table 5). Using mass-based variables, the assigned PFTs again accounted for much of the variation in $R_{dark,m}^{25}$ in the *GlobResp* database (Table 5), with the 'null' model explaining 54% of variation in $R_{dark,m}^{25}$. Inclusion of additional leaf-trait (but not climate) fixed terms resulted in 78% of variation in $R_{dark,m}^{25}$ being accounted for (Fig. 7b). For both the area- and mass-based mixed-effect models, the 'best' predictive model (as assessed by AIC criterion; Table S4) yielded predictive PFT-specific equations (Table 6). Supporting Information provides comparison of models using alternative PFT classifications (*JULES* & *LPJ*; Table S5); these analyses revealed that replacing *JULES* PFTs with those of *LPJ* did not improve the power of the predictive models, as shown by the lower AIC values for a model that used *JULES*-PFTs compared to one using *LPJ*-PFTs (Table S5).

Discussion

Recognising that leaf respiration is not adequately represented in Terrestrial Biome Models and the land surface component of Earth System Models (Leuzinger & Thomas, 2011; Huntingford *et al.*, 2013) – reflecting the previous lack of data to constrain estimates of leaf R_{dark} - and that improving predictions of future vegetation-climate scenarios requires global variation in leaf R_{dark} to be more thoroughly characterised (Atkin *et al.*, 2014), we compiled and analysed a new, large global database of leaf R_{dark}, climate conditions and associated traits. Our findings revealed systematic variation in leaf R_{dark} in contrasting environments, particularly regarding to site-to-site differences in growth temperature and, to a lesser extent, aridity. Importantly, analysis of the *GlobResp* database has yielded a range of equations (suitable for TBMs and land surface components of ESMs) to predict variations in R_{dark} using information on associated traits (particularly photosynthetic capacity, as well as leaf structure and chemistry) and growth temperature at each site.

Global patterns in leaf respiration: role of environmental gradients

Our results suggest, irrespective of whether rates are expressed on an area or mass basis, that the global pattern is one of increasing rates of leaf R_{dark} with site growth T (Figs. 4 and S4) when moving from the cold, dry arctic tundra to the warm, moist tropics. Importantly, however, such increases in leaf R_{dark} are far less than expected given the large range of growth temperatures across sites. One would expect the variation in TWQ across our sites (*c*. 20ºC) to be associated with a *c*. four-fold increase in R_{dark}^{TWQ} (assuming that R_{dark} roughly doubles for every instantaneous 10ºC rise in T) rather than the observed *c*. two-fold increases (Fig. 4). Underpinning this constrained variation in R_{dark}^{TWQ} are markedly *faster* area- and mass-based rates of leaf R_{dark} at 25ºC (R_{dark}^{25}) at the coldest sites, and *slower* R_{dark}^{25} at warmer sites near the equator (Figs 4 and S4).

Earlier studies of temperature responses were contradictory: some report faster area- and/or mass-based rates of R_{dark}^{25} at cold sites (Stocker, 1935; Wager, 1941; Semikhatova *et al.*, 1992; Semikhatova *et al.*, 2007), whilst others have found similar mass-based rates of R_{dark}^{25} and $R_{dark,m}^{25} \leftrightarrow [N]_m$ relationships in (woody) plants growing in cold and warm habitats (Reich *et al.*, 1998b; Wright *et al.*, 2006). Our new global database, which includes data from Reich *et al.* (1998b) and Wright *et al.* (2006), contains numerous, previously unpublished data for tropical forest and arctic tundra sites (Tables 1 and S1), greatly expanding the thermal range and species coverage. Whilst one might argue that the faster area- and mass-based R_{dark}^{25} in cold habitats (Figs 4 and S4) is a result of the inclusion of tundra herbs/grasses in the *GlobResp* database, growth T (i.e. TWQ) remained important when analysing $R_{dark}^{25} \leftrightarrow V_{cmax}^{25}$ and $R_{dark}^{25} \leftrightarrow [N]$ relationships within a single, globally-distributed PFT (broadleaved trees; Figs 5c and 6c). Moreover, the significant negative

524 $R_{dark,a}^{25}$↔TWQ and $R_{dark,m}^{25}$↔TWQ relationships (Fig. 4) were maintained when data were restricted
525 to broadleaved trees (data not shown), albeit with a diminished slope for $R_{dark,m}^{25}$↔TWQ
526 relationships. So, when analysed at the global level, our key finding is that rates of R_{dark}^{25} do differ
527 between cold and warm sites.

528 Faster R_{dark}^{25} in plants growing in cold habitats compared to those in warm habitats could
529 reflect phenotypic (acclimation) or genotypic differences across gradients in growth *T*. The ability
530 of leaf R_{dark} to acclimate to sustained changes in growth *T* appears widespread among different PFTs
531 (Atkin & Tjoelker, 2003; Campbell *et al.*, 2007), although there is some evidence that broad-leaved
532 trees may have a greater capacity to acclimate than their conifer counterparts (Tjoelker *et al.*, 1999).
533 Acclimation to low growth *T* is linked to reversible adjustments in respiratory metabolism (Atkin &
534 Tjoelker, 2003). Rapid leaf R_{dark} are inherent in a number of species characteristic of cold habitats
535 (Larigauderie & Körner, 1995; Xiang *et al.*, 2013). Similarly, there is evidence that within species,
536 genotypes from cold habitats can exhibit inherently faster leaf R_{dark} than genotypes from warmer
537 habitats (Mooney, 1963; Oleksyn *et al.*, 1998). However, the pattern (both among and within species)
538 is far from consistent (Chapin & Oechel, 1983; Atkin & Day, 1990; Collier, 1996).

539 Another site factor that might influence R_{dark}^{25} is site water availability or aridity (Figs 4 and
540 S3; Tables 4 and 5). In our study, faster leaf R_{dark}^{25} occurred at the driest sites; similar findings were
541 reported by Wright *et al.* (2006). Although literature reviews suggest drought-mediated increases in
542 leaf R_{dark} are rare (Flexas *et al.*, 2005; Atkin & Macherel, 2009), there are reports showing that drought
543 can indeed increase leaf R_{dark} (Slot *et al.*, 2008; Metcalfe *et al.*, 2010) and taxa present at drier sites
544 may also exhibit drought adaptations. However, given our reliance on calculated values of aridity
545 that may not reflect water availability/loss at field-relevant scales, we suggest that further work is
546 needed to confirm the extent to which R_{dark}^{25} varies in response to aridity gradients.
547

548 ## Relationships linking respiration to other leaf traits

549 Including V_{cmax}^{25} as an explanatory variable markedly improved predictions of R_{dark}^{25}, both on an area
550 and mass basis. V_{cmax}^{25} also accounted for a greater proportion of variation in R_{dark}^{25} than did leaf [N]
551 or [P], highlighting the strong functional interdependency between photosynthetic capacity and
552 R_{dark}^{25}. Past studies have reported that variation in R_{dark} is tightly coupled to variation in
553 photosynthesis (Reich *et al.*, 1998b; Loveys *et al.*, 2003; Whitehead *et al.*, 2004), underpinned by
554 chloroplast-mitochondrion interdependence in the light and dark (Krömer, 1995; Noguchi & Yoshida,
555 2008), and energy costs associated with phloem loading (Bouma *et al.*, 1995). Thus, the simplifying
556 assumption by *JULES* and other modelling frameworks (Schwalm *et al.*, 2010; Smith & Dukes, 2013)
557 that $R_{dark,a}^{25}$ is proportional to $V_{cmax,a}^{25}$ (Cox *et al.*, 1998) is robustly supported by our global analysis.
558 However, even though there was no significant $R_{dark,a}^{25}$↔$V_{cmax,a}^{25}$ relationship for C_3 herbs/grasses in

559 Figure 5a, overall this PFT exhibited faster rates of $R_{dark,a}^{25}$ at a given $V_{cmax,a}^{25}$ compared to other
560 PFTs (Fig. 5a), with average $R_{dark,a}^{25}$:$V_{cmax,a}^{25}$ ratios being 0.078 for C_3 herbs, 0.045 for shrubs, 0.033
561 for broad-leaved trees and 0.038 for needle-leaved trees. Moreover, area or mass-based R_{dark}^{25} at any
562 given V_{cmax}^{25} differed among thermally contrasting sites, being faster at colder sites (Figs 5b,e; Table
563 S3). Given these issues, it is crucial that in TBMs and ESMs that link $R_{dark,a}^{25}$ to $V_{cmax,a}^{25}$, account is
564 taken of PFTs and the impact of site growth T on the balance between repiratory and photosynthetic
565 metabolism.

566 Our documentation of new predictive $R_{dark,a}^{25} \leftrightarrow [N]_a$ relationships, to account for variation
567 among PFTs and site growth T (Fig. 6), provides an opportunity to improve the next generation of
568 ESMs. We found that leaf R_{dark}^{25} at any given leaf [N] was faster in C_3 forbs/grasses than in their
569 shrub and tree counterparts (both on an area and mass basis), supporting the findings of Reich *et al.*
570 (2008). In C_3 herbs/grasses, faster rates of R_{dark}^{25} at any given leaf [N] likely reflect greater relative
571 allocation of leaf N to metabolic processes than to structural or defensive roles (Evans, 1989;
572 Takashima *et al.*, 2004; Harrison *et al.*, 2009), combined with high demands for respiratory products.
573 In addition to PFT-dependent changes in $R_{dark}^{25} \leftrightarrow [N]$ relationships, we also found that rates of leaf
574 R_{dark}^{25} at any given leaf [N] were faster in plants growing at colder sites. This finding held when all
575 PFTs were considered together, and also within the single, widespread PFT of broadleaved trees.
576 Faster leaf R_{dark}^{25} at a given [N] therefore appears to be a general trait associated with leaf
577 development in cold habitats (Atkin *et al.*, 2008).
578

579 ## Variability in leaf respiration rates within individual ecosystems

580 A key feature of scatterplots such as in Fig. 4 (which presents species means at each site) was the
581 substantial variation in species-mean values of R_{dark} at any given latitude, or TWQ, or indeed, within
582 any given site (frequently 5-10 fold). This is in line with the diversity often reported in other leaf
583 functional traits (chemical, structural and metabolic) within natural ecosystems (Wright *et al.*, 2004;
584 Fyllas *et al.*, 2009; Asner *et al.*, 2014). Furthermore, the range of variation in species-mean values
585 of R_{dark} was far larger than the two-fold shift in mean R_{dark} observed along major geographic
586 gradients. Our understanding of which of these factors account for the wide range of respiratory
587 rates exhibited by co-existing species is still rather poor (Atkin *et al.*, 2014). At an ecological level,
588 the wide range in R_{dark} may reflect differences among co-existing species [e.g. position along the
589 'leaf economic spectrum' (Wright *et al.*, 2004); position within the conceptual 'competitive-stress
590 tolerator-ruderal (CSR)' space (Grime, 1977)].
591

Formulating equations that predict global variability in leaf respiration

One of our objectives was to develop equations that accurately predict mean rates of leaf R_{dark}^{25} observed across the globe. Our final, parsimonious mixed-effects models accounted for 70% of the variation in area-based R_{dark}^{25} (Fig. 7a) and 78% of the variation in mass-based R_{dark}^{25} (Fig. 7b). Such models provide equations that enable R_{dark}^{25} to be predicted using inputs from fixed terms such as PFT, growth T and leaf physiology/chemistry. Here, we discuss the fixed effects of the area- and mass-based models.

For the area-based model, PFT category was the most important explanatory factor [e.g. in a model with no random effects, the *JULES* PFT classification alone accounted for 27% of the variability in $R_{dark,a}^{25}$], followed by $V_{cmax,a}^{25}$, $[P]_a$, TWQ and $[N]_a$ (Table 5a). Moreover, a comparative model that included random components, and where fixed effects were limited to the PFT classes, was still able to explain 43% of the variation in $R_{dark,a}^{25}$, suggesting that while these PFTs represent a simplification of floristic complexity, they nevertheless help account for much of the global variation in area-based R_{dark}^{25}.

Interestingly, introducing information on phenological habit (i.e. evergreen vs deciduous) and biome by replacing the *JULES* PFTs with those of *LPJ* did not improve the quality of the predictive model (Table S5). This may appear counterintuitive, but could have arisen because the additional information contained in the *LPJ*-PFT classifications was already captured in the 'best' predictive model's explanatory variables (i.e. M_a, $[N]_a$, $[P]_a$, and TWQ) shown in Table 5.

The final 'best' predictive model retained $V_{cmax,a}^{25}$, providing further support for a coupling of photosynthetic and respiratory metabolism (Krömer, 1995; Hoefnagel *et al.*, 1998; Noguchi & Yoshida, 2008). In terms of leaf chemistry, inclusion of $[N]_a$ reflects the coupling of respiratory and N metabolism (Tcherkez *et al.*, 2005), and energy demands associated with protein turnover (Penning de Vries, 1975; Bouma *et al.*, 1994; Zagdanska, 1995). Moreover, as $[N]_a$ is important to $V_{cmax,a}^{25}$, inclusion of $V_{cmax,a}^{25}$ in the model may to some extent obscure the role of $[N]_a$ *per se*. The significant interaction of PFT and $[N]_a$ demonstrates (Table 5) that variation in leaf $[N]_a$ has greater proportional effects on $R_{dark,a}^{25}$ in some PFTs (e.g. C_3 herbs/grasses) than in others (e.g. broad-leaved trees), for the reasons outlined above. Retention of $[P]_a$ in the preferred model suggests that latitudinal variation in foliar [P] (Fig. S2) plays an important role in facilitating faster rates of leaf $R_{dark,a}^{25}$ at the cold high-latitude sites (Figs 4, S4) whilst limiting rates at P-deficient sites in some regions of the tropics (Townsend *et al.*, 2007; Asner *et al.*, 2014). These findings are likely to have particular relevance for predictions of $R_{dark,a}^{25}$ in TBMs that include dynamic representation of N and P cycling (Thornton *et al.*, 2007; Zaehle *et al.*, 2014).

While PFT category remained an explanatory factor in the final model for mass-based R_{dark}^{25} (Table 5), $V_{cmax,m}^{25}$ emerged as the single most important factor accounting for variability in $R_{dark,m}^{25}$.

Importantly, all climate variables were excluded from the model, including site growth T (TWQ). Does this mean that variation in $R_{dark,m}^{25}$ is unrelated to site growth T, as previously suggested (Wright *et al.*, 2006)? Not necessarily; variation in R_{dark}^{25} on both area and mass bases was tightly linked to variation in site growth T (TWQ, Fig. 5). The absence of TWQ in the mass-based mixed model likely arose from the influence of site growth T on leaf $[N]_m$, leaf $[P]_m$ and M_a; all three traits vary in response to differences in site growth T (Reich & Oleksyn, 2004; Wright *et al.*, 2004; Poorter *et al.*, 2009).

In the preferred models for area- and mass-based R_{dark}^{25}, little of the response variance not accounted for by the fixed terms was related to phylogeny, as represented by 'family' (Fig. S8); by contrast, a substantial component (23-73%) of the response variance not accounted for by the fixed terms was related to differences among sites (Fig. S9). This suggests that other 'site' factors (including environmental and methodological differences) may have played an important role in determining variation in $R_{dark,a}^{25}$. Soil characteristics may be important, including availability of nutrients such as calcium, potassium and magnesium (Broadley *et al.*, 2004). In addition, rates of R_{dark}^{25} are sensitive to prevailing ambient T and soil water content in the days preceding measurement (Gorsuch *et al.*, 2010; Searle *et al.*, 2011). Given this, one would not expect long-term climate averages to fully capture the actual environment experienced by plants.

Looking forward: improving representation of leaf respiration in Earth System Models

The most direct way of improving representation of leaf respiration in TBMs and the land surface components of ESMs is to formulate equations that describe patterns in R_{dark}^{25} using leaf trait and climate parameters already incorporated into those models. Our study provides PFT-, leaf-trait- and climate-based equations, depending on which leaf traits are used in a particular model framework to predict variation in R_{dark}^{25} (e.g. area or mass-based [N], or photosynthetic capacity, Tables 5, S4 and S5). Application of such equations would enable prediction of R_{dark}^{25} for biogeographical regions for which the PFT composition is known. The *GlobResp* database will also assist in the development of land surface models that use a trait-continuum approach, where bivariate trait associations and trade-offs are included directly in the models, rather than strictly PFT-categorical approach. For an overview of the issues relevant to incorporation of trait–climate relationships in TBMs, readers are directed to recent discussion papers (Scheiter *et al.*, 2013; Verheijen *et al.*, 2013; Higgins *et al.*, 2014).

Other challenges to incorporating leaf respiration in ESMs include: (i) establishing models of diel variations in leaf R_{dark} – here, understanding the extent to which our daytime measurements of R_{dark} differ from fluxes measured at night will be of interest; (ii) accounting for the appropriate level of thermal acclimation of leaf R_{dark}^{25} to dynamic changes in prevailing growth T and soil moisture at all geographical positions; and, (iii) identifying the extent to which light inhibition of leaf respiration (Kok, 1948; Brooks & Farquhar, 1985; Hurry *et al.*, 2005) varies among PFTs and biomes, over the

range of leaf *T*s experienced by leaves during the day. Although much progress has been made (King *et al.*, 2006; Atkin *et al.*, 2008; Smith & Dukes, 2013; Wythers *et al.*, 2013), accounting for temperature acclimation and light inhibition of leaf *R* in TBMs and associated land surface components of ESMs remains a considerable challenge (Atkin *et al.*, 2014). The equations we provide here that predict current biogeographical variations in leaf R_{dark} at a standard *T* (typically 25°C) are driven by some unquantified combination of acclimation responses and genotypic (adaptive) differences. Further work is needed, however, to establish criteria that will enable environment and genotypic variations in light inhibition of leaf respiration to be predicted; here, recent studies linking light inhibition to photorespiratory metabolism (Griffin & Turnbull, 2013; Ayub *et al.*, 2014) may provide directions for future research. Achieving these goals will be assisted by compilation of data not only from the sites shown in Figure 1, but also from geographic regions currently poorly represented; additional data from Africa, Asia and Europe are needed to enable global historical biogeographic/phylogenetic effects on leaf R_{dark} to be tested. In the long term, a wider goal is development of a mechanistic model that accounts for genotypic-developmental-environmentally-mediated variations in leaf R_{dark}.

Currently, many TBM and ESMs predict photosynthetic capacity (V_{cmax}^{25}) and R_{dark}^{25} based on assumed [N] values for each PFT. In using this approach, differences among plants within a PFT (e.g. genotypic differences and/or plasticity responses to the growth environment) are unspecified. Our mixed-effects models suggest that PFTs capture a substantial amount of species variation across diverse sites and their use is reasonable as a first approximation for the purposes of modelling. In the application of PFT-based modelling, the growth *T*-dependent (TWQ) variations in R_{dark}^{25} within widely distributed PFTs (e.g. broadleaved trees) provide a means to predict *T*-adjustments in R_{dark} at the global scale. For example, predicted R_{dark}^{25} declines 18% from 1.0 to 0.82 μmol m^{-2} s^{-1} when site temperature (TWQ) increases from 20 to 25°C (Table 6). Assuming a static PFT (e.g. no species turnover or differential acclimation/adaptation), these new equations (Table 6, and associated ESM equations in Table S4) provide a first-order approximation of the acclimation response of R_{dark}^{25} of a given PFT to a cooler past world, or warmer future world. They also demonstrate that predictions based on PFT, leaf traits and TWQ provide a powerful improvement in the representation of leaf respiration in ESMs that seek to describe the role of terrestrial ecosystems in an evolving global climate and carbon cycle.

Acknowledgements: We thank the *New Phytologist* Trust for its generous support of the 8th *New Phytologist* Workshop ('*Improving representation of leaf respiration in large-scale predictive climate-vegetation models'*) held at the Australian National University in 2013. Support for the workshop was also provided by the Research School of Biology, ANU. The study was also supported

by the *TRY* initiative on plant traits (http://www.try-db.org). The *TRY* initiative and database is hosted, developed and maintained at the Max Planck Institute for Biogeochemistry, Jena, Germany and is/has been supported by DIVERSITAS, IGBP, the Global Land Project, the UK Natural Environment Research Council (NERC) through QUEST (Quantifying and Understanding the Earth System), the French Foundation for Biodiversity Research (FRB), and GIS *Climat Environnement et Société*. We thank Ben Long and Kaoru Kitajima for providing valuable data, input in earlier analyses/discussions and/or comments on draft versions of this manuscript. The support of the Australian Research Council to OKA (FT0991448, DP0986823, DP1093759, DP130101252 and CE140100008) and PM (FT110100457) is acknowledged, and OKA, KB, MB and ML also acknowledge the support of the Australian SuperSite Network, part of the Australian Government's Terrestrial Ecosystem Research Network (www.tern.org.au) and PM the support of UK NERC (NE/C51621X/1, 709 NE/F002149/1). Collection of unpublished trait and respiration data from 19 RAINFOR floristic inventory plots was supported by a Moore Foundation grant to OP, YM, and Jon Lloyd.

References

Allen SE. 1974. *Chemical Analysis of Ecological Materials*. Oxford: Blackwell Scientific Publications.

Amthor JS. 2000. The McCree-de Wit-Penning de Vries-Thornley respiration paradigms: 30 years later. *Annals of Botany* **86**: 1-20.

Archibold OW. 1995. *Ecology of world vegetation*. London, UK: Chapman and Hall.

Asner GP, Martin RE, Tupayachi R, Anderson CB, Sinca F, Carranza-Jiménez L, Martinez P. 2014. Amazonian functional diversity from forest canopy chemical assembly. *Proceedings of the National Academy of Sciences, USA* **111**: 5604–5609.

Atkin OK, Atkinson LJ, Fisher RA, Campbell CD, Zaragoza-Castells J, Pitchford J, Woodward FI, Hurry V. 2008. Using temperature-dependent changes in leaf scaling relationships to quantitatively account for thermal acclimation of respiration in a coupled global climate-vegetation model. *Global Change Biology* **14**: 2709-2726.

Atkin OK, Bruhn D, Tjoelker MG 2005. Response of plant respiration to changes in temperature: Mechanisms and consequences of variations in Q_{10} values and acclimation. In: Lambers H, Ribas-Carbó M eds. *Plant respiration: from cell to ecosystem*. Dordrecht: Springer, 95-135.

Atkin OK, Day DA. 1990. A comparison of the respiratory processes and growth rates of selected Australian alpine and related lowland plant species. *Australian Journal of Plant Physiology* **17**: 517-526.

Atkin OK, Evans JR, Siebke K. 1998. Relationship between the inhibition of leaf respiration by light and enhancement of leaf dark respiration following light treatment. *Australian Journal of Plant Physiology* **25**: 437-443.

Atkin OK, Holly C, Ball MC. 2000. Acclimation of snow gum (*Eucalyptus pauciflora*) leaf respiration to seasonal and diurnal variations in temperature: the importance of changes in the capacity and temperature sensitivity of respiration. *Plant, Cell & Environment* **23**: 15-26.

Atkin OK, Macherel D. 2009. The crucial role of plant mitochondria in orchestrating drought tolerance. *Annals of Botany* **103**: 581-597.

Atkin OK, Meir P, Turnbull MH. 2014. Improving representation of leaf respiration in large-scale predictive climate–vegetation models. *New Phytologist* **202**: 743-748.

Atkin OK, Scheurwater I, Pons TL. 2007. Respiration as a percentage of daily photosynthesis in whole plants is homeostatic at moderate, but not high, growth temperatures. *New Phytologist* **174**: 367-380.

Atkin OK, Tjoelker MG. 2003. Thermal acclimation and the dynamic response of plant respiration to temperature. *Trends in Plant Science* **8**: 343-351.

Atkin OK, Turnbull MH, Zaragoza-Castells J, Fyllas NM, Lloyd J, Meir P, Griffin KL. 2013. Light inhibition of leaf respiration as soil fertility declines along a post-glacial chronosequence in New Zealand: an analysis using the Kok method. *Plant and Soil* **367**: 163-182.

Ayub G, Smith RA, Tissue DT, Atkin OK. 2011. Impacts of drought on leaf respiration in darkness and light in *Eucalyptus saligna* exposed to industrial-age atmospheric CO_2 and growth temperature. *New Phytologist* **190**: 1003.

Ayub G, Zaragoza-Castells J, Griffin KL, Atkin OK. 2014. Leaf respiration in darkness and in the light under pre-industrial, current and elevated atmospheric CO_2 concentrations. *Plant Science* **226**: 120-130.

Azcón-Bieto J, Lambers H, Day DA. 1983. Effect of photosynthesis and carbohydrate status on respiratory rates and the involvement of the alternative pathway in leaf respiration. *Plant Physiology* **72**: 598-603.

Azcón-Bieto J, Osmond CB. 1983. Relationship between photosynthesis and respiration. The effect of carbohydrate status on the rate of CO_2 production by respiration in darkened and illuminated wheat leaves. *Plant Physiology* **71**: 574-581.

Badger MR, Collatz GJ. 1977. Studies on the kinetic mechanism of ribulose-1,5-bisphosphate carboxylase and oxygenase reactions, with particular reference to the effect of temperature on kinetic parameters. *Carnegie Institution of Washington Yearbook* **76**: 355-361.

Bartoli CG, Gomez F, Gergoff G, Guiamet JJ, Puntarulo S. 2005. Up-regulation of the mitochondrial alternative oxidase pathway enhances photosynthetic electron transport under drought conditions. *Journal of Experimental Botany* **56**: 1269-1276.

Bolstad PV, Mitchell K, Vose JM. 1999. Foliar temperature-respiration response functions for broad-leaved tree species in the southern appalachians. *Tree Physiology* **19**: 871-878.

Bolstad PV, Reich P, Lee T. 2003. Rapid temperature acclimation of leaf respiration rates in *Quercus alba* and *Quercus rubra Tree Physiology* **23**: 969-976.

Booth BBB, Jones CD, Collins M, Totterdell IJ, Cox PM, Sitch S, Huntingford C, Betts RA, Harris GR, Lloyd J. 2012. High sensitivity of future global warming to land carbon cycle processes. *Environmental Research Letters* **7**: 024002.

Bouma TJ, De VR, Van LPH, De KMJ, Lambers H. 1995. The respiratory energy requirements involved in nocturnal carbohydrate export from starch-storing mature source leaves and their contribution to leaf dark respiration. *Journal of Experimental Botany* **46**: 1185-1194.

Bouma TJ, Devisser R, Janssen JHJA, Dekock MJ, Vanleeuwen PH, Lambers H. 1994. Respiratory energy requirements and rate of protein turnover *in vivo* determined by the use of an inhibitor of protein synthesis and a probe to assess its effect. *Physiologia Plantarum* **92**: 585-594.

Broadley MR, Bowen HC, Cotterill HL, Hammond JP, Meacham MC, Mead A, White PJ. 2004. Phylogenetic variation in the shoot mineral concentration of angiosperms. *Journal of Experimental Botany* **55**: 321-336.

Brooks A, Farquhar GD. 1985. Effect of temperature on the CO_2/O_2 specificity of ribulose-1,5-biphosphate carboxylase/oxygenase and the rate of respiration in the light. Estimates from gas exchange measurements on spinach. *Planta* **165**: 397-406.

Campbell C, Atkinson L, Zaragoza-Castells J, Lundmark M, Atkin O, Hurry V. 2007. Acclimation of photosynthesis and respiration is asynchronous in response to changes in temperature regardless of plant functional group. *New Phytologist* **176**: 375-389.

Canadell JG, Le Quere C, Raupach MR, Field CB, Buitenhuis ET, Ciais P, Conway TJ, Gillett NP, Houghton RA, Marland G. 2007. Contributions to accelerating atmospheric CO_2 growth from economic activity, carbon intensity, and efficiency of natural sinks. *Proceedings of the National Academy of Sciences, USA* **104**: 18866-18870.

Chapin FS, Oechel WC. 1983. Photosynthesis, respiration, and phosphate absorption by *Carex aquatilis* ecotypes along latitudinal and local environmental gradients. *Ecology* **64**: 743-751.

Chazdon RL, Kaufmann S. 1993. Plasticity of leaf anatomy of two rainforest shrubs in relation to photosynethetic light acclimation. *Functional Ecology* **7**: 385-394.

Clark DB, Mercado LM, Sitch S, Jones CD, Gedney N, Best MJ, Pryor M, Rooney GG, Essery RLH, Blyth E, Boucher O, Harding RJ, Huntingford C, Cox PM. 2011. The Joint UK Land Environment Simulator (JULES), model description - Part 2: Carbon fluxes and vegetation dynamics. *Geoscientific Model Development* **4**: 701-722.

Collier DE. 1996. No difference in leaf respiration rates among temperate, subarctic, and arctic species grown under controlled conditions. *Canadian Journal of Botany* **74**: 317-320.

Cox PM, Betts RA, Jones CD, Spall SA, Totterdell IJ. 2000. Acceleration of global warming due to carbon-cycle feedbacks in a coupled climate model. *Nature* **408**: 184-187.

Cox PM, Huntingford C, Harding RJ. 1998. A canopy conductance and photosynthesis model for use in a GCM land surface scheme. *Journal of Hydrology* **212**: 79-94.

Craine JM, Berin DM, Reich PB, Tilman GD, Knops JMH. 1999. Measurement of leaf longevity of 14 species of grasses and forbs using a novel approach. *New Phytologist* **142**: 475-481.

Crous KY, Zaragoza-Castells J, LÖW M, Ellsworth DS, Tissue DT, Tjoelker MG, Barton CVM, Gimeno TE, Atkin OK. 2011. Seasonal acclimation of leaf respiration in *Eucalyptus saligna* trees: impacts of elevated atmospheric CO_2 and summer drought. *Global Change Biology* **17**: 1560-1576.

Dillaway DN, Kruger EL. 2011. Leaf respiratory acclimation to climate: comparisons among boreal and temperate tree species along a latitudinal transect. *Tree Physiology* **31**: 1114-1127.

Evans JR. 1989. Photosynthesis and nitrogen relationships in leaves of C_3 plants. *Oecologia* **78**: 9-19.

Evans JR, Von Caemmerer S, Setchell BA, Hudson GS. 1994. The relationship between CO_2 transfer conductance and leaf anatomy in transgenic tobacco with a reduced content of Rubisco. *Australian Journal of Plant Physiology* **21**: 475-495.

Falster DS, Warton DI, Wright IJ. 2006. SMATR: Standardised major axis tests and routines, version 2.0. .

Farquhar GD, von Caemmerer S, Berry JA. 1980. A biochemical model of photosynthetic CO_2 assimilation in leaves of C_3 species. *Planta* **149**: 78-90.

Fisher JB, Huntzinger DN, Schwalm CR, Sitch S. 2014. Modeling the terrestrial biosphere. *Annual Review of Environment and Resources* **39**: 91-123.

Flexas J, Galmés J, Ribas-Carbó M, Medrano H, Lambers H 2005. The effects of water stress on plant respiration. In: Govindjee ed. *Volume 18. Plant respiration: from cell to ecosystem*. Dordrecht: Springer, 85-94.

Fyllas NM, Patino S, Baker TR, Bielefeld Nardoto G, Martinelli LA, Quesada CA, Paiva R, Schwarz M, Horna V, Mercado LM, Santos A, Arroyo L, Jim´enez EM, Luiz˜ao FJ, Neill A, Silva N, Prieto A, Rudas A, Silviera M, Vieira ICG, Lopez-Gonzalez G, Malhi Y, Phillips OL, Lloyd J. 2009. Basin-wide variations in foliar properties of Amazonian forest: phylogeny, soils and climate. *Biogeosciences* **6**: 2677–2708.

García-Núñez C, Azócar A, Rada F. 1995. Photosynthetic acclimation to light in juveniles of two cloud-forest tree species. *Trees-Structure and Function* **10**: 114-124.

Gifford RM. 2003. Plant respiration in productivity models: conceptualisation, representation and issues for global terrestrial carbon-cycle research. *Functional Plant Biology* **30**: 171-186.

Gimeno TE, Sommerville KE, Valladares F, Atkin OK. 2010. Homeostasis of respiration under drought and its important consequences for foliar carbon balance in a drier climate: insights from two contrasting *Acacia* species. *Functional Plant Biology* **37**: 323-333.

Gorsuch PA, Pandey S, Atkin OK. 2010. Temporal heterogeneity of cold acclimation phenotypes in *Arabidopsis* leaves. *Plant, Cell & Environment* **33**: 244-258.

Griffin KL, Turnbull MH. 2013. Light saturated RuBP oxygenation by Rubisco is a robust predictor of light inhibition of respiration in *Triticum aestivum* L. *Plant Biol* **1**: 1438-8677.

Grime JP. 1977. Evidence for the existence of three primary strategies in plants and its relevance to ecological and evolutionary theory. *The American Naturalist* **111**: 1169–1194.

Grueters U. 1998. *Der Kohlenstoffhaushalt von Weizen in der Interaktion erho¨hter CO_2/O_3 Konzentrationen und Stickstoffversorgung.* PhD thesis, Justus-Liebig-University Giessen.

Harrison MT, Edwards EJ, Farquhar GD, Nicotra AB, Evans JR. 2009. Nitrogen in cell walls of sclerophyllous leaves accounts for little of the variation in photosynthetic nitrogen-use efficiency. *Plant, Cell & Environment* **32**: 259-270.

Heskel MA, Bitterman D, Atkin OK, Turnbull MH, Griffin KL. 2014. Seasonality of foliar respiration in two dominant plant species from the Arctic tundra: response to long-term warming and short-term temperature variability. *Functional Plant Biology* **41**: 287-300.

Higgins SI, Langan L, Scheiter S. 2014. Progress in DGVMs: a comment on "Impacts of trait variation through observed trait–climate relationships on performance of an Earth system model: a conceptual analysis" by Verheijen et al. (2013). *Biogeosciences Discuss.* **11**: 4483-4492.

Hijmans RJ, Cameron SE, Parra JL, Jones PG, Jarvis A. 2005. Very high resolution interpolated climate surfaces for global land areas. *International Journal of Climatology* **25**: 1965-1978.

Hoefnagel MHN, Atkin OK, Wiskich JT. 1998. Interdependence between chloroplasts and mitochondria in the light and the dark. *Biochimica Et Biophysica Acta-Bioenergetics* **1366**: 235-255.

Huntingford C, Zelazowski P, Galbraith D, Mercado LM, Sitch S, Fisher R, Lomas M, Walker AP, Jones CD, Booth BBB, Malhi Y, Hemming D, Kay G, Good P, Lewis SL, Phillips OL, Atkin OK, Lloyd J, Gloor E, Zaragoza-Castells J, Meir P, Betts R, Harris PP, Nobre C, Marengo J, Cox PM. 2013. Simulated resilience of tropical rainforests to CO_2-induced climate change. *Nature Geoscience* **6**: 268–273.

Hurry V, Igamberdiev AU, Keerberg O, Pärnik TR, Atkin OK, Zaragoza-Castells J, Gardestrøm P 2005. Respiration in photosynthetic cells: gas exchange components, interactions with photorespiration and the operation of mitochondria in the light. In: Lambers H, Ribas-Carb¢ M eds. *Advances in Photosynthesis and Respiration*. Dordrecht: Kluwer Academic Publishers, 43-61.

IPCC. 2013. *Climate Change 2013: The Physical Science Basis*. Cambridge, UK and New York, USA: Cambridge University Press.

Kamaluddin M, Grace J. 1993. Growth and photosynthesis of tropical forest tree seedlings (*Bischofia javanica* Blume) as influenced by a change in light availability. *Tree Physiology* **13**: 189-201.

Kattge J, Díaz S, Lavorel S, Prentice IC, Leadley P, Bönisch G, Garnier E, Westoby M, Reich PB, Wright IJ, Cornelissen JHC, Violle C, Harrison SP, van Bodegom PM, Reichstein M, Enquist BJ, Soudzilovskaia NA, Ackerly DD, Anand M, Atkin O, Bahn M, Baker TR, Baldocchi D, Bekker R, Blanco CC, Blonder B, Bond WJ, Bradstock R, Bunker DE, Casanoves F, Cavender-Bares J, Chambers JQ, Chapin Iii FS, Chave J, Coomes D, Cornwell WK, Craine JM, Dobrin BH, Duarte L, Durka W, Elser J, Esser G, Estiarte M, Fagan WF, Fang J, Fernández-Méndez F, Fidelis A, Finegan B, Flores O, Ford H, Frank D, Freschet GT, Fyllas NM, Gallagher RV, Green WA, Gutierrez AG, Hickler T, Higgins SI, Hodgson JG, Jalili A, Jansen S, Joly CA, Kerkhoff AJ, Kirkup D, Kitajima K, Kleyer M, Klotz S, Knops JMH, Kramer K, Kühn I, Kurokawa H, Laughlin D, Lee TD, Leishman M, Lens F, Lenz T, Lewis SL, Lloyd J, Llusià J, Louault F, Ma S, Mahecha MD, Manning P, Massad T, Medlyn BE, Messier J, Moles AT, Müller SC, Nadrowski K, Naeem S, Niinemets Ü, Nöllert S, Nüske A, Ogaya R, Oleksyn J, Onipchenko VG, Onoda Y, Ordoñez J, Overbeck G, Ozinga WA, Patiño S, Paula S, Pausas JG, Peñuelas J, Phillips OL, Pillar V, Poorter H, Poorter L, Poschlod P, Prinzing A, Proulx R, Rammig A, Reinsch S, Reu B, Sack L, Salgado-Negret B, Sardans J, Shiodera S, Shipley B, Siefert A, Sosinski E, Soussana JF, Swaine E, Swenson N, Thompson K, Thornton P, Waldram M, Weiher E, White M, White S, Wright SJ, Yguel B, Zaehle S, Zanne AE, Wirth C. 2011. TRY – a global database of plant traits. *Global Change Biology* **17**: 2905–2935.

King AW, Gunderson CA, Post WM, Weston DJ, Wullschleger SD. 2006. Plant respiration in a warmer world. *Science* **312**: 536-537.

Kitajima K, Mulkey SS, Wright SJ. 1997. Seasonal leaf phenotypes in the canopy of a tropical dry forest: photosynthetic characteristics and associated traits. *Oecologia* **109**: 490-498.

Kloeppel BD, Abrams MD. 1995. Ecophysiological attributes of the native *Acer saccharum* and the exotic *Acer platanoides* in urban oak forests in Pennsylvania, USA. *Tree Physiology* **15**: 739-746.

Kloeppel BD, Abrams MD, Kubiske ME. 1993. Seasonal ecophysiology and leaf morphology of four successional Pennsylvania barrens species in open versus understory environments. *Canadian Journal of Forest Research* **23**: 181-189.

Kloeppel BD, Kubiske ME, Abrams MD. 1994. Seasonal tissue water relations of four successional Pennsylvania barrens species in open and understory environments. *International Journal of Plant Sciences* **155**: 73-79.

Kok B. 1948. A critical consideration of the quantum yield of *Chlorella*-photosynthesis. *Enzymologia* **13**: 1-56.

Krömer S. 1995. Respiration during photosynthesis. *Annual Review of Plant Physiology & Plant Molecular Biology* **46**: 45-70.
Kruse J, Rennenberg H, Adams MA. 2011. Steps towards a mechanistic understanding of respiratory temperature responses. *New Phytologist* **189**: 659-677.
Lambers H 1985. Respiration in intact plants and tissues: its regulation and dependence on environmental factors, metabolism and invaded organisms. *Encyclopedia of Plant Physiology. Volume 18, (Douce, R. & Day, D. A.)*. New York: Springer-Verlag, 417-473.
Larigauderie A, Körner C. 1995. Acclimation of leaf dark respiration to temperature in alpine and lowland plant species. *Annals of Botany* **76**: 245-252.
Lee TD, Reich PB, Bolstad PV. 2005. Acclimation of leaf respiration to temperature is rapid and related to specific leaf area, soluble sugars and leaf nitrogen across three temperate deciduous tree species. *Functional Ecology* **19**: 640-647.
Leuzinger S, Thomas RQ. 2011. How do we improve Earth system models? Integrating Earth system models, ecosystem models, experiments and long-term data. *New Phytologist* **191**: 15-18.
Lopez-Gonzalez G, Lewis SL, Burkitt M, Phillips OL. 2011. ForestPlots.net: a web application and research tool to manage and analyse tropical forest plot data. *Journal of Vegetation Science* **22**: 610-613.
Loveys BR, Atkinson LJ, Sherlock DJ, Roberts RL, Fitter AH, Atkin OK. 2003. Thermal acclimation of leaf and root respiration: an investigation comparing inherently fast- and slow-growing plant species. *Global Change Biology* **9**: 895-910.
Lusk CH, Reich PB. 2000. Relationships of leaf dark respiration with light environment and tissue nitrogen content in juveniles of 11 cold-temperate tree species. *Oecologia* **123**: 318-329.
Machado JL, Reich PB. 2006. Dark respiration rate increases with plant size in saplings of three temperate tree species despite decreasing tissue nitrogen and nonstructural carbohydrates. *Tree Physiology* **26**: 915-923.
Meir P, Kruijt B, Broadmeadow M, Barbosa E, Kull O, Carswell F, Nobre A, Jarvis PG. 2002. Acclimation of photosynthetic capacity to irradiance in tree canopies in relation to leaf nitrogen concentration and leaf mass per unit area. *Plant, Cell & Environment* **25**: 343-357.
Meir P, Levy PE, Grace J, Jarvis PG. 2007. Photosynthetic parameters from two contrasting woody vegetation types in West Africa. *Plant Ecology* **192**: 277-287.
Metcalfe DB, Lobo-do-Vale R, Chaves MM, Maroco JP, Aragao L, Malhi Y, Da Costa AL, Braga AP, Goncalves PL, De Athaydes J, Da Costa M, Almeida SS, Campbell C, Hurry V, Williams M, Meir P. 2010. Impacts of experimentally imposed drought on leaf respiration and morphology in an Amazon rain forest. *Functional Ecology* **24**: 524-533.
Mitchell KA, Bolstad PV, Vose JM. 1999. Interspecific and environmentally induced variation in foliar dark respiration among eighteen southeastern deciduous tree species. *Tree Physiology* **19**: 861-870.
Miyazawa S, Satomi S, Terashima I. 1998. Slow leaf development of evergreen broad-leaved tree species in Japanese warm temperate forests. *Annals of Botany* **82**: 859-869.
Mooney HA. 1963. Physiological ecology of coastal, subalpine, and alpine populations of *Polygonum bistortoides Ecology* **44**: 812-816.
Mooney HA, Field C, Gulmon SL, Rundel P, Kruger FJ. 1983. Photosynthetic characteristic of South African sclerophylls. *Oecologia* **58**: 398-401.
Niinemets U. 1999. Components of leaf dry mass per area - thickness and density - alter leaf photosynthetic capacity in reverse directions in woody plants. *New Phytologist* **144**: 35-47.
Noguchi K, Yoshida K. 2008. Interaction between photosynthesis and respiration in illuminated leaves. *Mitochondrion* **8**: 87-99.
Oberbauer SF, Strain BR. 1985. Effects of light regime on the growth and physiology of *Pentaclethra macroloba* (Mimosaceae) in Costa Rica. *Journal of Tropical Ecology* **1**: 303-320.
Oberbauer SF, Strain BR. 1986. Effects of canopy position and irradiance on the leaf physiology and morphology of *Pentaclethra macroloba* (Mimosaceae). *American Journal of Botany* **73**: 409-416.
Oleksyn J, Modrzynski J, Tjoelker MG, Zytkowiak R, Reich PB, Karolewski P. 1998. Growth and physiology of *Picea abies* populations from elevational transects: common garden evidence for altitudinal ecotypes and cold adaptation. *Functional Ecology* **12**: 573-590.

Ow LF, Whitehead D, Walcroft AS, Turnbull MH. 2010. Seasonal variation in foliar carbon exchange in *Pinus radiata* and *Populus deltoides*: respiration acclimates fully to changes in temperature but photosynthesis does not. *Global Change Biology* **16**: 288-302.

Penning de Vries FWT. 1975. The cost of maintenance processes in plant cells. *Annals of Botany* **39**: 77-92.

Piao SL, Luyssaert S, Ciais P, Janssens IA, Chen AP, Cao C, Fang JY, Friedlingstein P, Luo YQ, Wang SP. 2010. Forest annual carbon cost: a global-scale analysis of autotrophic respiration. *Ecology* **91**: 652-661.

Poorter H, Niinemets U, Poorter L, Wright IJ, Villar R. 2009. Causes and consequences of variation in leaf mass per area (LMA): a meta-analysis. *New Phytologist* **182**: 565-588.

Poorter L, Bongers F. 2006. Leaf traits are good predictors of plant performance across 53 rain forest species. *Ecology* **87**: 1733-1743.

Prentice IC, Cowling SA 2013. Dynamic Global Vegetation Models. In: Levin SA ed. *Encyclopedia of Biodiversity (Second Edition)*. Waltham: Academic Press, 670-689.

Prentice IC, Farquhar GD, Fasham MJR, Goulden ML, Heimann M, Jaramillo VJ, Kheshi HS, Le Quere C, Scholes RJ, Wallace DWR 2001. The carbon cycle and atmospheric carbon dioxide. In: al. JTHe ed. *Contribution of Working Group I to the Third Assessment Report of the Intergovernmental Panel on Climate Change*. Cambridge: Cambridge University Press, 183-237.

Reich PB, Ellsworth DS, Walters MB. 1998a. Leaf structure (specific leaf area) modulates photosynthesis-nitrogen relations: evidence from within and across species and functional groups. *Functional Ecology* **12**: 948-958.

Reich PB, Ellsworth DS, Walters MB, Vose JM, Gresham C, Volin JC, Bowman WD. 1999. Generality of leaf trait relationships: A test across six biomes. *Ecology* **80**: 1955-1969.

Reich PB, Oleksyn J. 2004. Global patterns of plant leaf N and P in relation to temperature and latitude. *Proceedings of the National Academy of Sciences, USA* **101**: 11001-11006.

Reich PB, Tjoelker MG, Machado JL, Oleksyn J. 2006. Universal scaling of respiratory metabolism, size and nitrogen in plants. *Nature* **439**: 457-461.

Reich PB, Tjoelker MG, Pregitzer KS, Wright IJ, Oleksyn J, Machado JL. 2008. Scaling of respiration to nitrogen in leaves, stems and roots of higher land plants. *Ecology Letters* **11**: 793-801.

Reich PB, Walters MB, Ellsworth DS, Vose JM, Volin JC, Gresham C, Bowman WD. 1998b. Relationships of leaf dark respiration to leaf nitrogen, specific leaf area and leaf life-span: a test across biomes and functional groups. *Oecologia* **114**: 471-482.

Reich PB, Walters MB, Tjoelker MG, Vanderklein D, Buschena C. 1998c. Photosynthesis and respiration rates depend on leaf and root morphology and nitrogen concentration in nine boreal tree species differing in relative growth rate. *Functional Ecology* **12**: 395-405.

Ryan MG. 1995. Foliar maintenance respiration of subalpine and boreal trees and shrubs in relation to nitrogen content. *Plant, Cell & Environment* **18**: 765-772.

Scheiter S, Langan L, Higgins SI. 2013. Next-generation dynamic global vegetation models: learning from community ecology. *New Phytologist* **198**: 957-969.

Schulze ED, Kelliher FM, Körner C, Lloyd J, Leuning R. 1994. Relationships among maximum stomatal conductance, ecosystem surface conductance, carbon assimilation rate, and plant nitrogen nutrition - a global ecology scaling exercise. *Annual Review of Ecology and Systematics* **25**: 629-660.

Schwalm CR, Williams CA, Schaefer K, Anderson R, Arain MA, Baker I, Barr A, Black TA, Chen GS, Chen JM, Ciais P, Davis KJ, Desai A, Dietze M, Dragoni D, Fischer ML, Flanagan LB, Grant R, Gu LH, Hollinger D, Izaurralde RC, Kucharik C, Lafleur P, Law BE, Li LH, Li ZP, Liu SG, Lokupitiya E, Luo YQ, Ma SY, Margolis H, Matamala R, McCaughey H, Monson RK, Oechel WC, Peng CH, Poulter B, Price DT, Riciutto DM, Riley W, Sahoo AK, Sprintsin M, Sun JF, Tian HQ, Tonitto C, Verbeeck H, Verma SB. 2010. A model-data intercomparison of CO_2 exchange across North America: Results from the North American Carbon Program site synthesis. *Journal of Geophysical Research-Biogeosciences* **115**.

Searle SY, Thomas S, Griffin KL, Horton T, Kornfeld A, Yakir D, Hurry V, Turnbull MH. 2011. Leaf respiration and alternative oxidase in field-grown alpine grasses respond to natural changes in temperature and light. *New Phytologist* **189**: 1027-1039.

Semikhatova OA, Gerasimenko TV, Ivanova TI 1992. Photosynthesis, respiration, and growth of plants in the Soviet Arctic. In: Chapin FS, Jefferies RL, Reynolds JF, Shaver GR, Svoboda J eds. *Arctic Ecosystems in a Changing Climate*. San Diego: Academic Press, 169-192.

Semikhatova OA, Ivanova TI, Kirpichnikova OV. 2007. Comparative study of dark respiration in plants inhabiting arctic (Wrangel Island) and temperate climate zones. *Russian Journal of Plant Physiology* **54**: 582-588.

Sendall KM, Reich PB. 2013. Variation in leaf and twig CO_2 flux as a function of plant size: a comparison of seedlings, saplings and trees. *Tree Physiology* 33: 713-729.

Sitch S, Huntingford C, Gedney N, Levy PE, Lomas M, Piao SL, Betts R, Ciais P, Cox P, Friedlingstein P, Jones CD, Prentice IC, Woodward FI. 2008. Evaluation of the terrestrial carbon cycle, future plant geography and climate-carbon cycle feedbacks using five Dynamic Global Vegetation Models (DGVMs). *Global Change Biology* **14**: 2015-2039.

Sitch S, Smith B, Prentice IC, Arneth A, Bondeau A, Cramer W, Kaplan JO, Levis S, Lucht W, Sykes MT, Thonicke K, Venevsky S. 2003. Evaluation of ecosystem dynamics, plant geography and terrestrial carbon cycling in the LPJ dynamic global vegetation model. *Global Change Biology* **9**: 161-185.

Slot M, Rey-Sánchez C, Gerber S, Lichstein JW, Winter K, Kitajima K. 2014a. Thermal acclimation of leaf respiration of tropical trees and lianas: response to experimental canopy warming, and consequences for tropical forest carbon balance. *Global Change Biology* **20:** 2915–2926.

Slot M, Rey-Sánchez C, Winter K, Kitajima K. 2014b. Trait-based scaling of temperature-dependent foliar respiration in a species-rich tropical forest canopy. *Functional Ecology* **28:** 1074–1086.

Slot M, Wright SJ, Kitajima K. 2013. Foliar respiration and its temperature sensitivity in trees and lianas: *in situ* measurements in the upper canopy of a tropical forest. *Tree Physiology* **33**: 505-515.

Slot M, Zaragoza-Castells J, Atkin OK. 2008. Transient shade and drought have divergent impacts on the temperature sensitivity of dark respiration in leaves of Geum urbanum. *Functional Plant Biology* **35**: 1135-1146.

Smith NG, Dukes JS. 2013. Plant respiration and photosynthesis in global-scale models: incorporating acclimation to temperature and CO_2. *Global Change Biology* **19**: 45-63.

Stocker O. 1935. Assimilation und Atmung westjavanischer Tropenbäume. *Planta* **24**: 402-445.

Swaine EK. 2007. *Ecological and evolutionary drivers of plant community assembly in a Bornean rain forest.* University of Aberdeen Aberdeen.

Takashima T, Hikosaka K, Hirose T. 2004. Photosynthesis or persistence: nitrogen allocation in leaves of evergreen and deciduous Quercus species. *Plant, Cell & Environment* **27**: 1047-1054.

Tcherkez G, Boex-Fontvieille E, Mahe A, Hodges M. 2012. Respiratory carbon fluxes in leaves. *Current Opinion in Plant Biology* **15**: 308-314.

Tcherkez G, Cornic G, Bligny R, Gout E, Ghashghaie J. 2005. *In vivo* respiratory metabolism of illuminated leaves. *Plant Physiology* **138**: 1596-1606.

Thornton PE, Lamarque JF, Rosenbloom NA, Mahowald NM. 2007. Influence of carbon-nitrogen cycle coupling on land model response to CO_2 fertilization and climate variability. *Global Biogeochemical Cycles* **21**: GB4018

Thornton PE, Law BE, Gholz HL, Clark KL, Falge E, Ellsworth DS, Goldstein AH, Monson RK, Hollinger D, Falk M, Chen J, Sparks JP. 2002. Modeling and measuring the effects of disturbance history and climate on carbon and water budgets in evergreen needleleaf forests. *Agricultural and Forest Meteorology* **113**: 185-222.

Tjoelker MG, Craine JM, Wedin D, Reich PB, Tilman D. 2005. Linking leaf and root trait syndromes among 39 grassland and savannah species. *New Phytologist* **167**: 493-508.

Tjoelker MG, Oleksyn J, Lorenc-Plucinska G, Reich PB. 2009. Acclimation of respiratory temperature responses in northern and southern populations of *Pinus banksiana*. *New Phytologist* **181**: 218-229.

Tjoelker MG, Oleksyn J, Reich PB. 1999. Acclimation of respiration to temperature and CO_2 in seedlings of boreal tree species in relation to plant size and relative growth rate. *Global Change Biology* **5**: 679-691.

Tjoelker MG, Oleksyn J, Reich PB. 2001. Modelling respiration of vegetation: evidence for a general temperature-dependent Q_{10}. *Global Change Biology* **7**: 223-230.

Tjoelker MG, Oleksyn J, Reich PB, Zytkowiak R. 2008. Coupling of respiration, nitrogen, and sugars underlies convergent temperature acclimation in *Pinus banksiana* across wide-ranging sites and populations. *Global Change Biology* **14**: 782-797.
Townsend AR, Cleveland CC, Asner GP, Bustamante MMC. 2007. Controls over foliar N : P ratios in tropical rain forests. *Ecology* **88**: 107-118.
Turnbull MH, Tissue DT, Griffin KL, Richardson SJ, Peltzer DA, Whitehead D. 2005. Respiration characteristics in temperate rainforest tree species differ along a long-term soil-development chronosequence. *Oecologia* **143**: 271-279.
UNEP. 1997. *World Atlas of Desertification*. London: United Nations Environment Programme.
Veneklaas EJ, Poot P. 2003. Seasonal patterns in water use and leaf turnover of different plant functional types in a species-rich woodland, south-western Australia. *Plant and Soil* **257**: 295-304.
Verheijen LM, Brovkin V, Aerts R, Bonisch G, Cornelissen JHC, Kattge J, Reich PB, Wright IJ, van Bodegom PM. 2013. Impacts of trait variation through observed trait-climate relationships on performance of an Earth system model: a conceptual analysis. *Biogeosciences* **10**: 5497-5515.
von Caemmerer S, Evans JR, Hudson GS, Andrews TJ. 1994. The kinetics of ribulose-1,5-bisphosphate carboxylase/oxygenase in vivo inferred from measurements of photosynthesis in leaves of transgenic tobacco. *Planta* **195**: 88-97.
Wager HG. 1941. On the respiration and carbon assimilation rates of some arctic plants as related to temperature. *New Phytologist* **40**: 1-19.
Warton DI, Duursma RA, Falster DS, Taskinen S. 2012. SMART 3-an R package for estimation and inference about allometric lines. *Methods in Ecology and Evolution* **3**: 257-259.
Warton DI, Wright IJ, Falster DS, Westoby M. 2006. Bivariate line-fitting methods for allometry. *Biological Reviews* **81**: 259-291.
Weerasinghe LK, Creek D, Crous KY, Xiang S, Liddell MJ, Turnbull MH, Atkin OK. 2014. Canopy position affects the relationships between leaf respiration and associated traits in a tropical rainforest in Far North Queensland. *Tree Physiology* **34**: 564-584.
Whitehead D, Griffin KL, Turnbull MH, Tissue DT, Engel VC, Brown KJ, Schuster WSF, Walcroft AS. 2004. Response of total night-time respiration to differences in total daily photosynthesis for leaves in a *Quercus rubra* L. canopy: implications for modelling canopy CO_2 exchange *Global Change Biology* **10**: 925-938.
Woodward FI, Lomas MR, Betts RA. 1998. Vegetation-climate feedbacks in a greenhouse world. *Philosophical Transactions of the Royal Society of London Series B-Biological Sciences* **353**: 29-38.
Wright IJ, Reich PB, Atkin OK, Lusk CH, Tjoelker MG, Westoby M. 2006. Irradiance, temperature and rainfall influence leaf dark respiration in woody plants: evidence from comparisons across 20 sites. *New Phytologist* **169**: 309-319.
Wright IJ, Reich PB, Westoby M. 2001. Strategy shifts in leaf physiology, structure and nutrient content between species of high- and low-rainfall and high- and low-nutrient habitats. *Functional Ecology* **15**: 423-434.
Wright IJ, Reich PB, Westoby M, Ackerly DD, Baruch Z, Bongers F, Cavender-Bares J, Chapin T, Cornelissen JHC, Diemer M, Flexas J, Garnier E, Groom PK, Gulias J, Hikosaka K, Lamont BB, Lee T, Lee W, Lusk C, Midgley JJ, Navas ML, Niinemets U, Oleksyn J, Osada N, Poorter H, Poot P, Prior L, Pyankov VI, Roumet C, Thomas SC, Tjoelker MG, Veneklaas EJ, Villar R. 2004. The worldwide leaf economics spectrum. *Nature* **428**: 821-827.
Wright IJ, Westoby M. 2002. Leaves at low versus high rainfall: coordination of structure, lifespan and physiology. *New Phytologist* **155**: 403-416.
Wythers KR, Reich PB, Bradford JB. 2013. Incorporating temperature-sensitive Q_{10} and foliar respiration acclimation algorithms modifies modeled ecosystem responses to global change. *Journal of Geophysical Research: Biogeosciences* **118**: 77-90.
Xiang S, Reich PB, Sun S, Atkin OK. 2013. Contrasting leaf trait scaling relationships in tropical and temperate wet forest species. *Functional Ecology* **27**: 522-534.
Zaehle S, Medlyn BE, De Kauwe MG, Walker AP, Dietze MC, Hickler T, Luo Y, Wang Y-P, El-Masri B, Thornton P, Jain A, Wang S, Warlind D, Weng E, Parton W, Iversen CM, Gallet-Budynek A, McCarthy H, Finzi A, Hanson PJ, Prentice IC, Oren R, Norby RJ. 2014. Evaluation of 11 terrestrial

carbon–nitrogen cycle models against observations from two temperate Free-Air CO_2 Enrichment studies. *New Phytologist* **202**: 803-822.

Zagdanska B. 1995. Respiratory energy demand for protein turnover and ion transport in wheat leaves upon water deficit. *Physiologia Plantarum* **95**: 428-436.

Zaragoza-Castells J, Sanchez-Gomez D, Hartley IP, Matesanz S, Valladares F, Lloyd J, Atkin OK. 2008. Climate-dependent variations in leaf respiration in a dry-land, low productivity Mediterranean forest: the importance of acclimation in both high-light and shaded habitats. *Functional Ecology* **22**: 172-184.

Zomer RJ, Trabucco A, Bossio DA, Verchot LV. 2008. Climate change mitigation: A spatial analysis of global land suitability for clean development mechanism afforestation and reforestation. *Agriculture, Ecosystems & Environment* **126**: 67-80.

Zotz G, Winter K 1996. Diel patterns of CO_2 exchange in rainforest canopy plants. In: Mulkey SS, Chazdon RL, Smith AP eds. *Tropical forest plant ecophysiology* New York: Chapman & Hall, 89-113.

Zuur AF, Ieno EN, Walker N, Saveliev AA, Smith GM. 2009. *Mixed effects models and extensions in ecology with R*. New York: Springer Science+Business Media

Supporting Information

Additional supporting information may be found in the online version of this article.

Methods S1: Sampling methods and measurements protocols for previously unpublished data.

Methods S2: Details on methodology used to temperature normalize respiration rates

Table S1. Details on unpublished databases used in global data base of R_{dark}.

Table S2. Details on published databases used in global data base of R_{dark}.

Table S3. Standardized Major Axis regression slopes for relationships in Figs 5 & 6.

Table S4. Comparison of mixed-effects models with area-based R_{dark}^{25}as the response variable

Table S5. Comparison of mixed-effects models using different plant functional types (PFT) classifications, with R_{dark}^{25} as the response variable.

Figure S1. Comparison of R_{dark}^{25}, calculated assuming either a fixed Q_{10} or a T-dependent Q_{10}

Figure S2. Relationships between leaf structural/chemical composition traits and TWQ

Figure S3. R_{dark}-aridity index relationships, excluding data from a high-rainfall site in NZ

Figure S4. R_{dark}-MMT relationships for those sites were the month of measurement was known

Figure S5. Testing key assumptions for mixed effects models –heterogeneity and normality.

Figure S6. Model validation graphs for the area-based mixed effects model

Figure S7. Standardised residuals against fitted values for variables not used in mixed model

Figure S8. Dotchart of the area-based mixed model's random intercepts by Family

Figure S9. Dotchart of the area-based mixed model's random intercepts by site

Table 1. Sample sites and climate conditions at which leaf dark respiration (R_{dark}) was measured.

Country/Region	Biomes	Altitude (m asl)	MAT (°C)	TWQ (°C)	MAP (mm)	PWQ (mm)	AI	No. species	PFTs present (*JULES*)
USA-AK	Tu	720	-11.3	8.2	225	113	0.61	37	BIT, C3H, S
Russia-Siberia	BF	217	-10.8	15.4	254	122	0.46	3	BIT, NIT
USA-CO	Tu	3,360	-2.6	7.5	811	203	1.20	10	BIT, C3H, NIT, S
USA-MN	BF, TeDF, TeG	365	4.4	18.4	735	303	0.87	53	BIT, C3H, C4H, NIT, S
USA-IA	TeDF	385	7.1	20.2	865	315	0.83	11	BIT, NIT
USA-WI	TeDF, TeG	293	7.7	20.6	880	315	0.93	15	BIT, C3H, NIT
USA-MI	TeDF	200	8.6	19.9	944	268	0.98	1	NIT
Germany	TeDF	60	9.1	17.2	704	190	0.92	9	BIT, NIT
USA-NY	TeDF	225	9.4	20.8	1,173	308	1.20	3	BIT
USA-PA	TeDF	355	9.5	19.9	915	262	0.91	3	BIT
Spain	TeW	1,017	10.7	19.2	487	99	0.48	1	BIT
Australia-TAS	TeRF	144	11.0	14.7	1,325	211	1.58	14	BIT, S
Chile	TeRF	434	11.1	15.4	1,467	103	1.40	18	BIT, NIT
USA-TN	TeDF	775	11.2	20.1	1,554	389	1.34	13	BIT, C3H, NIT, S
New Zealand	TeRF	202	11.3	15.9	4,014	1,011	4.50	16	BIT, NIT, S
USA-NC	TeDF	850	11.4	20.0	1,852	444	1.52	15	BIT, NIT
USA-NM	Sa	1,620	12.5	22.2	275	127	0.19	9	BIT, NIT, S
Australia-ACT	TeW	572	13.0	20.7	722	271	0.58	6	BIT, NIT, S
Japan	TeDF	20	14.9	23.7	1,619	433	1.92	4	BIT
Sth Africa	TeW	600	16.6	21.0	754	67	0.57	5	BIT, S
Peru-Andes	TrRF_up	2,380	16.7	17.7	1,297	373	0.79	82	BIT, C3H
Australia-SA	TeW	35	17.3	23.6	255	52	0.17	10	BIT, C3H, S
Australia-NSW	TeW	140	17.3	23.2	820	215	0.29	70	BIT, C3H, C4H, NIT, S
USA-SC	TeDF	3	17.7	25.8	1,339	469	1.02	10	BIT, C3H, NIT, S
Australia-WA	TeW	204	18.7	24.5	463	47	0.32	55	BIT, C3H, S
Australia-FNQ	TrRF_lw	513	22.4	25.1	1,990	934	1.35	45	BIT, S
Cameroon	TrRF_lw	550	24.0	24.8	1,729	417	1.13	6	BIT, C3H
Venezuela	TrRF_lw	492	24.4	24.7	3,092	693	1.61	10	BIT, S
Bolivia	TrRF_lw	400	25.3	27.0	1,020	436	0.57	50	BIT
Suriname	TrRF_lw	215	25.4	26.3	2,224	165	1.37	25	BIT, C3H, C4H, S
Peru-Amazon	TrRF_lw	164	25.4	26.2	2,567	828	1.50	214	BIT, S
Bangladesh	TrRF_lw	21	25.5	28.5	1,970	736	1.34	1	BIT
Costa Rica	TrRF_lw	135	25.7	26.7	4,141	747	2.64	2	BIT, S
French Guiana	TrRF_lw	21	25.8	26.2	2,824	222	1.88	70	BIT
Malaysia-Borneo	TrRF_lw	20	26.7	27.1	2,471	501	1.64	29	BIT, S
Brazil-Amazon	TrRF_lw	115	27.0	27.6	2,232	401	1.39	9	BIT
Panama	TrRF_lw	98	27.0	27.7	1,822	300	1.19	18	BIT
Niger	Sa	280	28.2	31.4	618	55	0.30	3	BIT, S

Sites shown in order from increasing mean annual temperature (MAT). Where multiple sites were found within a region, values represent the mean values of all sites, weighted for the number of species at each site (see Tables S1 and S2 in Supporting Information for further details). Data on climate are from the *WorldClim* data base (Hijmans *et al.*, 2005). Number of species measured at each site are shown, as are the number of observational rows of data contained in the *GlobResp* database. For the latter, an observational row represents individual measurements for all unpublished data (See Table S1 in Supporting Information), while for published data (SI Table S2) observational rows in many cases represent mean values of species:site combinations. *JULES* (Clark *et al.*, 2011) plant functional types (PFTs) at each site shown, according to: BIT, broad-leaved tree; C3H, C_3 metabolism herb/grass; C4H, C_4 metabolism herb/grass; NIT, needle-leaved tree; S, shrub. Biome classes: BF, boreal forests; TeDF, temperate deciduous forest; TeG, temperate grassland; TeRF, temperate rainforest; TeW, temperate woodland; TrRF_lw, lowland tropical rainforest (<1500 asl); TrRF_up, upland tropical rainforest (>1500 asl); Tu, tundra. Abbreviations: mean temperature of the warmest quarter (i.e. warmest 3-month period per year; TWQ), mean annual precipitation (MAP), mean precipitation of the warmest quarter (PWQ), aridity index (AI) calculated as the ratio of MAP to mean annual potential evapotranspiration (UNEP, 1997; Zomer *et al.*, 2008). Australia-ACT, Australian Capital Territory; Australia-FNQ, Far North Queensland; Australia-NSW, New South Wales; Australia-TAS, Tasmania; Australia-WA, Western Australia; USA-AK, Alaska; USA-CO, Colorado; USA-MN, Minnesota; USA-IA, Iowa; USA-WI, Wisconsin; USA-MI, Michigan; USA-PA, Pennsylvania; USA-NY, New York; USA-NC, North Carolina; USA-TN, Tennessee; USA-NM, New Mexico; USA-SC, South Carolina.

Table 2. Details of plant functional types (PFTs) contained in *GlobResp* database.

ESM framework	Plant functional types (PFTs)	No. sites	Min. latitude	Max. latitude	No. species
JULES	BlT	94	-43.42	68.63	642
	C3H	14	-34.04	68.63	75
	C4H	3	-33.84	45.41	8
	NlT	20	-43.31	62.25	24
	S	32	-43.42	68.63	124
LPJ	BorDcBl	10	40.05	68.63	18
	BorDcNl	3	33.33	62.25	2
	BorEvNl	6	40.05	62.25	10
	TmpDcBl	25	-43.41	50.60	46
	TmpEvBl	33	-43.42	68.63	193
	TmpEvNl	13	-43.31	50.60	18
	TmpH	12	-34.04	68.63	79
	TrpDcBl	20	-15.78	13.20	50
	TrpEvBl	39	-17.68	24.20	468
	TrpH	3	-13.11	3.38	4

PFTs for two Earth System Model frameworks are shown: *JULES* (Clark *et al.*, 2011) and *LPJ* (Sitch *et al.*, 2003). For each PFT, the number of field sites and species are shown, as is the maximum absolute latitude and longitude of the PFT distribution. For *JULES*, the following PFTs are shown: BlT, broad-leaved tree; C3H, C_3 metabolism herb/grass; C4H, C_4 metabolism herb/grass; NlT, needle-leaved tree; S, shrub. For *LPJ*, the following PFTs are shown: BorDcBl, boreal deciduous broad-leaved tree/shrub; BorDcNl, boreal deciduous needle-leaved tree/shrub; BorEvNl, boreal evergreen needle-leaved tree/shrub; TmpDcBl, temperate deciduous broad-leaved tree/shrub; TmpEvBl, temperate evergreen broad-leaved tree/shrub; TmpEvNl, temperate evergreen needle-leaved tree/shrub; TmpH, temperate herb/grass; TrpDcBl, tropical deciduous broad-leaved tree/shrub; TrpEvBl, tropical evergreen broad-leaved tree/shrub; TrpH, tropical herb/grass. Note: in some cases, individual species occurred at multiple sites in multiple biomes. Finally, an overwhelming majority of the shrubs (S) were evergreen (123 species:site combinations) compared to deciduous shrubs (11 species:site combinations)

Table 3. Correlations between log_{10} transformed leaf respiration (R_{dark}) and location/climate (see Figure 4).

Response variable		Latitude							TWQ, both hemispheres							Aridity index, both hemispheres						
	Hemisphere	*df*	*p* value	r^2	Intercept	Slope	CI slope, lower	CI slope, higher	*df*	*p* value	r^2	Intercept	Slope	CI slope, lower	CI slope, higher	*df*	*p* value	r^2	Intercept	Slope	CI slope, lower	CI slope, higher
$logR_{dark,a}^{25}$	Nth	404	< 0.0001	0.189	-0.130	0.005	0.004	0.006	1,104	< 0.0001	0.139	0.467	-0.019	-0.022	-0.016	1,069	<0.0001	0.038	0.119	-0.069	-0.090	-0.048
	Sth	698	< 0.0001	0.071	-0.063	0.005	0.004	0.007														
$logR_{dark,a}^{TWQ}$	Nth	404	< 0.0001	0.039	-0.028	-0.002	-0.003	-0.001	1,104	< 0.0001	0.066	-0.329	0.013	0.010	0.015	1,069	<0.0001	0.016	0.011	-0.043	-0.063	-0.023
	Sth	698	0.740	0.000	N/A	N/A	N/A	N/A														
$logR_{dark,m}^{25}$	Nth	421	< 0.0001	0.148	0.908	0.006	0.004	0.007	1,111	< 0.0001	0.074	1.342	-0.015	-0.019	-0.012	1,076	<0.0001	0.019	1.065	-0.054	-0.077	-0.031
	Sth	688	0.824	0.000	N/A	N/A	N/A	N/A														
$LogR_{dark,m}^{TWQ}$	Nth	421	0.006	0.018	1.008	-0.002	-0.003	-0.001	1,111	< 0.0001	0.083	0.546	0.016	0.013	0.019	1,076	0.031	0.004	0.950	-0.026	-0.049	-0.002
	Sth	688	< 0.0001	0.061	0.991	-0.005	-0.007	-0.004														

For each correlation between the *y*-axis leaf trait and *x*-axis location/climate parameter, the number of degrees of freedom (df), probability value (*p-value*) and coefficient of determination (r^2) and 95% confidence intervals (CI) are shown. Traits shown are: $R_{dark,a}^{25}$ and $R_{dark,a}^{TWQ}$, predicted area-based leaf R_{dark} rates (μmol CO_2 m^{-2} s^{-1}) at 25°C and TWQ (mean daily temperature of the warmest quarter), respectively; leaf $R_{dark,m}^{25}$ and $R_{dark,m}^{TWQ}$, predicted mass-based R_{dark} rates (nmol CO_2 g^{-1} s^{-1}) at 25°C and TWQ, respectively. TWQ at each site were obtained using site information and the *WorldClim* data base (Hijmans *et al.*, 2005). Aridity index calculated as the ratio of mean annual precipitation (MAP) to mean annual potential evapotranspiration (PET) (UNEP, 1997; Zomer *et al.*, 2008). Abbreviations: N/A, not applicable.

Table 4. Regression equations expressing area- and mass-based leaf dark respiration at 25°C (R_{dark}^{25}) as function of other leaf traits and site climate.

Dependent variable	Input: independent variables *(Backwards-Stepwise Regression)*	Output: selected equations *(Multiple Linear Regression)*	*Multiple linear regression parameters*							
			n	r^2	*PRESS* statistic	Standardized partial regression coefficients				
						β_1	β_2	β_3	β_4	β_5
Area-based $log_{10}\ R_{dark,a}^{25}$	*Leaf traits* (all log_{10}): $[N]_a$, M_a	$\log_{10}R_{dark,a}^{25} = -0.469 + (0.329*\log_{10}N_a) + (0.204*\log_{10}M_a)$	1038	0.168	57.71	0.270 ($\log_{10}N_a$)	0.186 ($\log_{10}M_a$)			
	Leaf traits (all log_{10}): $[N]_a$, $[P]_a$, M_a	$\log_{10}R_{dark,a}^{25} = 0.076 + (0.304*\log_{10}P_a) + (0.140*\log_{10}M_a)$	730	0.156	40.95	0.338 ($\log_{10}P_a$)	0.112 ($\log_{10}M_a$)			
	Leaf traits (all log_{10}): $[N]_a$, $[P]_a$, M_a, $V_{cmax,a}^{25}$	$\log_{10}R_{dark,a}^{25} = -0.241 + (0.235*\log_{10}P_a) + (0.050*\log_{10}M_a) (0.290*\log_{10}V_{cmax,a}^{25})$	703	0.221	34.79	0.269 ($\log_{10}P_a$)	0.041 ($\log_{10}M_a$)	0.285 ($\log_{10}V_{cmax}$)		
	Climate parameters: TWQ, PWQ, AI	$\log_{10}R_{dark,a}^{25} = 0.451 - (0.0153*TWQ) - (0.00016*PWQ)$	1114	0.171	61.86	-0.297 (TWQ)	-0.196 (PWQ)			
	Leaf traits (all log_{10}) *and climate parameters*: $[N]_a$, $[P]_a$, M_a, $V_{cmax,a}^{25}$, TWQ, PWQ	$\log_{10}R_{dark,a}^{25} = -0.563 + (0.292*\log_{10}M_a) + (0.119*\log_{10}P_a) + (0.221*V_{cmax,a}^{25}) - (0.0147*TWQ) - (0.00012*PWQ)$	703	0.353	29.06	0.238 ($\log_{10}M_a$)	0.136 ($\log_{10}P_a$)	0.243 ($\log_{10}V_{cmax}$)	-0.304 (TWQ)	-0.165 (PWQ)
Mass-based $log_{10}\ R_{dark,m}^{25}$	*Leaf traits* (all log_{10}): $[N]_m$, SLA	$\log_{10}R_{dark,m}^{25} = 0.0932 + (0.475*\log_{10}SLA) + (0.364*\log_{10}N_m)$	1037	0.314	57.78	0.392 ($\log_{10}SLA$)	0.244 ($\log_{10}N_m$)			
	Leaf traits (all log_{10}): $[N]_m$, $[P]_m$, SLA	$\log_{10}R_{dark,m}^{25} = 0.495 + (0.556*\log_{10}SLA) + (0.333*\log_{10}P_m)$	730	0.336	40.68	0.396 ($\log_{10}SLA$)	0.315 ($\log_{10}P_m$)			
	Leaf traits (all log_{10}): $[N]_m$, $[P]_m$, SLA, $V_{cmax,m}^{25}$	$\log_{10}R_{dark,m}^{25} = -0.061 + (0.432*\log_{10}SLA) + (0.264*\log_{10}P_m) + (0.274*\log_{10}V_{cmax,m}^{25})$	703	0.407	34.80	0.307 ($\log_{10}SLA$)	0.252 ($\log_{10}P_m$)	0.263 ($\log_{10}V_{cmax}$)		
	Climate parameters: TWQ, PWQ, AI	$\log_{10}R_{dark,m}^{25} = 1.353 - (0.0157*TWQ) - (0.000018*AI)$	1121	0.087	83.22	-0.276 (TWQ)	0.112 (AI)			
	Leaf traits (all log_{10}) *and climate parameters*: $[N]_m$, $[P]_m$, SLA, $V_{cmax,m}^{25}$, TWQ, AI	$\log_{10}R_{dark,m}^{25} = 0.249 + (0.526*\log_{10}SLA) + (0.0705*\log_{10}P_m) + (0.281*\log_{10}V_{cmax,m}^{25}) - (0.0184*TWQ) - (0.000015*AI)$	703	0.497	29.72	0.374 ($\log_{10}SLA$)	0.067 ($\log_{10}P_m$)	0.270 ($\log_{10}V_{cmax}$)	-0.333 (TWQ)	0.111 (AI)

All leaf trait data were log_{10} transformed. To select the best fitting equation from a group of input independent variables (e.g. leaf trait, climate or the combination of trait plus climate), data were explored using *Backwards-Stepwise Regression* – this revealed that chosen parameters exhibited *variance inflation factors* (VIF) less than 2.0 (i.e. minimal multi-collinearity); it also identified best-fit parameters (using *F*-to-remove criterion). Thereafter, multiple regression analyses were conducted to estimate predictive equations for the chosen variables. All selected variables were significant ($P<0.001$). The *PRESS* statistic (predicted residual error sum of squares) provides a measure of how well each regression model predicts the observations, with smaller *PRESS* indicating better predictive capability. Relative contributions of leaf trait and climate variables to each regression can be gauged from their standardized partial regression coefficients (β_1-β_5, depending on model equation). Abbreviations: M_a, leaf mass per unit leaf area (g m^{-2}); SLA, leaf area per unit leaf mass (m^2 kg^{-1}); $[N]_a$ and $[N]_m$, area- (g m^{-2}) and mass-based (mg g^{-1}) leaf nitrogen concentration, respectively; $[P]_a$ and $[P]_m$, area- (g m^{-2}) and mass-based (mg g^{-1}) leaf phosphorus concentration, respectively; $V_{cmax,a}^{25}$ (μmol CO_2 m^{-2} s^{-1}) and $V_{cmax,m}^{25}$ (nmol CO_2 g^{-1} s^{-1}), predicted area- and mass-based capacity for CO_2 fixation by Rubisco at 25°C, respectively; $R_{dark,a}^{25}$ (μmol CO_2 m^{-2} s^{-1}) and $R_{dark,m}^{25}$ (nmol CO_2 g^{-1} s^{-1}), predicted area- and mass-based leaf R_{dark} rates at 25°C, respectively; mean temperature of the warmest quarter (i.e. warmest 3-month period per year; TWQ, °C), mean annual precipitation (MAP, mm yr^{-1}), mean precipitation of the warmest quarter (PWQ), aridity index (AI) calculated as the ratio of MAP to mean annual potential evapotranspiration (UNEP, 1997; Zomer *et al.*, 2008). TWQ at each site were obtained using site information and the *WorldClim* data base (Hijmans *et al.*, 2005).

Table 5. Two linear mixed-effects models ('best' predictive model and a 'null', PFT only model), with (a) area-based (μmol CO_2 m^{-2} s^{-1}) and (b) mass-based (nmol CO_2 g^{-1} s^{-1}) leaf respiration at 25°C ($R_{dark,a}^{25}$ and $R_{dark,m}^{25}$, respectively) as the response variables, each showing fixed and random effects. See Table 6 for PFT-specific equations are shown that can be used to predict variability in $R_{dark,a}^{25}$ and $R_{dark,m}^{25}$ based on 'best' models.

(a) Area-based model

Fixed effects

	'Best' predictive model (PFTs, leaf traits and climate)			'Null' model (PFT only)		
Source	Value	s.e.	*t*-value	Value	s.e.	t-value
PFT-BlT	1.2636	0.033	38.551	1.3805	0.046	29.750
PFT-C3H	0.4708	0.141	3.348	0.5099	0.160	3.185
PFT-NlT	-0.3595	0.150	-2.392	-0.0558	0.179	-0.311
PFT-S	0.3290	0.064	5.163	0.3460	0.071	4.867
$[N]_a$	0.0728	0.018	4.124			
$[P]_a$	0.0015	0.000	7.389			
$V_{cmax,a}^{25}$	0.0095	0.001	15.241			
TWQ	-0.0358	0.006	-5.658			
Interaction: C3H x $[N]_a$	0.3394	0.069	4.892			
Interaction: NlT x $[N]_a$	0.0762	0.146	0.523			
Interaction: S x $[N]_a$	0.0687	0.053	1.295			

Random effects

	'Best' predictive model (PFTs, leaf traits and climate)			'Null' model	
Source	# levels $group^{-1}$	Residual variance	% of total	Residual variance	% of total
Intercept variance: species	531	0.009	7.1%	0.023	11.5%
Intercept variance: families	100	0.002	1.4%	0.004	2.1%
Intercept variance: sites	49	0.031	23.4%	0.073	36.2%
Residual error		0.091	68.2%	0.102	50.2%
Total		0.133	100.0%	0.202	100.0%

(b) Mass-based model

Fixed effects

	'Best' predictive model (PFTs, leaf traits and climate)			'Null' model (PFT only)		
Source	Value	s.e.	*t*-value	Value	s.e.	t-value
PFT-BlT	8.5341	2.091	4.081	10.8938	1.243	8.764
PFT-C3H	-5.6273	6.832	-0.824	10.0926	3.569	2.828
PFT-NlT	6.8086	16.683	0.408	-2.2741	3.553	-0.640
PFT-S	-2.9249	2.564	-1.141	1.8429	1.492	1.235
$[N]_m$	-0.1306	0.085	-1.531			
$[P]_m$	-0.5670	1.491	-0.380			
M_a	-0.0137	0.004	-3.040			
$V_{cmax,m}^{25}$	0.0111	0.002	6.459			
Interaction: C3H x $[N]_m$	0.7252	0.295	2.459			
Interaction: NlT x $[N]_m$	-0.7283	1.796	-0.405			
Interaction: S x $[N]_m$	0.1605	0.146	1.102			
Interaction: C3H x $[P]_m$	-4.2308	2.659	-1.591			
Interaction: NlT x $[P]_m$	0.4131	1.694	0.244			
Interaction: S x $[P]_m$	2.3333	1.790	1.303			
Interaction: $[N]_m$ x $[P]_m$	0.1876	0.062	3.026			

Random effects

	'Best' predictive model (PFTs, leaf traits and climate)			'Null' model	
Source	# levels $group^{-1}$	Residual variance	% of total	Residual variance	% of total
Intercept variance: families	100	0.373	0.7%	7.950	9.2%
Intercept variance: sites	49	37.745	73.2%	55.290	64.2%
Residual error		13.476	26.1%	22.850	26.5%
Total		51.594	100.0%	86.090	100.0%

For the 'best' models, parameter values, s.e. and t-values given for the continuous explanatory variables; explanatory variables (all un-transformed and centred on their means) are: (1) plant functional types (PFT), according to *JULES* (Clark *et al.*, 2011): BlT (broad-leaved tree), C3H (C_3 metabolism herbs/grasses), NlT (needle-leaved trees), and S (shrubs); (2) leaf nitrogen ([N]) and phosphorus ([P]) concentrations (g m^{-2} for area-based values and mg g^{-1} for mass based values), M_a (g m^{-2}) and Rubisco CO_2 fixation capacity at 25°C (V_{cmax}^{25}; μmol CO_2 m^{-2} s^{-1} and nmol CO_2 g^{-1} s^{-1} for area and mass-based values, respectively); and mean temperature of the warmest quarter (TWQ, °C) (Hijmans *et al.*, 2005). Figure S5 (Supp. Info.) assess heterogeneity and normality assumptions of the 'best' models, while Figure S6 shows model validation graphs for the area-based model fixed component explanatory variables; similarly, Fig. S7 shows details for variables omitted from the fixed components in the area-based model (M_a, AI and PWQ). The PFT-BlT values (first row) are based on the assumption that other variables were at their global mean values. The random effects tables, the intercept was allowed to vary among species, families and sites; residual errors shown are within species, families and sites. See Figure 7 for scatter plots of

modelled vs actual values of the 'best' models, both with and without inclusion of random effects. See also Table S4 (Supporting Information) for area-based model outputs for scenarios where different combinations of fixed effect parameters were included.

Table 6. PFT-specific equations (formulated from the 'best' mixed-effects models shown in Table 5) that can be used to predict variability in (a) area-based (μmol CO_2 m^{-2} s^{-1}) and (b) mass-based (nmol CO_2 g^{-1} s^{-1}) leaf respiration at 25°C ($R_{dark,a}^{25}$ and $R_{dark,m}^{25}$, respectively).

(a) PFT-specific equations to predict variability in $R_{dark,a}^{25}$ ('best' model)	(b) PFT-specific equations to predict variability in $R_{dark,m}^{25}$ ('best' model)
BlT: $R_{dark,a}^{25} = 1.2636 + (0.0728*[N]_a) + (0.015*[P]_a) + (0.0095*V_{cmax,a}^{25}) - (0.0358*TWQ)$	BlT: $R_{dark,m}^{25} = 8.5341-(0.1306*[N]_m)-(0.5670*[P]_m)-(0.0137*M_a) + (0.0111*V_{cmax,m}^{25}) + (0.1876*([N]_m x [P]_m)$
C3H: $R_{dark,a}^{25} = 1.7344+ (0.4122*[N]_a) + (0.015*[P]_a) + (0.0095*V_{cmax,a}^{25}) - (0.0358*TWQ)$	C3H: $R_{dark,m}^{25} = 2.9068+(0.5946*[N]_m)-(4.7978*[P]_m)-(0.0137*M_a)+(0.0111*V_{cmax,m}^{25})+(0.1876*([N]_m x [P]_m)$
NlT: $R_{dark,a}^{25} = 0.9041+ (0.1489*[N]_a) + (0.015*[P]_a) + (0.0095*V_{cmax,a}^{25}) - (0.0358*TWQ)$	NlT: $R_{dark,m}^{25} = 15.3427-(0.8589*[N]_m)-(0.1539*[P]_m)-(0.0137*M_a)+(0.0111*V_{cmax,m}^{25})+(0.1876*([N]_m x [P]_m)$
S: $R_{dark,a}^{25} = 1.5926+ (0.1415*[N]_a) + (0.015*[P]_a) + (0.0095*V_{cmax,a}^{25}) - (0.0358*TWQ)$	S: $R_{dark,m}^{25} = 5.6092+(0.0299*[N]_m)+(1.7663*[P]_m)-(0.0137*M_a)+(0.0111*V_{cmax,m}^{25})+(0.1876*([N]_m x [P]_m)$

Explanatory variables are: (1) plant functional types (PFT), according to *JULES* (Clark *et al.*, 2011): BlT (broad-leaved tree), C3H (C_3 metabolism herbs/grasses), NlT (needle-leaved trees), and S (shrubs); (2) leaf nitrogen ([N]) and phosphorus ([P]) concentrations (g m^{-2} for area-based values and mg g^{-1} for mass based values), and Rubisco CO_2 fixation capacity at 25°C (V_{cmax}^{25}; μmol CO_2 m^{-2} s^{-1} and nmol CO_2 g^{-1} s^{-1} for area and mass-based values, respectively); and mean temperature of the warmest quarter (TWQ, °C) (Hijmans *et al.*, 2005). Note – equations refer to un-transformed values of each response and explanatory variable**.** See also Table S4 (Supporting Information) for area-based model equations for scenarios where different combinations of fixed effect parameters were included.

Figure legends

Figure 1. Location (a) and climate envelope (b) of the sites at which leaf dark respiration (R_{dark}) and associated traits were measured. (a) shows silite locations on a global map showing spatial variability in mean annual temperatures (MAT); (b) shows plot of mean annual precipitation (MAP) vs MAT for each site (shown in biome classes). See Table 1 for summary of site information, and Table S1 and S2 (Supporting Information) for details on the latitude, longitude, altitude (height above sea level), MAT, mean temperature of the warmest quarter (i.e. warmest 3-month period per year; TWQ), MAP, mean precipitation of the warmest quarter (PWQ) and aridity index (AI, ratio of MAP to mean annual potential evapotranspiration). In (b), biomes categorization of each site is shown. Biome abbreviations: Tu, tundra; BF, boreal forest; TeDF, temperate deciduous forest; TeRF, temperate rainforest; TeW, temperate woodland; Sa, savana; TrRF_up, upland tropical rainforest (>1500 m asl); TrRF_low, lowland tropical rainforest (<1500 m asl). In (b), note the unusually high MAP at the Frans Josef TeRF site on the Sth Island of New Zealand.

Figure 2. Box plots showing modulation of leaf structural and chemical traits by *JULES* (Clark *et al.*, 2011) plant functional type (PFT) classifications. Traits shown are: (a) M_a, leaf mass per unit leaf area; (b) $[N]_a$, area-based leaf nitrogen concentration; and (c) $[P]_a$, area-based leaf phosphorous concentration. Data shown are for individual row observations contained in the *GlobResp* database (to give an indication of underlying data distribution). The central box in each box plot shows the interquartile range; the median is shown as the bold line within each box; whiskers extend 1.5 times the interquartile range or to the most extreme value, whichever is the smaller; any points outside these values are shown as individual points. Data for the following *JULES* (Clark *et al.*, 2011) plant functional type (PFT) classifications: BlT, broad-leaved tree; C3H, C_3 metabolism herb/grass; C4H, C_4 metabolism herb/grass; NlT, needle-leaved tree; S, shrub

Figure 3. Box plots showing modulation of carboxylation capacity of Rubisco (V_{cmax}) and leaf respiration (R_{dark}) in darkness by *JULES* (Clark *et al.*, 2011) plant functional type (PFT) classifications. Data shown are for individual row observations contained in the *GlobResp* database (to give an indication of underlying data distribution). Rates at 25ºC are shown. Traits shown are: (a) $V_{cmax,a}^{25}$ and (c) $V_{cmax,m}^{25}$: area- and mass-based carboxylation rates, respectively; (b) $R_{dark,a}^{25}$ and (d) $R_{dark,m}^{25}$: area- and mass-based respiration rates, respectively. Values of V_{cmax} at 25ºC were calculated according to Farquhar *et al*. (1980) assuming an activation energy (E_a) of 64.8 kJ mol^{-1}. Values of R_{dark} at 25ºC were calculated assuming a T-dependent Q_{10} (Tjoelker *et al.*, 2001) and equation 7 described in Atkin et al. (2005). The central box in each box plot shows the interquartile range; the median is shown as the bold line within each box; whiskers extend 1.5 times the interquartile range or to the most extreme value, whichever is the smaller; any points outside these values are shown as individual points. Data for the following *JULES* (Clark *et al.*, 2011) plant functional type (PFT) classifications: BlT, broad-leaved tree; C3H, C_3 metabolism herb/grass; NlT, needle-leaved tree; S, shrub. Data not shown for C_4 metabolism herbs/grasses, due to limited data availalbility.

Figure 4. Relationships between leaf R_{dark} (log_{10} scale) and location (absolute latitude) or climate [mean daily temperature of the warmest quarter (TWQ) & aridity index (AI)]. Traits shown are: $R_{dark,a}^{25}$, (a, b and c) and $R_{dark,a}^{TWQ}$ (d, e and f), predicted area-based R_{dark} rates at 25ºC and TWQ, respectively; $R_{dark,m}^{25}$ (g, h and i) and $R_{dark,m}^{TWQ}$ (j, k and l), predicted mass-based R_{dark} rates at 25ºC and TWQ, respectively. Values shown are averages for unique site:species combinations for rates at 25ºC and TWQ, calculated assuming a temperature-dependent Q_{10} (Tjoelker *et al.*, 2001) and equation 7 described in Atkin et al. (2005). Values at the TWQ of each replicate were calculated using climate/location data from the *WorldClim* data base (Hijmans *et al.*, 2005). Aridity index calculated as the ratio of mean annual precipitation (MAP) to mean annual potential evapotranspiration (PET) (UNEP, 1997). In plots against latitude, northern and southern latitudes shown as blue and red symbols, respectively. Solid lines in each plot show regression lines where the relationships were significant; dashed lines show the prediction intervals (two-times the standard deviation) around the predicted relationship. See Table 3 for correlations between log_{10} transformed R_{dark} and location/climate. Note: see Figure S3 (Supporting Information) for relationships beween R_{dark} and AI, excluding data from the exceptionally high rainfall sites at Frans Josef on the Sth Island of New Zealand.

Figure 5. Patterning of area- and mass-based R_{dark}^{25} – V_{cmax}^{25} relationships by *JULES* PFTs (a and d); TWQ categories (5ºC intervals) – all data (b and e); and TWQ categories (5ºC intervals) – broad-leaved trees only (c and f). All values shown on a log_{10} scale. Values shown are averages for unique site:species combinations. Upper panels (a, b and c) show area-based values, while lower panels (d, e and f) show mass-based values. *JULES* PFTs: BlT, broad-leaved tree; C3H, C_3 metabolism herb/grass; NlT, needle-leaved tree; S, shrub. TWQ classes: 1st <10ºC; 2nd 10-15ºC; 3rd 15-20ºC; 4th 20-25ºC; 5th >25ºC. Values of R_{dark} at 25ºC were calculated assuming a *T*-dependent Q_{10} (Tjoelker *et al.*, 2001) and equation 7 described in Atkin *et al*. (2005). Values V_{cmax} at 25ºC were calculated according to Farquhar *et al*. (1980) assuming an activation energy (E_a) of 64.8 kJ mol^{-1}. See Table S3 for SMA regression outputs.

Figure 6. Patterning of area- and mass-based R_{dark}^{25} – N relationships by *JULES* PFTs (a and d); TWQ categories (5ºC intervals) – all data (b and e); and TWQ categories (5ºC intervals) – broad-leaved trees only (c and f). Values shown are averages for unique site:species combinations. All values shown on a log_{10} scale. *JULES* PFTs: BlT, broad-leaved tree; C3H, C_3 metabolism herb/grass; NlT, needle-leaved tree; S, shrub. TWQ classes: 1st <10ºC; 2nd 10-15ºC; 3rd 15-20ºC; 4th 20-25ºC; 5th >25ºC. Values of R_{dark} at 25ºC were calculated assuming a *T*-dependent Q_{10} (Tjoelker *et al.*, 2001) and equation 7 described in Atkin et al. (2005). See Table S3 for SMA regression outputs.

Figure 7. Scatterplots for (a) area-based, and (b) mass-based linear mixed-effects model's goodness of fits, including fixed and random terms. Observed values of leaf respiration at 25ºC (R_{dark}^{25}) are plotted against model predictions (using the 'best' predictive models detailed in Table 5). For the area-based model (a), the fixed component explanatory variables were: (1) plant functional types (PFT), according to *JULES* (Clark *et al.*, 2011); (2) area-based leaf nitrogen ($[N]_a$) and phosphorus ($[P]_a$) concentrations, and Rubisco CO_2 fixation capacity at 25ºC ($V_{cmax,a}^{25}$); and mean temperature of the warmest quarter (TWQ) (Hijmans *et al.*, 2005). For the mass-based model (b), the fixed component explanatory variables were: (1) plant functional types (PFT); (2) mass-based leaf nitrogen ($[N]_m$) and phosphorus ($[P]_m$) concentrations, Rubisco CO_2 fixation capacity at 25ºC ($V_{cmax,m}^{25}$), and leaf mass per unit leaf area (M_a).

Figure 1. Location (a) and climate envelope (b) of the sites at which leaf dark respiration (R_{dark}) and associated traits were measured. (a) shows site locations on a global map showing spatial variability in mean annual temperatures (MAT); (b) shows plot of mean annual precipitation (MAP) vs MAT for each site (shown in biome classes). See Table 1 for summary of site information, and Table S1 and S2 (Supporting Information) for details on the latitude, longitude, altitude (height above sea level), MAT, mean temperature of the warmest quarter (i.e. warmest 3-month period per year; TWQ), MAP, mean precipitation of the warmest quarter (PWQ) and aridity index (AI, ratio of MAP to mean annual potential evapotranspiration). In (b), biomes categorization of each site is shown. Biome abbreviations: Tu, tundra; BF, boreal forest; TeDF, temperate deciduous forest; TeRF, temperate rainforest; TeW, temperate woodland; Sa, savana; TrRF_up, upland tropical rainforest (>1500 m asl); TrRF_low, lowland tropical rainforest (<1500 m asl). In (b), note the unusually high MAP at the Frans Josef TeRF site on the Sth Island of New Zealand.

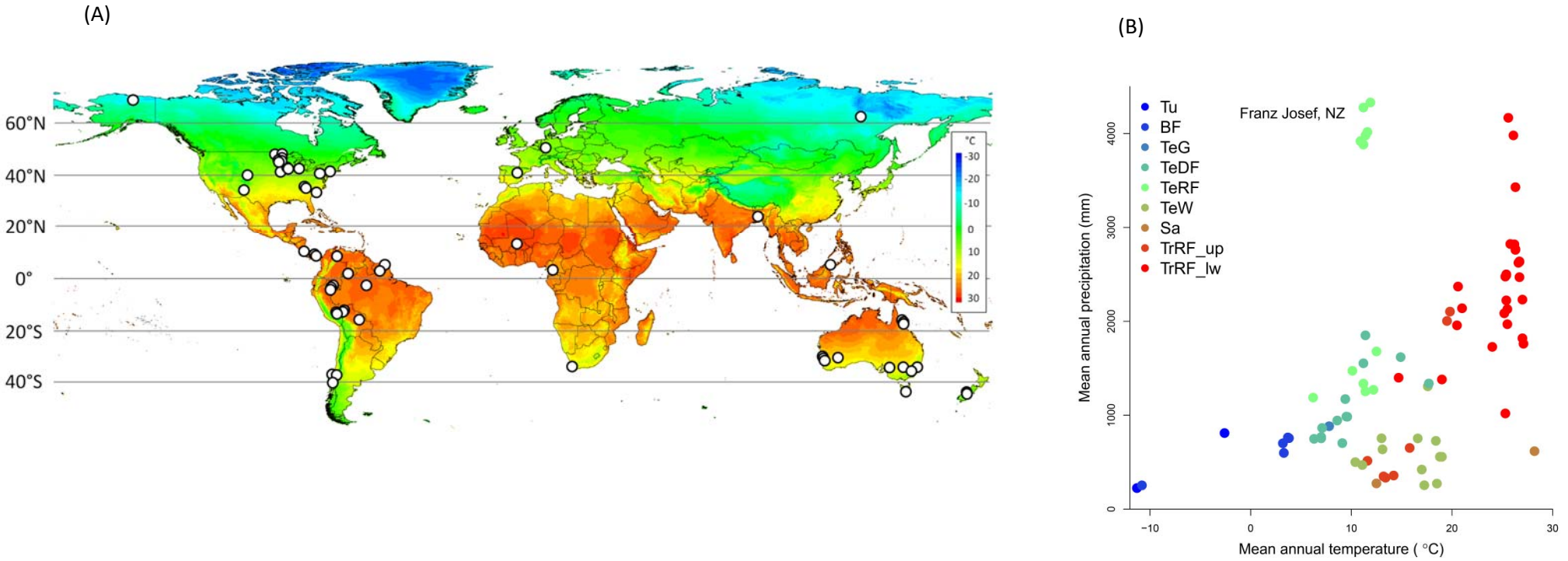

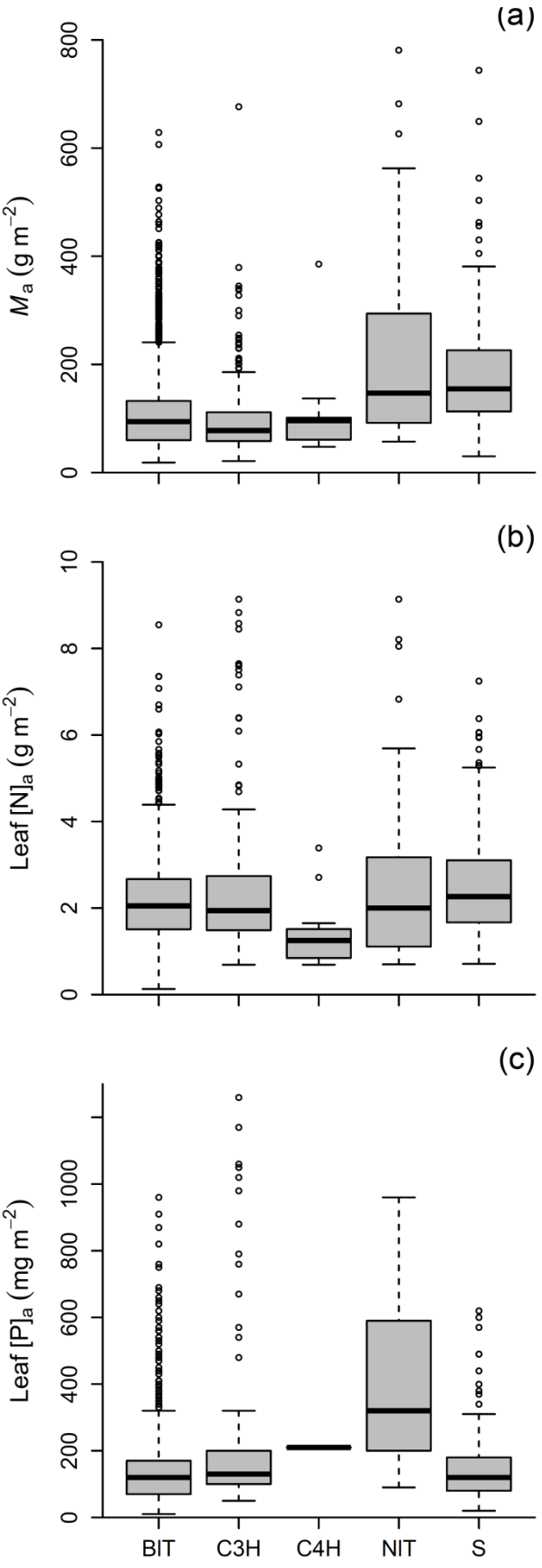

Figure 2. Box plots showing modulation of leaf structural and chemical traits by *JULES* (Clark *et al.*, 2011) plant functional type (PFT) classifications. Traits shown are: (a) M_a, leaf mass per unit leaf area; (b) $[N]_a$, area-based leaf nitrogen concentration; and (c) $[P]_a$, area-based leaf phosphorous concentration. Data shown are for individual observations. The central box in each box plot shows the interquartile range; the median is shown as the bold line within each box; whiskers extend 1.5 times the interquartile range or to the most extreme value, whichever is the smaller; any points outside these values are shown as individual points. Data for the following *JULES* (Clark *et al.*, 2011) plant functional type (PFT) classifications: BlT, broad-leaved tree; C3H, C_3 metabolism herb/grass; C4H, C_4 metabolism herb/grass; NlT, needle-leaved tree; S, shrub.

Figure 3. Box plots showing modulation of carboxylation capacity of Rubisco (V_{cmax}) and leaf respiration (R_{dark}) in darkness by *JULES* (Clark *et al.*, 2011) plant functional type (PFT) classifications. Data shown are for individual row observations contained in the *GlobResp* database (to give an indication of underlying data distribution). Rates at 25°C are shown. Traits shown are: (a) $V_{cmax,a}^{25}$ and (c) $V_{cmax,m}^{25}$: area- and mass-based carboxylation rates, respectively; (b) $R_{dark,a}^{25}$ and (d) $R_{dark,m}^{25}$: area- and mass-based respiration rates, respectively. Values of V_{cmax} at 25°C were calculated according to Farquhar *et al*. (1980) assuming an activation energy (E_a) of 64.8 kJ mol^{-1}. Values of R_{dark} at 25°C were calculated assuming a T-dependent Q_{10} (Tjoelker *et al.*, 2001) and equation 7 described in Atkin et al. (2005). The central box in each box plot shows the interquartile range; the median is shown as the bold line within each box; whiskers extend 1.5 times the interquartile range or to the most extreme value, whichever is the smaller; any points outside these values are shown as individual points. Data for the following *JULES* (Clark *et al.*, 2011) plant functional type (PFT) classifications: BlT, broad-leaved tree; C3H, C_3 metabolism herb/grass; NlT, needle-leaved tree; S, shrub. Data not shown for C_4 metabolism herbs/grasses, due to limited data availalbility.

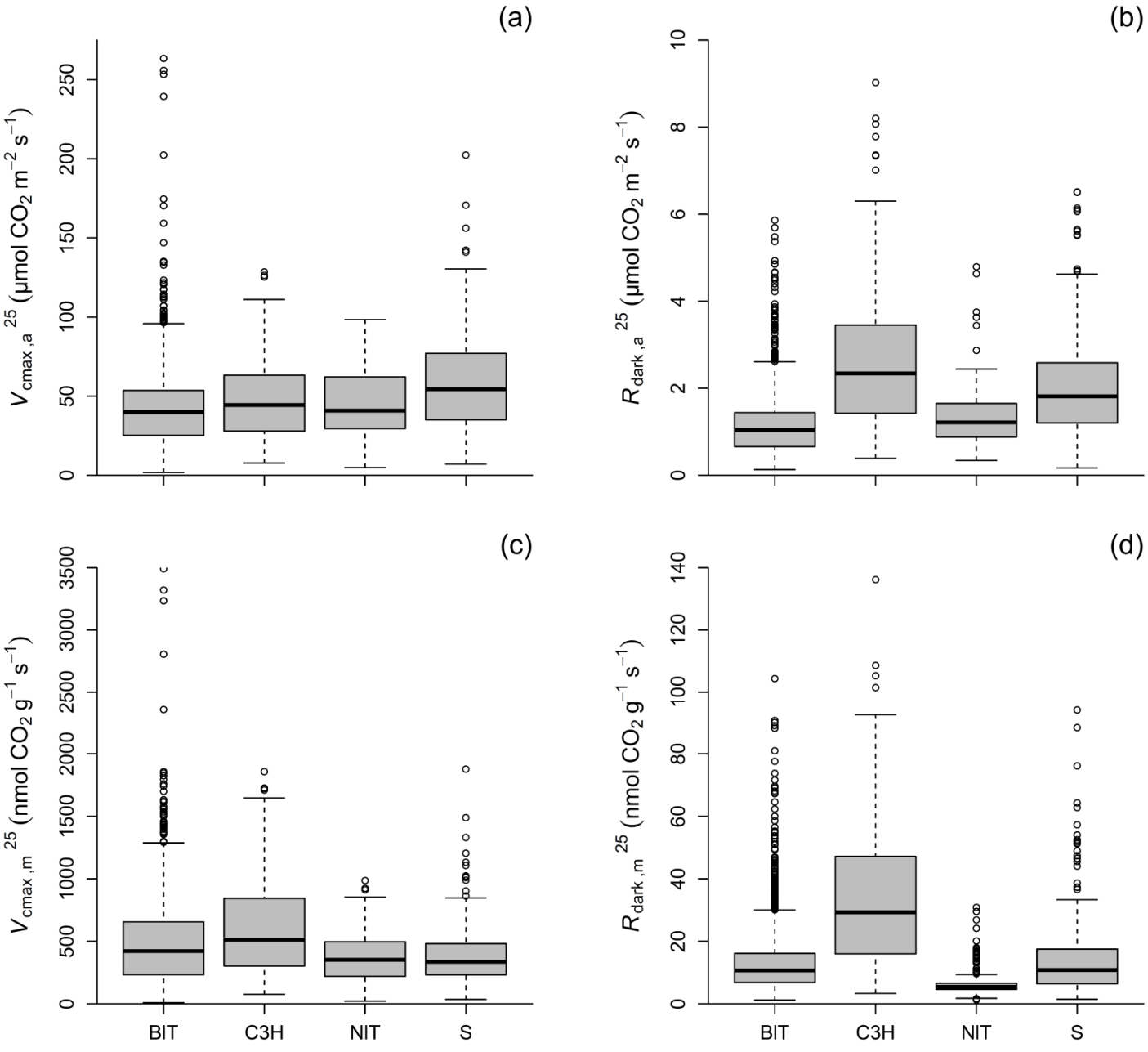

Figure 4. Relationships between leaf R_{dark} (log_{10} scale) and location (absolute latitude) or climate [mean daily temperature of the warmest quarter (TWQ) & aridity index (AI)]. Traits shown are: $R_{dark,a}^{25}$, (a, b and c) and $R_{dark,a}^{TWQ}$ (d, e and f), predicted area-based R_{dark} rates at 25°C and TWQ, respectively; $R_{dark,m}^{25}$ (g, h and i) and $R_{dark,m}^{TWQ}$ (j, k and l), predicted mass-based R_{dark} rates at 25°C and TWQ, respectively. Values shown are averages for unique site:species combinations for rates at 25°C and TWQ, calculated assuming a temperature-dependent Q_{10} (Tjoelker *et al.*, 2001) and equation 7 described in Atkin et al. (2005). Values at the TWQ of each replicate were calculated using climate/location data from the *WorldClim* data base (Hijmans *et al.*, 2005). Aridity index calculated as the ratio of mean annual precipitation (MAP) to mean annual potential evapotranspiration (PET) (UNEP, 1997). In plots against latitude, northern and southern latitudes shown as blue and red symbols, respectively. Solid lines in each plot show regression lines where the relationships were significant; dashed lines show the prediction intervals (two-times the standard deviation) around the predicted relationship. See Table 3 for correlations between log_{10} transformed R_{dark} and location/climate. Note: see Figure S3 (Supporting Information) for relationships beween R_{dark} and AI, excluding data from the exceptionally high rainfall sites at Frans Josef on the Sth Island of New Zealand.

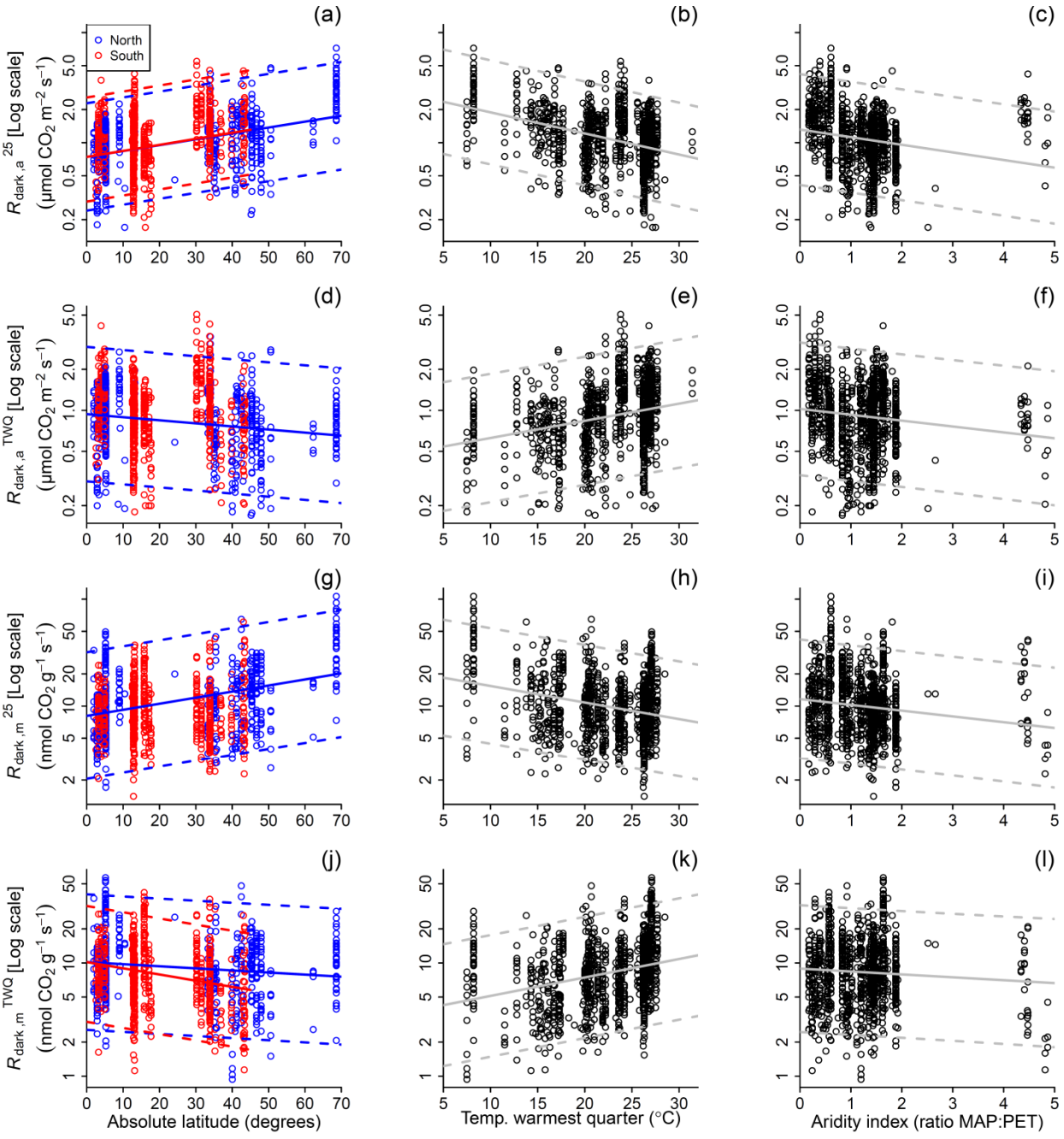

Figure 5. Patterning of area- and mass-based R_{dark}^{25} – V_{cmax}^{25} relationships by *JULES* PFTs (a and d); TWQ categories (5°C intervals) – all data (b and e); and TWQ categories (5°C intervals) – broad-leaved trees only (c and f). All values shown on a $\log_{10}$ scale. Values shown are averages for unique site:species combinations. Upper panels (a, b and c) show area-based values, while lower panels (d, e and f) show mass-based values. *JULES* PFTs: BlT, broad-leaved tree; C3H, C_3 metabolism herb/grass; NlT, needle-leaved tree; S, shrub. TWQ classes: 1st <10°C; 2nd 10-15°C; 3rd 15-20°C; 4th 20-25°C; 5th >25°C. Values of R_{dark} at 25°C were calculated assuming a *T*-dependent Q_{10} (Tjoelker *et al.*, 2001) and equation 7 described in Atkin *et al*. (2005). Values V_{cmax} at 25°C were calculated according to Farquhar *et al*. (1980) assuming an activation energy (E_a) of 64.8 kJ mol^{-1}. See Table S3 for SMA regression outputs.

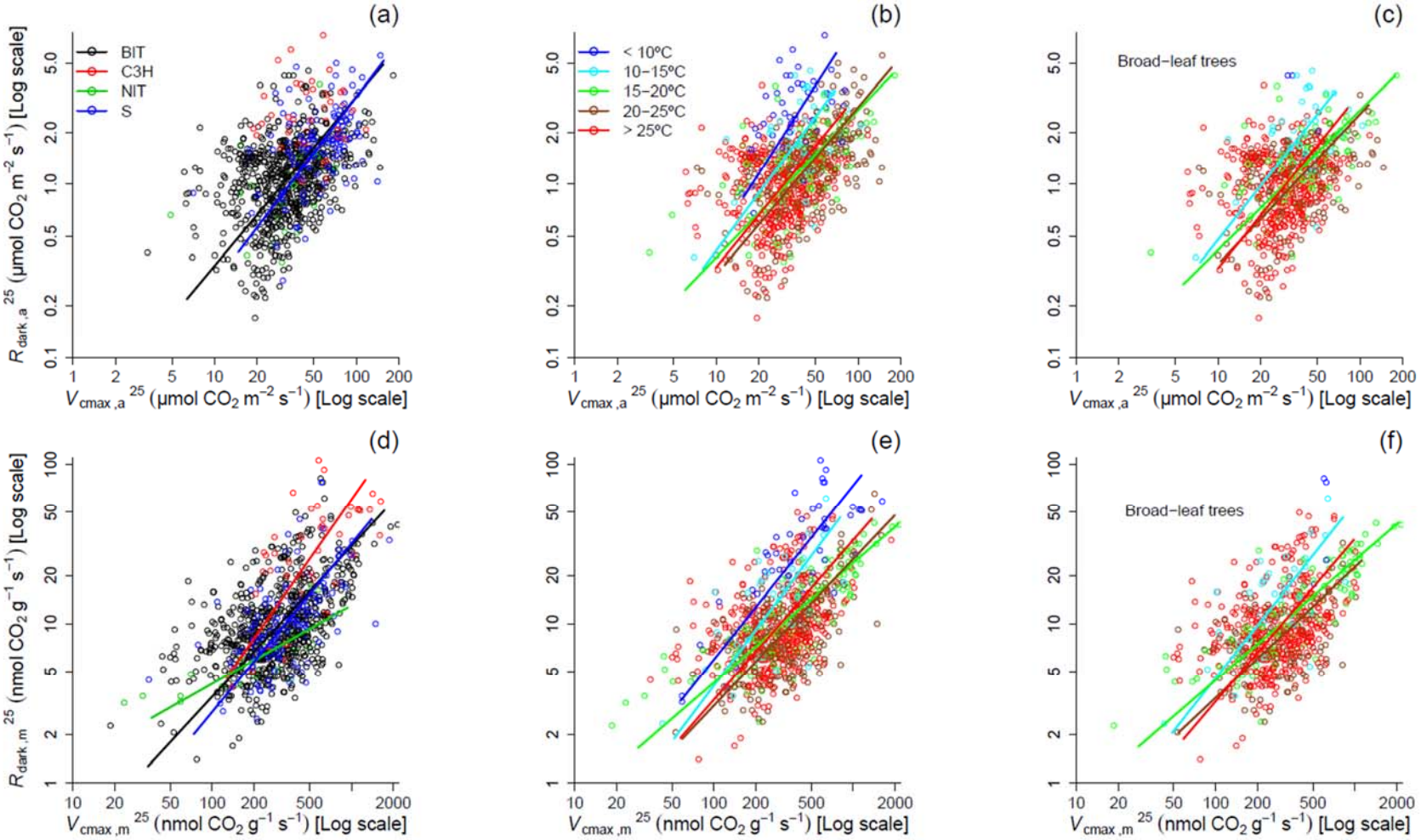

Figure 6. Patterning of area- and mass-based R_{dark}^{25} – N relationships by *JULES* PFTs (a and d); TWQ categories (5°C intervals) – all data (b and e); and TWQ categories (5°C intervals) – broad-leaved trees only (c and f). Values shown are averages for unique site:species combinations. All values shown on a $\log_{10}$ scale. *JULES* PFTs: BlT, broad-leaved tree; C3H, C_3 metabolism herb/grass; NlT, needle-leaved tree; S, shrub. TWQ classes: 1st <10°C; 2nd 10-15°C; 3rd 15-20°C; 4th 20-25°C; 5th >25°C. Values of R_{dark} at 25°C were calculated assuming a *T*-dependent Q_{10} (Tjoelker *et al.*, 2001) and equation 7 described in Atkin et al. (2005). See Table S3 for SMA regression outputs.

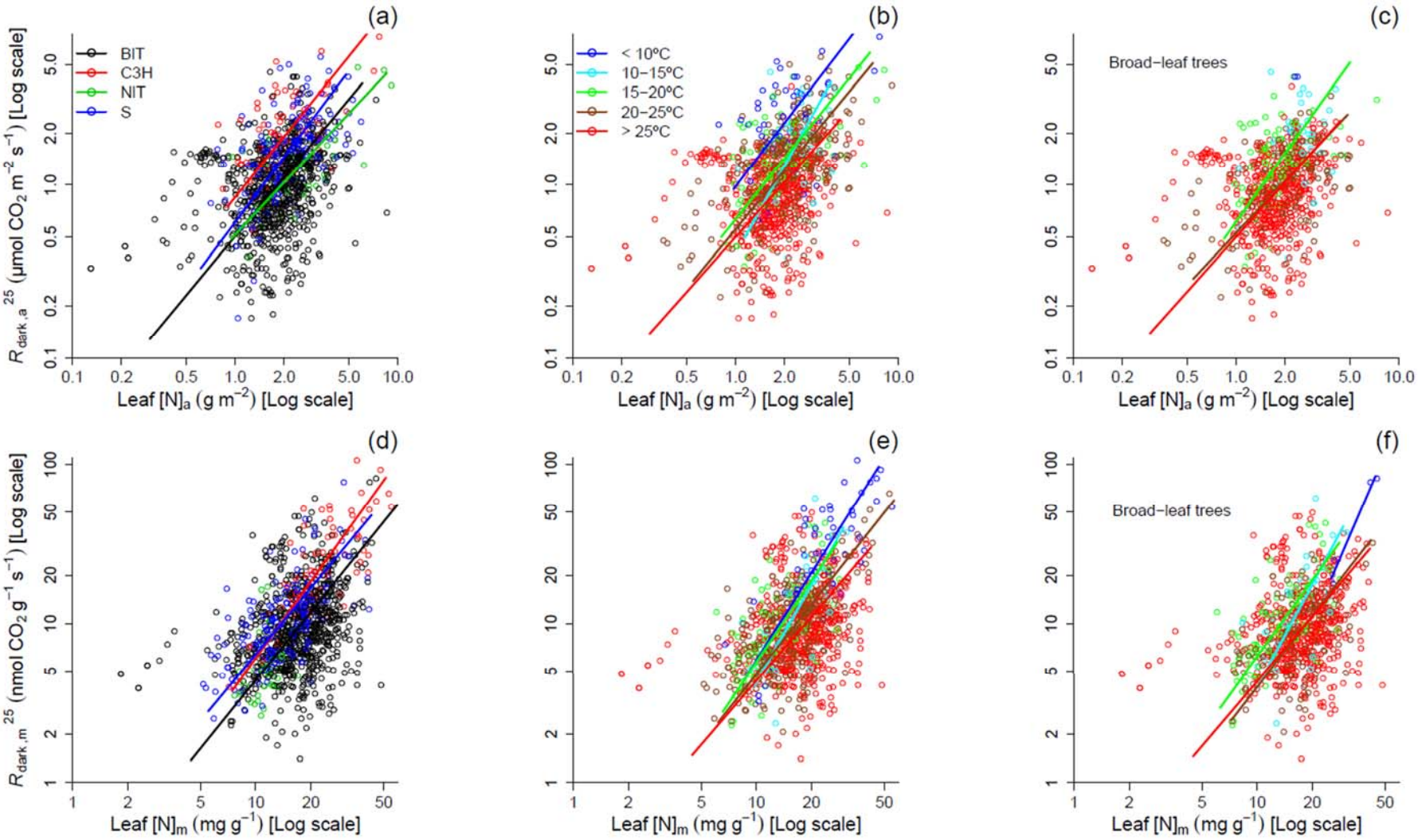
(a)
BIT
C3H
NIT
S
$R_{dark,a}^{25}$ (μmol CO_2 m^{-2} s^{-1}) [Log scale]
Leaf $[N]_a$ (g m^{-2}) [Log scale]
(b)
< 10°C
10–15°C
15–20°C
20–25°C
> 25°C
Leaf $[N]_a$ (g m^{-2}) [Log scale]
(c)
Broad−leaf trees
Leaf $[N]_a$ (g m^{-2}) [Log scale]
(d)
$R_{dark,m}^{25}$ (nmol CO_2 g^{-1} s^{-1}) [Log scale]
Leaf $[N]_m$ (mg g^{-1}) [Log scale]
(e)
Leaf $[N]_m$ (mg g^{-1}) [Log scale]
(f)
Broad−leaf trees
Leaf $[N]_m$ (mg g^{-1}) [Log scale]

Figure 7. Scatterplots for (a) area-based, and (b) mass-based linear mixed-effects model's goodness of fits, including fixed and random terms. Observed values of leaf respiration at 25°C (R_{dark}^{25}) are plotted against model predictions (using the 'best' predictive models detailed in Table 5). For the area-based model (a), the fixed component explanatory variables were: (1) plant functional types (PFT), according to *JULES* (Clark *et al.*, 2011); (2) area-based leaf nitrogen ($[N]_a$) and phosphorus ($[P]_a$) concentrations, and Rubisco CO_2 fixation capacity at 25°C ($V_{cmax,a}^{25}$); and mean temperature of the warmest quarter (TWQ) (Hijmans *et al.*, 2005). For the mass-based model (b), the fixed component explanatory variables were: (1) plant functional types (PFT); (2) mass-based leaf nitrogen ($[N]_m$) and phosphorus ($[P]_m$) concentrations, Rubisco CO_2 fixation capacity at 25°C ($V_{cmax,m}^{25}$), and leaf mass per unit leaf area (M_a).

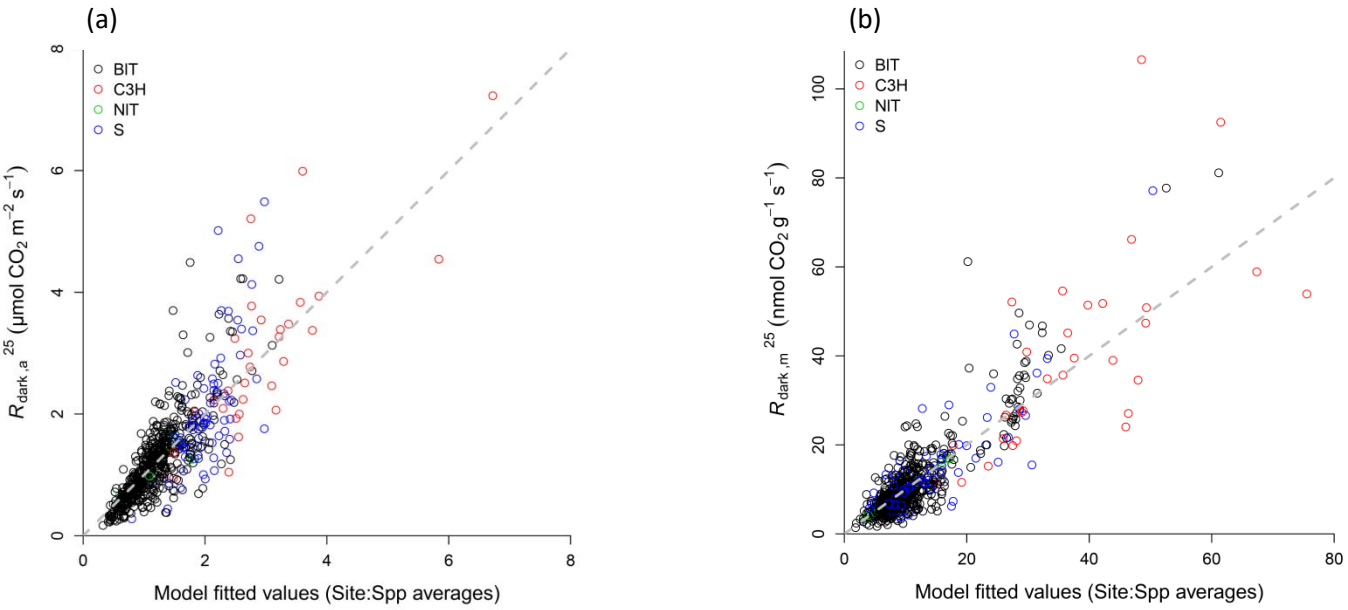

Supporting Information

Authors: Atkin, Bloomfield, Reich, Tjoelker et al.

Title: Global variability in leaf respiration in relation to climate, plant functional types and leaf traits

Methods S1: Sampling methods and measurements protocols - unpublished data collected at sites detailed in Table S1.

Species identification

For work undertaken at the RAINFOR plots in Sth America (http://www.rainfor.org/en/project/field-campaigns), voucher specimens were collected and identified according to Lopez-Gonzalez *et al.* (2011). For Sth American plots associated with the Carnegie Institution *Spectranomics project* (http://spectranomics.ciw.edu), botanical vouchers were identified as detailed in Asner *et al*. (2014). Species identification at the TERN Supersites (http://www.tern.org.au/Australian-SuperSite-Network-pg17873.html) in Australia were indentified by CSIRO, university and/or forest service botanical staff at each site.

Sampling method (1): Ex situ measurements made using cut branches

Branches being sampled in the morning from the sun-facing upper canopy of individual plants; leaves had experienced at least two hours direct sunlight before branches were sampled. Branches were re-cut under water immediately after detachment. Thereafter, branches were transported to a nearby laboratory located for *ex situ* measurements of net CO_2 exchange.

Sampling method (2) In situ measurements using attached branches

Leaf gas exchange measured using attached, sun-facing upper canopy leaves of individual plants, typically between 9 am and 1 pm for most sites, with the exception of measurements in Sth America, Siberia and Spain, where measurements were made upto 4 pm.

Measurement methods – leaf gas exchange

(1) Measurements of respiration (R_{dark}) and light-saturated photosynthesis under ambient [CO_2] (A_{sat}) and elevated [CO_2] (A_{max}): Most recent, fully expanded leaves were selected for measurement of net CO_2 exchange rates, using Licor 6400 Portable Photosynthesis Systems (Li-6400, LiCor, Lincoln, NE) using a 6 cm^2 leaf chamber with red-blue light source (6400-18 RGB Light Source, Licor, Lincoln, NE). Measurements were made at a relative humidity of 60-70%, and at the prevailing ambient day-time T of each site (6-41°C, depending on site location). Leaves were first exposed to saturating irradiance (1000 - 2000 µmol photons m^{-2} s^{-1}, depending on speices and site) and an reference line atmospheric [CO_2] of 400 ppm for 10 minutes, after which rates of light-saturated net photosynthesis (A_{sat}) was measured following equilibrium. Thereafter, atmospheric [CO_2] was increased to 1500-2000 ppm (depending on site location), with CO_2-saturated, light-saturated rates of net photosynthesis (A_{max}) then being measured. Finally, which leaves were placed in darkness for 30-45 mins [to avoid post-illumination transients; (Azcón-Bieto & Osmond, 1983; Atkin *et al.*, 1998)] and rates of leaf respiration in darkness (R_{dark}) measured. Flow rates

through the leaf chamber were set to 500 and 300 µmol s^{-1} for measurements under light-saturation and darkness, respectively.

(2) Measurements of R_{dark} and A_{sat}: As for (1), but without measurements made at saturating atmospheric [CO_2] (i.e. no estimate of A_{max}).

(3) Measurements of R_{dark} and A_{sat} (from A-I curves): As for (1), but with measurements of A_{sat} being limited to measurements made at an atmospheric [CO_2] of 400 ppm (i.e. no estimate of A_{max}) as part of studies of the Kok-effect (Kok, 1948) using light-response curves of net CO_2 exchange (Atkin *et al.*, 2013; Heskel *et al.*, 2014). Measurements commenced at 1800 µmol photons m^{-2} s^{-1} and decreased to 1500, 100 and then at 5 µmol photons m^{-2} s^{-1} intervals to darkness, where R_{dark} was measured. Measurements took place at the prevailing day-time air T at each site (RH 60-70%). An equilibrium period of two minutes was allowed at each irradiance level before net CO_2 exchange was measured. During measurements, CO_2 flow rates in the leaf cuvette were set to 500 µmol s^{-1} for the measurements made at 1800 µmol photons m^{-2} s^{-1} and 300 µmol s^{-1} for those in darkness.

Leaf area, mass and nutrient concentration measurements

At most sites, leaf area was typically determined on a 600 dots/inch flatbed top-illumination optical scanner, with area being quantified subsequently using *Image J* software (http://imagej.nih.gov/ij/). The scanned leaves were then dried at 70°C for a minimum of 72 h before dry mass (DM) was measured. Leaf mass per area was then calculated as grams DM m^2. For sites where both leaf N and P values were reported, concentratons of the two elements were determined with a LaChat QuikChem 8500 Series 2 Flow Injection Analysis System (Lachat Instruments, Milwaukee, WI, USA) using Kjeldahl acid digests (Allen, 1974). For sites where only leaf N was reported, samples were ground using a hammer mill (31–700 Hammer Mill; Glen Creston, Stanmore, UK), weighed into tin cups and combusted using a Carlo-Erba elemental analyser NA1500 (Thermo Fisher Scientific, Milan, Italy).

Methods S2: Temperature normalization of respiration rates

To enable comparisons of leaf R_{dark}, we calculated rates both for a common temperature (i.e. 25°C) and the estimated growth T at each site (TWQ and MMT). To estimate rates of R_{dark} (R_2) at at given T (T_2), we calculated rates R_{dark} at 25ºC (R_{dark}^{25}), TWQ (R_{dark}^{TWQ}) and MMT (R_{dark}^{MMT}) assuming a fixed Q_{10} of 2.23 (Atkin *et al.*, 2005) using the equation:

$$R_2 = R_1 Q_{10}^{[\frac{(T_2 - T_1)}{10}]} \qquad \text{Eqn 1}$$

where R_1 represents the rate of R_{dark} at the measurement T (T_1). This approach assumes that the Q_{10} remains constant across a range of leaf T - global surveys of the T-dependence of R_{dark} have shown, however, that the Q_{10} declines with increasing leaf T (Tjoelker *et al.*, 2001; Atkin & Tjoelker, 2003). Given this, we also calculated R_{dark}^{25}, R_{dark}^{TWQ} and R_{dark}^{MMT} using a T-dependent Q_{10} (herein called '*var* Q_{10}')according to:

$$R_2 = R_1(3.09 - 0.043\left[\frac{(T_2 + T_1)}{2}\right])^{[\frac{T_2 - T_1}{10}]} \qquad \text{Eqn 2}$$

Comparison of area-based rates of R_{dark}^{25} calculated using Eqns 1 and 2 revealed little overall difference in predicted rates at 25ºC (r^2 = 0.995, Fig. S1). Estimates of R_{dark}^{TWQ} were likewise similar, irrespecitive of the equation used (r^2 = 0.991, Fig. S1). For subsequent analyses, we used Eqn 2 (i.e. *var* Q_{10}) when estimating rates of R_{dark}^{25}, R_{dark}^{TWQ} and R_{dark}^{MMT}.

Table S1. Details on unpublished databases used in *GlobResp* database of leaf respiration (R_{dark}). Shown are individual sample sites, climate and measurement conditions of the sites at which R_{dark} was measured. Sites shown in order from decreasing latitude from north to south. Data on climate are from the *WorldClim* data base (Hijmans *et al.*, 2005). Number of species, plants measured and *JULES* plant functional types (PFTs) at each site shown, according to: BlT, broad-leaved tree; C3H, C_3 metabolism herb/grass; C4H, C_4 metabolism herb/grass; NlT, needle-leaved tree; S, shrub. Biome classes: BF, boreal forests; TeDF, temperate deciduous forest; TeG, temperate grassland; TeRF, temperate rainforest; TeW, temperate woodland; TrRF_lw, lowland tropical rainforest (<1500 asl); TrRF_up, upland tropical rainforest (>1500 asl); Tu, tundra. Abbreviations: mean temperature of the warmest quarter (i.e. warmest 3-month period per year; TWQ), mean annual precipitation (MAP), mean precipitation of the warmest quarter (PWQ), aridity index (AI) calculated as the ratio of MAP to mean annual potential evapotranspiration (UNEP, 1997; Zomer et al., 2008). Australia-ACT, Australian Capital Territory; Australia-FNQ, Far North Queensland; Australia-TAS, Tasmania; Australia-WA, Western Australia; USA-AK, Alaska; USA-MN, Minnesota; USA-NY, New York; See Methods S1 text in Supporting Information for details on sampling methods and measurement protocols.

Country/Region	Biome	Latitude	Longitude	Altitude (m asl)	MAT (°C)	TWQ (°C)	MAP (mm)	PWQ (mm)	AI	No. species	No. measurements	PFTs present	Sampling method (Methods S1)	Measurement method (Methods S2)	Primary person responsible for collection of unpublished data (& senior associate)
USA-AK	Tu	68.630	-149.600	720	-11.3	8.2	225	113	0.608	37	204	BlT, C3H, S	(1)	(3)	N. Mirotchnick (K. Griffin)
Russia-Siberia	BF	62.252	129.621	218	-10.8	15.4	254	122	0.458	3	40	BlT, NlT	(2)	(2)	J. Zaragoza-Castells (O. Atkin)
Russia-Siberia	BF	62.250	129.621	216	-10.8	15.4	254	122	0.458	2	30	BlT, NlT	(2)	(2)	J. Zaragoza-Castells (O. Atkin)
USA-MN	BF	47.944	-91.755	426	3.7	17.3	763	308	0.976	11	182	BlT, NlT	(1)	(2)	P. Reich
USA-MN	BF	46.704	-92.525	385	3.2	17.7	702	288	0.832	7	199	BlT	(1)	(2)	P. Reich
USA-MN	TeDF	45.169	-92.762	210	7.0	21.1	769	315	0.832	1	18	BlT	(1)	(2)	K. Sendall (P. Reich)
USA-NY	TeDF	41.420	-74.010	225	9.4	20.8	1,173	308	1.204	3	21	BlT	(1)	(3)	K. Griffin
USA-NY	TeDF	41.420	-74.010	225	9.4	20.8	1,173	308	1.204	3	18	BlT	(1)	(3)	K. Griffin
Spain	TeW	40.809	-2.237	980	10.4	18.9	501	102	0.496	1	28	BlT	(2)	(2)	J. Zaragoza-Castells (O. Atkin)
Spain	TeW	40.805	-2.227	1,060	11.1	19.6	471	95	0.464	1	24	BlT	(2)	(2)	J. Zaragoza-Castells (O. Atkin)
French Guiana	TrRF_lw	5.270	-52.920	21	25.8	26.2	2,824	222	1.881	43	65	BlT	(1)	(1)	J. Zaragoza-Castells (P. Meir)
French Guiana	TrRF_lw	5.270	-52.920	21	25.8	26.2	2,824	222	1.881	43	78	BlT	(1)	(1)	J. Zaragoza-Castells (P. Meir)
Peru-Amazon	TrRF_lw	-3.252	-72.908	111	20.6	21.4	2,371	676	1.401	20	20	BlT	(1)	(1)	Y. Ishida (J. Lloyd/O. Atkin)
Peru-Amazon	TrRF_lw	-3.256	-72.894	111	26.2	26.7	2,821	681	1.667	18	18	BlT	(1)	(1)	Y. Ishida (J. Lloyd/O.Atkin)
Peru-Amazon	TrRF_lw	-3.941	-73.440	120	26.3	26.8	2,769	711	1.637	14	14	BlT, S	(1)	(1)	Y. Ishida (J. Lloyd/O.Atkin)
Peru-Amazon	TrRF_lw	-3.949	-73.435	120	26.3	26.8	2,769	711	1.638	17	18	BlT	(1)	(1)	Y. Ishida (J. Lloyd/O.Atkin)
Peru-Amazon	TrRF_lw	-3.954	-73.427	120	26.3	26.8	2,762	708	1.633	22	22	BlT	(1)	(1)	Y. Ishida (J. Lloyd/O.Atkin)
Peru-Amazon	TrRF_lw	-4.878	-73.630	124	26.7	27.0	2,634	618	1.506	14	15	BlT	(1)	(1)	Y. Ishida (J. Lloyd/O.Atkin)
Peru-Amazon	TrRF_lw	-4.899	-73.628	124	26.7	27.0	2,639	620	1.506	18	18	BlT	(1)	(1)	Y. Ishida (J. Lloyd/O.Atkin)
Peru-Amazon	TrRF_lw	-12.534	-69.054	200	25.5	26.4	2,131	686	1.215	5	5	BlT	(1)	(1)	R. Guerrieri (P. Meir/O.Atkin)
Peru-Amazon	TrRF_lw	-12.830	-69.271	220	25.3	26.3	2,477	957	1.436	64	65	BlT	(1)	(1)	J. Zaragoza-Castells & R. Guerrieri
Peru-Amazon	TrRF_lw	-12.831	-69.284	220	25.4	26.3	2,491	961	1.445	8	8	BlT	(1)	(1)	R. Guerrieri (P. Meir/O.Atkin)
Peru-Amazon	TrRF_lw	-12.839	-69.296	200	25.4	26.3	2,501	964	1.452	71	75	BlT	(1)	(1)	J. Zaragoza-Castells & R. Guerrieri (P. Meir/O.Atkin)
Peru-Andes	TrRF_up	-13.047	-71.542	1,750	19.5	20.3	2,005	574	1.196	17	20	BlT	(1)	(1)	R. Guerrieri (P. Meir/O.Atkin)
Peru-Andes	TrRF_up	-13.049	-71.537	1,500	20.6	21.4	2,371	676	1.402	14	16	BlT	(1)	(1)	R. Guerrieri (P. Meir/O.Atkin)
Peru-Andes	TrRF_up	-13.070	-71.556	1,800	19.8	20.6	2,104	602	1.249	20	20	BlT	(1)	(1)	R. Guerrieri (P. Meir/O.Atkin)

Peru-Andes	TrRF_up	-13.106	-71.589	2,750	15.8	16.8	652	188	0.423	10	11	BlT	(1)	(1)	R. Guerrieri (P. Meir/O.Atkin)
Peru-Andes	TrRF_up	-13.109	-71.600	3,000	14.2	15.3	359	103	0.244	8	8	BlT	(1)	(1)	R. Guerrieri (P. Meir/O.Atkin)
Peru-Andes	TrRF_up	-13.114	-71.607	3,450	11.6	12.8	515	160	0.367	13	14	BlT, C3H	(1)	(1)	R. Guerrieri (P. Meir/O.Atkin)
Peru-Andes	TrRF_up	-13.176	-71.595	3,000	13.2	14.3	349	101	0.24	14	16	BlT	(1)	(1)	R. Guerrieri (P. Meir/O.Atkin)
Peru-Andes	TrRF_up	-13.191	-71.588	3,000	13.4	14.5	335	97	0.23	7	7	BlT	(1)	(1)	R. Guerrieri (P. Meir/O.Atkin)
Australia-FNQ	TrRF_lw	-17.109	145.603	818	20.5	23.3	1,958	886	1.35	6	15	BlT	(1)	(3)	J. Zaragoza-Castells (O. Atkin/P.Meir)
Australia-FNQ	TrRF_lw	-17.120	145.632	728	21.0	23.8	2,140	954	1.471	16	56	BlT	(1)	(1)	L. Weerasinghe (O.Atkin)
Australia-FNQ	TrRF_lw	-17.682	145.534	1,040	19.0	22.2	1,382	641	0.943	10	24	BlT, S	(1)	(3)	J. Zaragoza-Castells(O. Atkin/P.Meir)
Australia-WA	TeW	-30.180	115.000	90	19.0	23.9	558	33	0.386	8	31	BlT, C3H, S	(2)	(1)	L. Weerasinghe (O. Atkin)
Australia-WA	TeW	-30.240	115.070	23	18.8	23.8	558	35	0.389	10	39	BlT, S	(2)	(1)	L. Weerasinghe (O. Atkin)
Australia-WA	TeW	-30.240	115.060	5	18.8	23.8	558	35	0.389	9	34	BlT, C3H, S	(2)	(1)	L. Weerasinghe (O. Atkin)
Australia-WA	TeW	-30.264	120.692	459	18.5	25.6	273	64	0.177	9	87	BlT, S	(1), (2)	(1)	K. Bloomfield (O. Atkin)
Australia-SA	TeW	-34.037	140.674	35	17.3	23.6	255	52	0.172	10	78	BlT, C3H, S	(1), (2)	(1)	K. Bloomfield (O. Atkin)
Australia-ACT	TeW	-35.276	149.109	601	13.1	19.8	637	162	0.509	5	18	BlT, S	(1), (2)	(3)	K. Crous (O. Atkin)
Australia-TAS	TeRF	-43.089	146.651	217	10.1	13.8	1,474	237	1.813	3	13	BlT	(1)	(1)	L. Weerasinghe (O. Atkin)
Australia-TAS	TeRF	-43.092	146.684	257	11.2	14.8	1,338	212	1.648	2	6	BlT, S	(1)	(1)	L. Weerasinghe (O. Atkin)
Australia-TAS	TeRF	-43.095	146.724	88	11.4	15.1	1,255	199	1.463	9	29	BlT, S	(1)	(1)	L. Weerasinghe (O. Atkin)

Table S2. Details on published databases used in *GlobResp* database of leaf respiration (R_{dark}). Shown are climate and measurement conditions of the sites at which R_{dark} was measured. Sites shown in order from decreasing latitude from north to south. Data on climate are from the *WorldClim* data base (Hijmans *et al.*, 2005). Number of species and *JULES* plant functional types (PFTs) at each site shown, according to: BlT, broad-leaved tree; C3H, C_3 metabolism herb/grass; C4H, C_4 metabolism herb/grass; NlT, needle-leaved tree; S, shrub. Biome classes: BF, boreal forests; TeDF, temperate deciduous forest; TeG, temperate grassland; TeRF, temperate rainforest; TeW, temperate woodland; TrRF_lw, lowland tropical rainforest (<1500 asl); Tu, tundra. Abbreviations: mean temperature of the warmest quarter (i.e. warmest 3-month period per year; TWQ), mean annual precipitation (MAP), mean precipitation of the warmest quarter (PWQ), aridity index (AI) calculated as the ratio of MAP to mean annual potential evapotranspiration (UNEP, 1997; Zomer et al., 2008). Australia-ACT, Australian Capital Territory; Australia-FNQ, Far North Queensland; Australia-NSW, New South Wales; Australia-WA, Western Australia; USA-AK, Alaska; USA-CO, Colorado; USA-MN, Minnesota; USA-IW, Iowa; USA-WI, Wisconsin; USA-MI, Michigan; USA-PN, Pennsylvania; USA-NC, North Carolina; USA-KT, Kentucky; USA-TN, Tennessee; USA-NM, New Mexico; USA-SC, South Carolina.

Country/Region	Biome	Latitude	Longitude	Altitude (m asl)	MAT (ºC)	TWQ (ºC)	MAP (mm)	PWQ (mm)	AI	No. species	PFTs present	Traits available in *GlobResp* database	References/Source
Germany	TeDF	50.600	8.700	60	9.1	17.2	704	190	0.917	9	BlT, NlT	R_{dark}, [N], M_a	Grueters (1998); Kattge *et al*. (2011)
USA-MN	BF	47.803	-95.007	400	3.3	18.3	599	278	0.749	1	NlT	R_{dark}, [N]	Tjoelker *et al.* (2008)
USA-MN	BF	46.721	-92.457	380	3.8	17.4	757	304	0.906	7	BlT	R_{dark}, [N]	Machado & Reich (2006)
USA-MN	BF	46.705	-92.525	380	3.7	17.4	764	308	0.905	7	BlT, NlT	R_{dark}, [N]	Tjoelker *et al.* (2008); Reich *et al*. (2008)
USA-MN	TeG	45.410	-93.210	300	6.3	20.4	749	314	0.835	35	BlT, C3H, C4H, S	A_{sat}, C_i, R_{dark}, [N], M_a	Craine *et al.* (1999); Tjoelker *et al*. (2005)
USA-MN	TeDF	45.410	-93.210	300	6.3	20.4	749	314	0.835	3	BlT	A_{sat}, C_i, R_{dark}, M_a	Tjoelker *et al*. (2005); Sendall & Reich (2013)
USA-MN	TeDF	44.996	-93.189	281	7.0	21.0	755	314	0.835	3	BlT	R_{dark}, [N], M_a	Lee *et al*. (2005); Kattge *et al*. (2011)
USA-WI	TeDF	42.980	-90.120	360	7.1	20.2	865	315	0.932	1	BlT	A_{sat}, R_{dark}, [N], M_a	Reich *et al.* (1998b)
USA-MI	TeDF	42.530	-85.855	200	8.6	19.9	944	268	0.98	1	NlT	R_{dark}, [N]	Tjoelker *et al.* (2008); Reich *et al*. (2008)
USA-WI	TeG	42.500	-90.000	275	7.8	20.7	884	315	0.925	15	BlT, C3H, NlT	A_{sat}, C_i, R_{dark}, [N], M_a	Reich *et al*. (1998a); Reich *et al.* (1998b)
USA-IA	TeDF	41.170	-92.870	385	7.1	20.2	865	315	0.834	11	BlT, NlT	R_{dark}, [N], M_a	Lusk & Reich (2000)
USA-PA	TeDF	40.82	-77.93	400	9.1	17.2	704	190	0.71	1	BlT	A_{sat}, R_{dark}, M_a	Kloeppel *et al.* (1993; 1994)
USA-PA	TeDF	40.8	-77.83	335	9.6	20.8	984	286	0.972	2	BlT	A_{sat}, C_i, R_{dark}, [N], M_a	Kloeppel & Abrams (1995)
USA-PA	TeDF	40.78	-77.88	348	9.5	20.6	986	285	0.986	1	BlT	A_{sat}, C_i, R_{dark}, [N], M_a	Kloeppel & Abrams (1995)
USA-CO	Tu	40.050	-105.600	3,360	-2.6	7.5	811	203	1.198	10	BlT, C3H, NlT, S	A_{sat}, C_i, R_{dark}, [N], M_a	Reich *et al.* (1998b)
Japan	TeDF	35.720	140.800	20	14.9	23.7	1,619	433	1.921	4	BlT	A_{sat}, R_{dark}, [N], M_a	Miyazawa *et al*. (1998)
USA-TN	TeDF	35.500	-83.500	775	11.2	20.1	1,554	389	1.335	13	BlT, C3H, NlT, S	A_{sat}, R_{dark}, [N], M_a	Bolstad *et al*. (1999)
USA-NC	TeDF	35.050	-83.420	850	11.4	20.0	1,852	444	1.521	15	BlT, NlT	R_{dark}, [N], M_a	Mitchell *et al*. (1999); Reich *et al.* (1998b)
USA-NM	Sa	34.000	-107.000	1,620	12.5	22.2	275	127	0.189	9	BlT, NlT, S	A_{sat}, C_i, R_{dark}, [N], M_a	Reich *et al.* (1998b)
USA-SC	TeDF	33.330	-79.220	3	17.7	25.8	1,339	469	1.02	10	BlT, C3H, NlT, S	R_{dark}, [N], M_a	Reich *et al*. (1998a; 1999)

Bangladesh	TrRF_lw	24.200	90.150	21	25.5	28.5	1,970	736	1.344	1	BlT	A_{sat}, R_{dark}, M_a	Kamaluddin & Grace (1993)
Niger	Sa	13.200	-2.230	280	28.2	31.4	618	55	0.304	3	BlT, S	A_{sat}, R_{dark}	Meir *et al.* (2007)
Costa Rica	TrRF_lw	10.470	-84.030	140	25.6	26.6	4,168	750	2.658	1	BlT	A_{sat}, C_i, R_{dark}, M_a	Oberbauer & Strain (1985); (1986)
Costa Rica	TrRF_lw	10.430	-83.980	105	26.1	27.2	3,981	731	2.515	1	S	A_{sat}, R_{dark}, [N], M_a	Chazdon & Kaufmann (1993)
Panama	TrRF_lw	9.170	-79.850	90	26.6	27.5	2,624	410	1.877	1	BlT	A_{sat}, C_i, R_{dark}, [N], M_a	Zotz & Winter (1996)
Panama	TrRF_lw	8.983	-79.550	100	27.0	27.7	1,820	300	1.186	13	BlT	A_{sat}, C_i, R_{dark}, [N], [P], M_a	Slot *et al.* (2014b)
Panama	TrRF_lw	8.970	-79.530	30	27.1	27.7	1,762	290	1.143	6	BlT	A_{sat}, C_i, R_{dark}, [N], M_a	Kitajima *et al.* (1997)
Venezuela	TrRF_lw	8.650	-71.400	2,350	14.7	15.1	1,400	458	1.053	1	BlT	A_{sat}, C_i, R_{dark}, [N], M_a	García-Núñez *et al*.(1995)
Malaysia	TrRF_lw	5.160	117.900	20	26.7	27.1	2,471	501	1.638	29	Malaysia-Borneo	A_{sat}, C_i, R_{dark}, [N], [P], M_a	Swaine (2007)
Cameroon	TrRF_lw	3.380	11.500	550	24.0	24.8	1,729	417	1.126	6	Cameroon	A_{sat}, R_{dark}, [N], M_a	Meir *et al.* (2007)
Suriname	TrRF_lw	2.854	-54.958	215	25.4	26.3	2,224	165	1.365	25	Suriname	A_{sat}, R_{dark}, [N], M_a	Kattge *et al*. (2011)
Venezuela	TrRF_lw	1.930	-67.050	120	26.3	26.6	3,430	740	1.725	9	Venezuela	A_{sat}, C_i, R_{dark}, [N], M_a	Reich *et al.* (1998b)
Brazil-Amazon	TrRF_lw	-2.580	-60.100	115	27.0	27.6	2,232	401	1.385	9	BlT	R_{dark}, [N], M_a	Meir *et al.* (2002)
Bolivia	TrRF_lw	-15.783	-62.917	400	25.3	27.0	1,020	436	0.57	50	BlT	A_{sat}, R_{dark}, [N], M_a	Poorter & Bongers (2006)
Australia-FNQ	TrRF_lw	-16.100	145.450	90	25.2	27.5	2,087	1,031	1.393	18	BlT	A_{sat}, C_i, R_{dark}, [N], [P], M_a	Weerasinghe *et al.* (2014)
Australia-WA	TeW	-31.500	115.690	15	18.4	23.6	728	39	0.541	25	BlT, C3H, S	A_{sat}, C_i, R_{dark}, [N], M_a	Wright *et al*. (2004)
Sth Africa	TeW	-33.830	18.830	600	16.6	21.0	754	67	0.572	5	BlT, S	A_{sat}, R_{dark}, [N], M_a	Mooney *et al*. (1983)
Australia-NSW	TeW	-33.840	145.880	223	17.0	24.2	422	98	0.294	19	BlT, C3H, NlT, S	A_{sat}, C_i, R_{dark}, [N], [P], M_a	Wright *et al.* (2001)
Australia-NSW	TeW	-33.840	145.880	223	17.0	24.2	422	98	0.294	21	BlT, C4H, S	A_{sat}, C_i, R_{dark}, [N], [P], M_a	Wright *et al.* (2001)
Australia-NSW	TeW	-33.860	151.210	39	17.6	21.9	1,309	358	NA	18	BlT, S	A_{sat}, C_i, R_{dark}, [N], [P], M_a	Wright *et al.* (2001)
Australia-NSW	TeW	-33.860	151.210	39	17.6	21.9	1,309	358	NA	17	BlT, S	A_{sat}, C_i, R_{dark}, [N], [P], M_a	Wright *et al.* (2001)
Australia-ACT	TeW	-35.312	149.058	560	13.0	21.0	755	314	0.601	1	NlT	A_{sat}, C_i, R_{dark}, [N], M_a	Reich *et al*. (1999))
Chile	TeRF	-36.840	-73.030	30	12.2	16.1	1,272	74	1.208	6	BlT	A_{sat}, C_i, R_{dark}, [N], M_a	Wright *et al. (*2006*)*
Chile	TeRF	-37.000	-71.470	1,000	6.2	11.5	1,189	74	1.119	5	BlT, NlT	A_{sat}, C_i, R_{dark}, [N], M_a	Wright *et al. (*2006*)*
Chile	TeRF	-39.800	-73.000	400	12.5	16.7	1,680	129	1.622	12	BlT	A_{sat}, C_i, R_{dark}, [N], M_a	Wright *et al. (*2006*)*
New Zealand	TeRF	-43.250	170.180	68	11.9	16.3	4,331	1,103	4.866	3	BlT, NlT	A_{sat}, C_i, R_{dark}, [N], [P], M_a	Atkin *et al.* (2013)
New Zealand	TeRF	-43.310	170.170	143	11.2	15.8	4,277	1,076	4.816	3	BlT, NlT	A_{sat}, C_i, R_{dark}, [N], [P], M_a	Atkin *et al.* (2013)
New Zealand	TeRF	-43.380	170.180	134	11.6	16.2	4,017	1,017	4.468	3	BlT	A_{sat}, C_i, R_{dark}, [N], [P], M_a	Atkin *et al.* (2013)
New Zealand	TeRF	-43.400	170.170	234	11.4	16.0	3,980	1,004	4.477	7	BlT	A_{sat}, C_i, R_{dark}, [N], [P], M_a	Atkin *et al.* (2013)

New Zealand	TeRF	-43.410	170.170	271	10.9	15.6	3,920	980	4.409	6	BIT, S	A_{sat}, C_i, R_{dark}, [N], [P], M_a	Atkin *et al.* (2013)
New Zealand	TeRF	-43.420	170.170	215	11.2	15.8	3,883	976	4.343	5	BIT, S	A_{sat}, C_i, R_{dark}, [N], [P], M_a	Atkin *et al.* (2013)

Table S3. Standardized Major Axis regression slopes and their confidence intervals for log-log transformed relationships shown in Figures 5 and 6 in the main text. Coefficients of determination (r^2) and significance values (p) of each bivariate relationship are shown. 95% confidence intervals (CI) of SMA slopes and y-axis intercepts are shown in parentheses. In cases where SMA tests for common slopes revealed no significant differences between the upper canopy and lower canopy groups (*i.e.* $P > 0.05$), when plotting bivariate relationships, common slopes were used (with CI of the common slopes provided). Where there was a significant difference in elevation of the common-slope SMA regressions, values for the y-axis intercept (elevation) are provided. Where appropriate, significant shifts along a common slopes are indicated. JULES PFTs: BlT, broad-leaved tree; C3H, C_3 metabolism herb/grass; C4H, C_4 metabolism herb/grass; NlT, needle-leaved tree; S, shrub. TWQ classes: <10ºC; 10-15ºC; 15-20ºC; 20-25ºC; >25ºC. *Abbreviations:* $R_{dark,a}^{25}$, predicted area-based R_{dark} at 25ºC; $R_{dark,m}^{25}$, mass-based R_{dark} at 25ºC; $V_{cmax,a}^{25}$, predicted area-based V_{cmax} at 25ºC; $V_{cmax,m}^{25}$, predicted mass-based V_{cmax} at 25ºC

Figure	Response	Bivariate	JULES PFTs	H0 #1: No difference in slope (p-value)	PFT or TWQ-class (ºC)	n	r^2	p	Slope	*Pairwise comparison*	Slope CI_low	Slope CI_high	Intercept	H0 #2: No difference in elevation (p-value)	Intercepts for a common slope	*Pairwise comparison (where relationship significant)*	H0 #3: No difference in 'shift'.p-value
5(a)	$R_{dark,a}^{25}$	$V_{cmax,a}^{25}$	All bar C4H	0.7017	BlT	691	0.12	< 0.0001	0.976		0.910	1.046	-1.445	< 0.0001	-1.470	*a*	< 0.0001
					C3H	45	0.00	***0.8940***	1.073		0.793	1.453	-1.414		-1.279		
					NlT	23	0.16	***0.0578***	0.949		0.633	1.422	-1.445		-1.510		
					S	115	0.16	< 0.0001	1.076		0.908	1.276	-1.647		-1.501	*a*	
5 (d)	$R_{dark,m}^{25}$	$V_{cmax,m}^{25}$	All bar C4H	< 0.0001	BlT	682	0.27	< 0.0001	0.946	b	0.887	1.009	-1.351				
					C3H	44	0.37	< 0.0001	1.247	a	0.977	1.592	-1.962				
					NlT	23	0.62	< 0.0001	0.494	c	0.375	0.651	-0.366				
					S	115	0.31	< 0.0001	1.057	a, b	0.906	1.234	-1.671				
5 (b)	$R_{dark,a}^{25}$	$V_{cmax,a}^{25}$	All bar C4H	0.0857	< 10	47	0.19	0.0023	1.273		0.974	1.662	-1.592	< 0.0001	-1.134	*d*	< 0.0001
					10 to 15	43	0.18	0.0042	1.103		0.832	1.461	-1.484		-1.287	*c*	
					15 to 20	121	0.33	< 0.0001	0.849		0.732	0.985	-1.270		-1.476	*a, b*	
					20 to 25	263	0.30	< 0.0001	0.966		0.872	1.069	-1.487		-1.507	*a*	
					> 25	400	0.03	0.0004	0.999		0.907	1.101	-1.475		-1.445	*b*	
5 (e)	$R_{dark,m}^{25}$	$V_{cmax,m}^{25}$	All bar C4H	< 0.0001	< 10	47	0.62	< 0.0001	1.093	a	0.909	1.314	-1.412				
					10 to 15	42	0.38	< 0.0001	1.165	a	0.908	1.496	-1.720				
					15 to 20	121	0.68	< 0.0001	0.752	b	0.679	0.832	-0.875				
					20 to 25	258	0.31	< 0.0001	0.920	a	0.831	1.019	-1.356				
					> 25	396	0.15	< 0.0001	1.002	a	0.914	1.098	-1.482				
5 (c)	$R_{dark,a}^{25}$	$V_{cmax,a}^{25}$	BlT only	0.0480	< 10	4	0.63	***0.2070***	-2.446		-9.686	-0.618	4.306	< 0.0001	-1.061		< 0.0001
					10 to 15	39	0.21	0.0036	1.033		0.771	1.384	-1.352		-1.204	*c*	
					15 to 20	101	0.35	< 0.0001	0.805		0.685	0.945	-1.183		-1.401	*b*	
					20 to 25	152	0.17	< 0.0001	0.865		0.747	1.001	-1.325		-1.440	*a*	
					> 25	395	0.03	0.0006	1.011		0.917	1.115	-1.494		-1.391	*b*	
5(f)	$R_{dark,m}^{25}$	$V_{cmax,a}^{25}$	BlT only	< 0.0001	< 10	4	0.41	***0.3627***	8.035		1.642	39.317	-20.639				
					10 to 15	39	0.40	< 0.0001	1.103	a	0.855	1.423	-1.549				
					15 to 20	101	0.72	< 0.0001	0.753	b	0.678	0.836	-0.862				
					20 to 25	147	0.15	< 0.0001	0.821	b	0.706	0.955	-1.109				
					> 25	391	0.13	< 0.0001	1.022	a	0.932	1.121	-1.533				
6(a)	$R_{dark,a}^{25}$	Leaf $[N]_a$	All bar C4H	0.5081	BlT	794	0.10	< 0.0001	1.134		1.061	1.211	-0.296	< 0.0001	-0.300	*a*	< 0.0001
					C3H	74	0.30	< 0.0001	1.169		0.961	1.421	-0.071		-0.065	*c*	
					NlT	30	0.32	0.0010	1.005		0.735	1.375	-0.287		-0.346	*a*	
					S	132	0.26	< 0.0001	1.257		1.084	1.458	-0.215		-0.180	*b*	
6 (d)	$R_{dark,m}^{25}$	Leaf $[N]_m$	All bar C4H	0.0093	BlT	805	0.11	< 0.0001	1.423	a	1.333	1.519	-0.781				
					C3H	74	0.60	< 0.0001	1.598	a	1.379	1.852	-0.818				
					NlT	39	0.09	***0.0576***	2.354		1.723	3.217	-1.763				
					S	132	0.43	< 0.0001	1.383	a	1.213	1.576	-0.579				
6 (b)	$R_{dark,a}^{25}$	Leaf $[N]_a$	All bar C4H	0.0512	< 10	47	0.14	0.0109	1.224	a, b	0.929	1.613	-0.008	< 0.0001	0.025	*a*	< 0.0001
					10 to 15	37	0.15	0.0170	1.700	a	1.245	2.320	-0.399		-0.187	*b,c*	
					15 to 20	92	0.25	< 0.0001	1.170	b	0.976	1.401	-0.198		-0.185	*b*	
					20 to 25	345	0.29	< 0.0001	1.141	b	1.043	1.248	-0.256		-0.251	*c*	
					> 25	509	0.04	< 0.0001	1.056	b	0.969	1.150	-0.301		-0.316	*d*	
6 (e)	$R_{dark,m}^{25}$	Leaf $[N]_m$	All bar C4H	0.0005	< 10	47	0.60	< 0.0001	1.821	a	1.508	2.198	-1.056				
					10 to 15	37	0.44	< 0.0001	2.040	a	1.583	2.629	-1.415				
					15 to 20	108	0.44	< 0.0001	1.695	a, b	1.468	1.956	-0.941				

					20 to 25	350	0.36	< 0.0001	1.451	b, c	1.334	1.579	-0.772
					> 25	508	0.06	< 0.0001	1.333	c	1.225	1.451	-0.695
6 (c)	$R_{dark,a}^{25}$	Leaf $[N]_a$	BIT only	0.0004	< 10	4	0.90	***0.0537***	10.773		4.514	25.707	-3.357
					10 to 15	34	0.10	***0.0714***	1.680		1.201	2.350	-0.389
					15 to 20	76	0.20	< 0.0001	1.320	a	1.075	1.621	-0.214
					20 to 25	186	0.28	< 0.0001	1.002	b	0.886	1.133	-0.278
					> 25	494	0.03	< 0.0001	1.050	b	0.963	1.146	-0.301
6 (f)	$R_{dark,m}^{25}$	Leaf $[N]_m$	BIT only	0.0041	< 10	4	0.97	0.0161	2.677	a	1.591	4.503	-2.491
					10 to 15	34	0.38	0.0001	2.140	a	1.616	2.833	-1.547
					15 to 20	85	0.44	< 0.0001	1.586	a, b	1.347	1.868	-0.799
					20 to 25	189	0.26	< 0.0001	1.479	b	1.307	1.674	-0.881
					> 25	493	0.05	< 0.0001	1.346	b	1.235	1.467	-0.713

Table S4. Comparison of linear mixed-effects models with area-based leaf respiration at 25°C ($R_{dark,a}^{25}$; µmol CO_2 m^{-2} s^{-1}) as the response variable (each showing fixed and random effects), with input data restricted to site:species means for which all potential fixed effect parameters were available. Several model frameworks are outlined (a 'best predictor model, followed by a null model using PFTs only as fixed factors, then models relevant to different model frameworks, here called 'ESM' frameworks), each containing different combinations of fixed effect parameter values (ESM#1-4; for details of each framework, see below). For the fixed effects sub-table, parameter values, s.e. and *t*-values given for the continuous explanatory variables; explanatory variables (all centred on their means) are: (1) plant functional types (PFT), according to *JULES* (Clark *et al.*, 2011): BlT (broad-leaved tree), C3H (C_3 metabolism herbs/grasses), NlT (needle-leaved trees), and S (shrubs); (2) area-based or mass-based leaf nitrogen [N_a (g m^{-2}) or N_m (mg g^{-1}), respectively] area-based phosphorus (P_a; g m^{-2}) concentrations, area-based Rubisco CO_2 fixation capacity at 25°C ($V_{cmax,a}^{25}$; µmol CO_2 m^{-2} s^{-1}), and mean temperature of the warmest quarter (TWQ; °C) (Hijmans *et al.*, 2005). The PFT-BlT values (first row) are based on the assumption that other variables were at their global mean values. In the 'best' model (i.e. same as that shown in Table 5 and Figure 9 in the main text), all available and relevant parameters were included in model selection (PFTs, $V_{cmax,a}^{25}$, N_a, P_a, TWQ, precipitation of the warmest quarter (PWQ) and aridity index (AI). The null model provides a model where fixed effect factor is limited to PFTs. For ESM#1, the model was limited to the following source fixed effect parameters: PFT, N_m and $V_{cmax,a}^{25}$ and TWQ. Here, our decision to include mass-based N was based on the fact that mass-based N is a predictive trait used in *JULES*, according to Schulze *et al.* (1994). For ESM#2, source fixed effect parameters were the same as for ESM#1, but without $V_{cmax,a}^{25}$. For ESM#3, input fixed effect parameters were: PFT, N_a and TWQ, while for ESM#4, they were PFT, $V_{cmax,a}^{25}$ and TWQ. In the random effect sub-table, the intercept was allowed to vary among species, families and sites; residual errors shown are within species, families, sites and investigators. Finally, predictive equations are shown that enable $R_{dark,a}^{25}$ to be predicted based on inputs according to the six models (see next page).

Table S4

	Best predictor model				Null model (PFT only)				ESM #1				ESM #2				ESM #3				ESM #4			
Fixed effect	Estimate	S.E.	t value		Estimate	S.E.	t value		Estimate	S.E.	t value		Estimate	S.E.	t value		Estimate	S.E.	t value		Estimate	S.E.	t value	
PFT_JULES_BlT (if other variables were at global mean)	1.2636	0.033	38.551		1.3805	0.046	29.750		1.2704	0.011	119.349		1.3000	0.012	105.939		1.2855	0.011	117.099		1.2618	0.011	118.611	
PFT_JULES_C3H	0.4708	0.141	3.348		0.5099	0.160	3.185		0.3591	0.027	13.135		0.3642	0.030	12.232		0.4395	0.028	15.657		0.4120	0.027	15.176	
PFT_JULES_NlT	-0.3595	0.150	-2.392		-0.0558	0.179	-0.311		0.0657	0.033	1.989		-0.0272	0.036	-0.748		-0.2566	0.036	-7.175		0.0259	0.033	0.782	
PFT_JULES_S	0.3290	0.064	5.163		0.3460	0.071	4.867		0.3028	0.015	20.290		0.2873	0.016	17.704		0.3188	0.015	20.655		0.3141	0.015	21.009	
Leaf [N] (units vary with model, see note below)	0.0728	0.018	4.124						0.0075	0.001	12.574		0.0104	0.001	16.077		0.2061	0.004	46.314					
Leaf_Pa	0.0015	0.000	7.389																					
Vcmax_a_25	0.0095	0.001	15.241						0.0114	0.000	58.237										0.0116	0.000	59.229	
MeanT_Warmest.Qtr	-0.0358	0.006	-5.658						-0.0338	0.002	-17.949		-0.0389	0.002	-17.983		-0.0402	0.002	-21.055		-0.0334	0.002	-17.766	
PFT_JULES_C3H : Leaf_Na	0.3394	0.069	4.892																					
PFT_JULES_NlT : Leaf_Na	0.0762	0.146	0.523																					
PFT_JULES_S : Leaf_Na	0.0687	0.053	1.295																					
Random effect	No. levels per group	Variance compone	% of total		Variance compone	% of total			No. levels per group	Variance compone	% of total		Variance compone	% of total			Variance compone	% of total			Variance compone	% of total		
Intercept variance: Among species	531	0.009	7.1%		0.023	11.5%			655	0.000	0.0%		0.000	0.0%			0.000	1.9%			0.000	0.0%		
Intercept variance: Among families	100	0.002	1.4%		0.004	2.1%			114	0.000	2.4%		0.001	3.0%			0.001	4.5%			0.000	2.6%		
Intercept variance: Among sites	49	0.031	23.4%		0.073	36.2%			64	0.005	32.8%		0.006	36.6%			0.005	31.1%			0.005	32.5%		
Residual (within species, families and sites plus real error)		0.091	68.2%		0.102	50.2%				0.009	64.8%		0.010	60.5%			0.009	62.4%			0.009	64.9%		
		0.133	100.0%		0.202	100.0%				0.014	100.0%		0.017	100.0%			0.015	100.0%			0.014	100.0%		
Likelihood ratio test		-595.2				-681.9				-633.7				-689.7				-653.1				-631.9		
Akaike (AIC)		1,220				1,380				1,289				1,399				1,326				1,284		
Bayesian (BIC)		1,288				1,416				1,341				1,446				1,373				1,331		
REML criterion at convergence		1,190				1,364				1,267				1,379				1,306				1,264		
Number of observations (Site:Spp averaged)	667								802															

Continuous explanatory variables HAVE been centred on their means.
Leaf N is included on an AREA basis in models: Best, Null and ESM 3. And on a MASS basis in ESM 1 and 2.
The Best and Null models are run on a smaller subset of data given the requirment for Leaf P values.

Table S4. Continued

Best predictor model (from Table 6 in the main text)

Broad-leaved trees: $R_{dark,a}^{25} = 1.236 + (0.0728*[N]_a) + (0.015*[P]_a) + (0.0095*V_{cmax,a}^{25}) – (0.0358*TWQ)$

C_3 herbs/grasses: $R_{dark,a}^{25} = 1.7344 + (0.4122*[N]_a) + (0.015*[P]_a) + (0.0095*V_{cmax,a}^{25}) – (0.0358*TWQ)$

Needle-leaved trees: $R_{dark,a}^{25} = 0.9041 + (0.1489*[N]_a) + (0.015*[P]_a) + (0.0095*V_{cmax,a}^{25}) – (0.0358*TWQ)$

Shrubs: $R_{dark,a}^{25} = 1.5926 + (0.1415*[N]_a) + (0.015*[P]_a) + (0.0095*V_{cmax,a}^{25}) – (0.0358*TWQ)$

Null model (PFT only) (from Table 6 in the main text)

Broad-leaved trees: $R_{dark,a}^{25} = 1.3805$

C_3 herbs/grasses: $R_{dark,a}^{25} = 1.8904$

Needle-leaved trees: $R_{dark,a}^{25} = 1.3247$

Shrubs: $R_{dark,a}^{25} = 1.7265$

ESM#1

Broad-leaved trees: $R_{dark,a}^{25} = 1.2704 + (0.0075*[N]_m) + (0.0114*V_{cmax,a}^{25}) – (0.0338*TWQ)$

C_3 herbs/grasses: $R_{dark,a}^{25} = 1.6295 + (0.0075*[N]_m) + (0.0114*V_{cmax,a}^{25}) – (0.0338*TWQ)$

Needle-leaved trees: $R_{dark,a}^{25} = 1.3361 + (0.0075*[N]_m) + (0.0114*V_{cmax,a}^{25}) – (0.0338*TWQ)$

Shrubs: $R_{dark,a}^{25} = 1.5732 + (0.0075*[N]_m) + (0.0114*V_{cmax,a}^{25}) – (0.0338*TWQ)$

ESM#2

Broad-leaved trees: $R_{dark,a}^{25} = 1.300 + (0.0104*[N]_m) – (0.0389*TWQ)$

C_3 herbs/grasses: $R_{dark,a}^{25} = 1.66642 + (0.0104*[N]_m) – (0.0389*TWQ)$

Needle-leaved trees: $R_{dark,a}^{25} = 1.2728 + (0.0104*[N]_m) – (0.0389*TWQ)$

Shrubs: $R_{dark,a}^{25} = 1.5875 + (0.0104*[N]_m) – (0.0389*TWQ)TWQ)$

ESM#3

Broad-leaved trees: $R_{dark\,a}^{25} = 1.2855 + (0.2061*[N]_a) – (0.0402*TWQ)$

C_3 herbs/grasses: $R_{dark,a}^{25} = 1.7250 + (0.2061*[N]_a) – (0.0402*TWQ)$

Needle-leaved trees: $R_{dark,a}^{25} = 1.0290 + (0.2061*[N]_a) – (0.0402*TWQ)$

Shrubs: $R_{dark,a}^{25} = 1.6043 + (0.2061*[N]_a) – (0.0402*TWQ)$

ESM#4

Broad-leaved trees: $R_{dark\,a}^{25} = 1.2818 + (0.0116 * V_{cmax,a}^{25}) – (0.0334*TWQ)$

C_3 herbs/grasses: $R_{dark,a}^{25} = 1.6737 + (0.0116 * V_{cmax,a}^{25}) – (0.0334*TWQ)$

Needle-leaved trees: $R_{dark,a}^{25} = 1.2877 + (0.0116 * V_{cmax,a}^{25}) – (0.0334*TWQ)$

Shrubs: $R_{dark,a}^{25} = 1.5758 + (0.0116 * V_{cmax,a}^{25}) – (0.0334*TWQ)$

Table S5. Comparison of linear mixed-effects models using different plant functional types (PFT) classifications, with leaf respiration at 25°C (R_{dark}^{25}) as the response variable. Two models are shown: (A) using area-based leaf respiration at 25°C ($R_{dark,a}^{25}$; μmol CO_2 m^{-2} s^{-1}); and, (B) mass-based leaf respiration at 25°C ($R_{dark,m}^{25}$; nmol CO_2 g^{-1} s^{-1}). For (A) and (B), two model frameworks are outlined (variants of ESM#3 model shown in Table S4, but with a larger number of observations reflecting the abundance of $[N]_a$ (g m^{-2}) and $[N]_m$ (mg g^{-1}) data), differing in the plant functional types (PFT) used: *JULES*(Clark *et al.*, 2011): BlT (broad-leaved tree), C3H (C_3 metabolism herbs/grasses), NlT (needle-leaved trees), and S (shrubs); and, *LPJ* (Sitch *et al.*, 2003): BorDcBl, boreal deciduous broad-leaved tree/shrub; BorDcNl, boreal deciduous needle-leaved tree/shrub; BorEvNl, boreal evergreen needle-leaved tree/shrub; TmpDcBl, temperate deciduous broad-leaved tree/shrub; TmpEvBl, temperate evergreen broad-leaved tree/shrub; TmpEvNl, temperate evergreen needle-leaved tree/shrub; TmpH, temperate herb/grass; TrpDcBl, tropical deciduous broad-leaved tree/shrub; TrpEvBl, tropical evergreen broad-leaved tree/shrub; TrpH, tropical herb/grass. For the fixed effects sub-tables, parameter values, s.e. and *t*-values given for the continuous explanatory variables; explanatory variables (all centred on their means) are: PFTs; area or mass-based leaf nitrogen (N_a and N_m, respectively) and mean temperature of the warmest quarter (TWQ) (Hijmans *et al.*, 2005). For *JULES*, the PFT-BlT values (first row) are based on the assumption that other variables were at their global mean values. Similarly, for *LPJ*, the PFT-BorDcBl (first row) are based on the assumption that other variables were at their global mean values. In the random effect sub-table, the intercept was allowed to vary among species, families and sites; residual errors shown are within species, families, sites and investigators.

(A) area-based

JULES			
Fixed effect	Estimate	S.E.	t value
PFT_JULES_BlT (if other variables were at global mean)	1.1911	0.034	35.041
PFT_JULES_C3H	0.3930	0.069	5.709
PFT_JULES_NlT	0.1392	0.091	1.536
PFT_JULES_S	0.3298	0.045	7.298
Leaf [N]_area	0.2589	0.014	18.973
MeanT_Warmest.Qtr	-0.0396	0.006	-6.381

LPJ			
Fixed effect	Estimate	S.E.	t value
PFT_LPJ _BorDcBl	1.3667	0.152	8.982
PFT_LPJ _BorDcNl	0.2756	0.166	1.659
PFT_LPJ_BorEvNl	-0.5574	0.234	-2.382
PFT_LPJ_TmpDcBl	-0.1969	0.152	-1.292
PFT_LPJ_TmpEvBl	0.0018	0.149	0.012
PFT_LPJ_TmpEvNl	-0.0581	0.177	-0.329
PFT_LPJ_TmpH	0.1723	0.151	1.141
PFT_LPJ_TrpDcBl	-0.1469	0.167	-0.881
PFT_LPJ_TrpEvBl	-0.1785	0.162	-1.104
PFT_LPJ_TrpH	0.0177	0.267	0.066
Leaf [N]_area	0.2592	0.014	18.407
MeanT_Warmest.Qtr	-0.0351	0.007	-4.743

Random effect	Variance component	% of total
Intercept variance: Among species	0.000	0.0%
Intercept variance: Among families	0.008	3.4%
Intercept variance: Among sites	0.056	24.1%
Residual (within species, families and sites plus real error)	0.167	72.5%
	0.230	100.0%
logLikelihood	-1,011	
Akaike (AIC)	2,041	
Bayesian (BIC)	2,091	
REML criterion at convergence	2,021	

Random effect	Variance component	% of total
Intercept variance: Among species	0.000	0.0%
Intercept variance: Among families	0.007	2.8%
Intercept variance: Among sites	0.061	25.7%
Residual (within species, families and sites plus real error)	0.170	71.5%
	0.237	100.0%
logLikelihood	-1,022	
Akaike (AIC)	2,075	
Bayesian (BIC)	2,154	
REML criterion at convergence	2,043	

Number of obs: 1025
Groups: Species, 833; Family, 129; Site, 81
Continuous explanatory variables HAVE been centred on their means

(B) mass-based

JULES			
Fixed effect	Estimate	S.E.	t value
PFT_JULES_BlT (if other variables were at global mean)	11.0413	0.068	161.680
PFT_JULES_C3H	4.1153	0.125	32.816
PFT_JULES_NlT	-2.0938	0.156	-13.408
PFT_JULES_S	1.6953	0.073	23.248
Leaf [N]_mass	0.4586	0.003	135.520
MeanT_Warmest.Qtr	-0.3842	0.013	-30.559

LPJ			
Fixed effect	Estimate	S.E.	t value
PFT_LPJ _BorDcBl	14.7990	0.254	58.233
PFT_LPJ _BorDcNl	0.7859	0.409	1.921
PFT_LPJ_BorEvNl	-7.7081	0.303	-25.481
PFT_LPJ_TmpDcBl	-2.8388	0.258	-11.000
PFT_LPJ_TmpEvBl	-3.5225	0.250	-14.069
PFT_LPJ_TmpEvNl	-5.7636	0.293	-19.703
PFT_LPJ_TmpH	0.2726	0.257	1.062
PFT_LPJ_TrpDcBl	-3.5374	0.288	-12.268
PFT_LPJ_TrpEvBl	-3.8196	0.275	-13.872
PFT_LPJ_TrpH	-2.3686	0.476	-4.974
Leaf [N]_mass	0.4567	0.003	133.980
MeanT_Warmest.Qtr	-0.3353	0.015	-23.104

Random effect	Variance component	% of total
Intercept variance: Among species	0.000	0.0%
Intercept variance: Among families	0.036	8.9%
Intercept variance: Among sites	0.258	64.3%
Residual (within species, families and sites plus real error)	0.108	26.9%
	0.401	100.0%
logLikelihood	-2,655	
Akaike (AIC)	5,330	
Bayesian (BIC)	5,379	
REML criterion at convergence	5,310	

Random effect	Variance component	% of total
Intercept variance: Among species	0.000	0.0%
Intercept variance: Among families	0.033	8.2%
Intercept variance: Among sites	0.262	65.0%
Residual (within species, families and sites plus real error)	0.108	26.8%
	0.403	100.0%
logLikelihood	-2,644	
Akaike (AIC)	5,319	
Bayesian (BIC)	5,398	
REML criterion at convergence	5,287	

Response variable is Rdarkm_25C_varQ10
Continuous explanatory variables HAVE been centred on their means
Number of obs: 1045
Groups: Species, 833; Family, 129; Site, 87

Figure S1. Comparison of area-based rates of leaf respiration in darkness (R_{dark}) at a common leaf temperature of 25°C, calculated assuming either a fixed Q_{10} of 2.23 (Atkin *et al.*, 2005) (using Eqn 1 in the main text) or assuming a *T*-dependent Q_{10} (Tjoelker *et al.*, 2001) (using Eqn 2 in the main text). $R_{dark,a}^{25}$ and $R_{dark,a}^{TWQ}$, predicted area-based R_{dark} rates (μmol CO_2 m^{-2} s^{-1}) at 25°C, and TWQ (mean *T* of the warmest quarter), respectively. Values at the TWQ of each replicate were calculated using climate data from the *WorldClim* data base (Hijmans *et al.*, 2005). Data shown are for individual observational rows in the global respiration database.

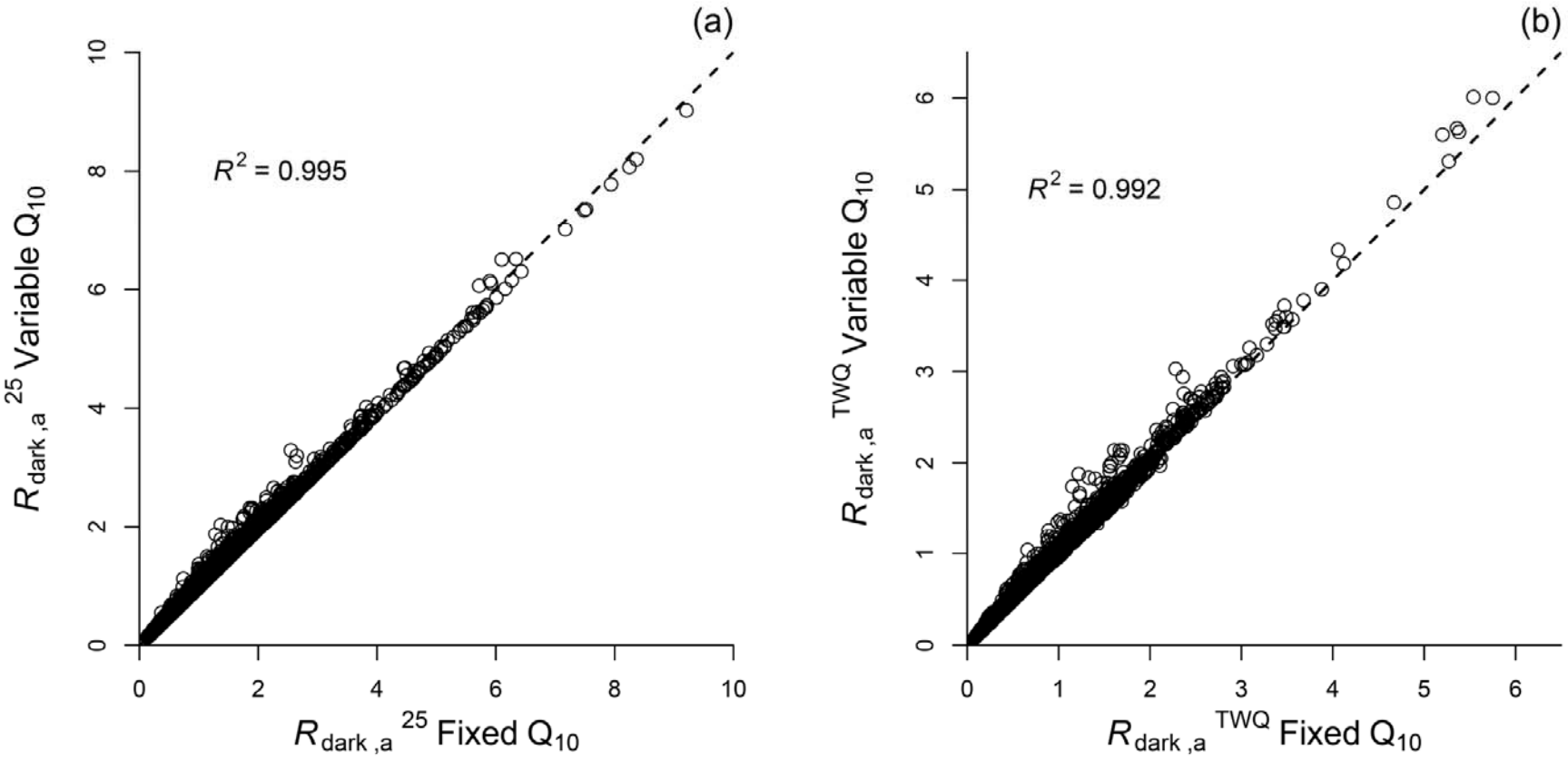

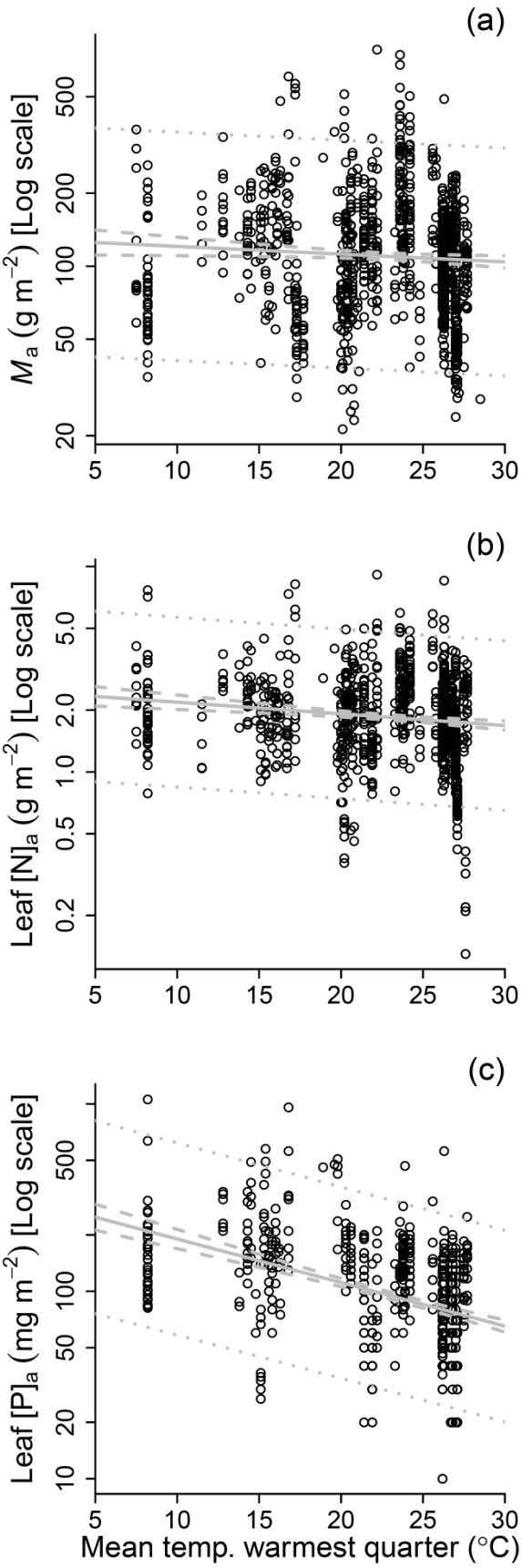

Figure S2. Relationships between leaf structural and chemical composition traits, and mean daily temperature of the warmest quarter (TWQ). Values shown are averages for unique site:species combinations in the global *GlobResp* database. Traits shown are: (a) M_a, leaf mass per unit leaf area; (b) $[N]_a$, area-based leaf nitrogen concentration; and (c) $[P]_a$, area-based leaf phosphorous concentration. TWQ at each site were obtained using site information and the *WorldClim* data base (Hijmans *et al.*, 2005). Solid grey line in each plot shows regression lines where the relationships were significant (with 95% confidence intervals shown as dashed line around the predicted relationship; the dotted lines show the prediction intervals (two-times the standard deviation) around the predicted relationship.

While the negative M_a↔TWQ (Fig. S2a) and $[N]_a$↔TWQ (Fig. 4b) relationships were both significant (M_a: $p<0.05$, $n=1092$; $[N]_a$: $p<0.0001$, $n=1029$), in neither case were the associations strong (M_a: Pearsons correlation (r) = -0.067, r^2 = 0.004; $[N]_a$: r = -0.134, r^2 = 0.018). By contrast, the negative $[P]_a$↔TWQ relationship (Fig. 4C) was more marked ($p<0.0001$, $n=728$, r = -0.418, r^2 = 0.174), with $[P]_a$ being highest at the coldest sites.

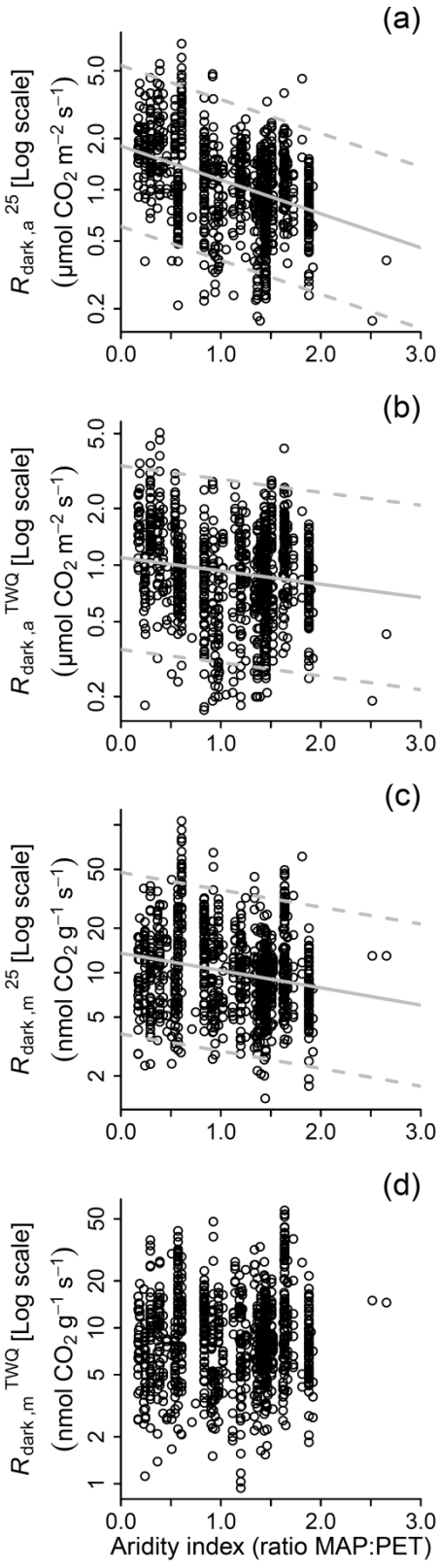

Figure S3. Site-species mean values leaf R_{dark} (log_{10} scale) relationships with aridity index (AI), excluding data from the exceptionally high-rainfall, Frans Josef Glacier (FJG) site in NZ. Traits shown are: $R_{dark,a}^{25}$, (a) and $R_{dark,a}^{TWQ}$ (b), predicted area-based R_{dark} rates at 25ºC and TWQ, respectively; $R_{dark,m}^{25}$ (c) and $R_{dark,m}^{TWQ}$ (d), predicted mass-based R_{dark} rates at 25ºC and TWQ, respectively. Values at 25ºC and TWQ were calculated assuming a temperature-dependent Q_{10} (Tjoelker *et al.*, 2001) and equation 7 described in Atkin et al. (2005). Values at the TWQ of each replicate were calculated using climate/location data from the *WorldClim* data base (Hijmans *et al.*, 2005). Aridity index calculated as the ratio of mean annual precipitation (MAP) to mean annual potential evapotranspiration (PET) (UNEP, 1997). Solid lines in each plot show regression lines where the relationships were significant; dashed lines show the prediction intervals (two-times the standard deviation) around the predicted relationship. See Figure 4 for the same figure where data from FJG were included.

Figure S4. Relationships between leaf R_{dark} (log_{10} scale) and measuring month mean daily temperature (MMT) for those sites where the month of measurement was known. Values shown are averages for unique site:species combinations, using previously unpublished data (Supporting Information Table S1). Traits shown are: (a) $R_{dark,a}^{25}$, predicted area-based R_{dark} at 25ºC; (b) $R_{dark,a}^{MMT}$, predicted area-based R_{dark} at MMT; (c) $R_{dark,m}^{25}$, mass-based R_{dark} at 25ºC; (d) $R_{dark,m}^{MMT}$, mass-based R_{dark} at MMT. Values at 25ºC and MMT were calculated assuming a *T*-dependent Q_{10} (Tjoelker *et al.*, 2001) and equation 7 described in Atkin et al. (2005). Values at the MMT of each replicate were calculated using climate/location data from the *WorldClim* data base (Hijmans *et al.*, 2005). Solid lines in each plot show regression lines where the relationships were significant; dashed lines show the prediction intervals (two-times the standard deviation) around the predicted relationship.

For $R_{dark,a}^{25}$, the negative relationship with MMT was significant (p<0.0001, n=677, r^2 = 0.192; $\log_{10} R_{dark,a}^{25}$ = 0.509 – 0.023*MMT) (Fig. S4a). Similarly, the $R_{dark,a}^{MMT}$↔MMT association (Fig. S4b) was significant (p<0.0001, n=677, r^2 = 0.041; $\log_{10} R_{dark,a}^{MMT}$ = -0.293 + 0.0095*MMT), as were the $R_{dark,m}^{25}$↔MMT (p<0.0001, n=667, r^2 = 0.184; $\log_{10} R_{dark,m}^{25}$ = 1.468 – 0.023*MMT) and $R_{dark,m}^{MMT}$↔MMT (p<0.0001, n=667, r^2 = 0.030; $\log_{10} R_{dark,m}^{MMT}$ = 0.666 + 0.009*MMT) relationships (Fig. S4c,d).

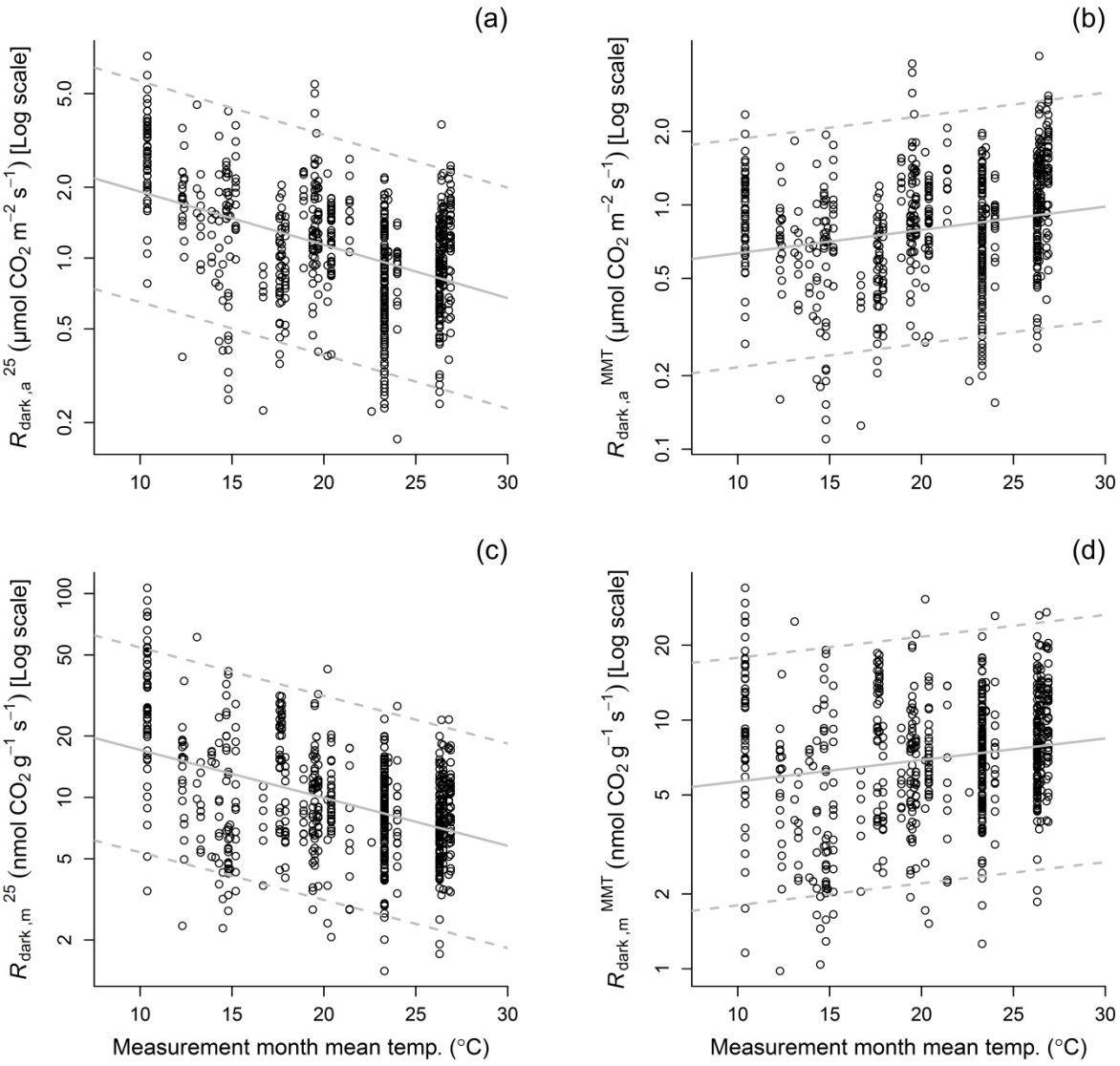

Figure S5. Testing key assumptions for area- and mass-based mixed effects models –heterogeneity and normality. See Table 5 in the main text for details on the models. The upper panel [(a) and (b)] refer to the model based on area-based values, while the lower panel [(c) and (d)] refers to the mass-based model.

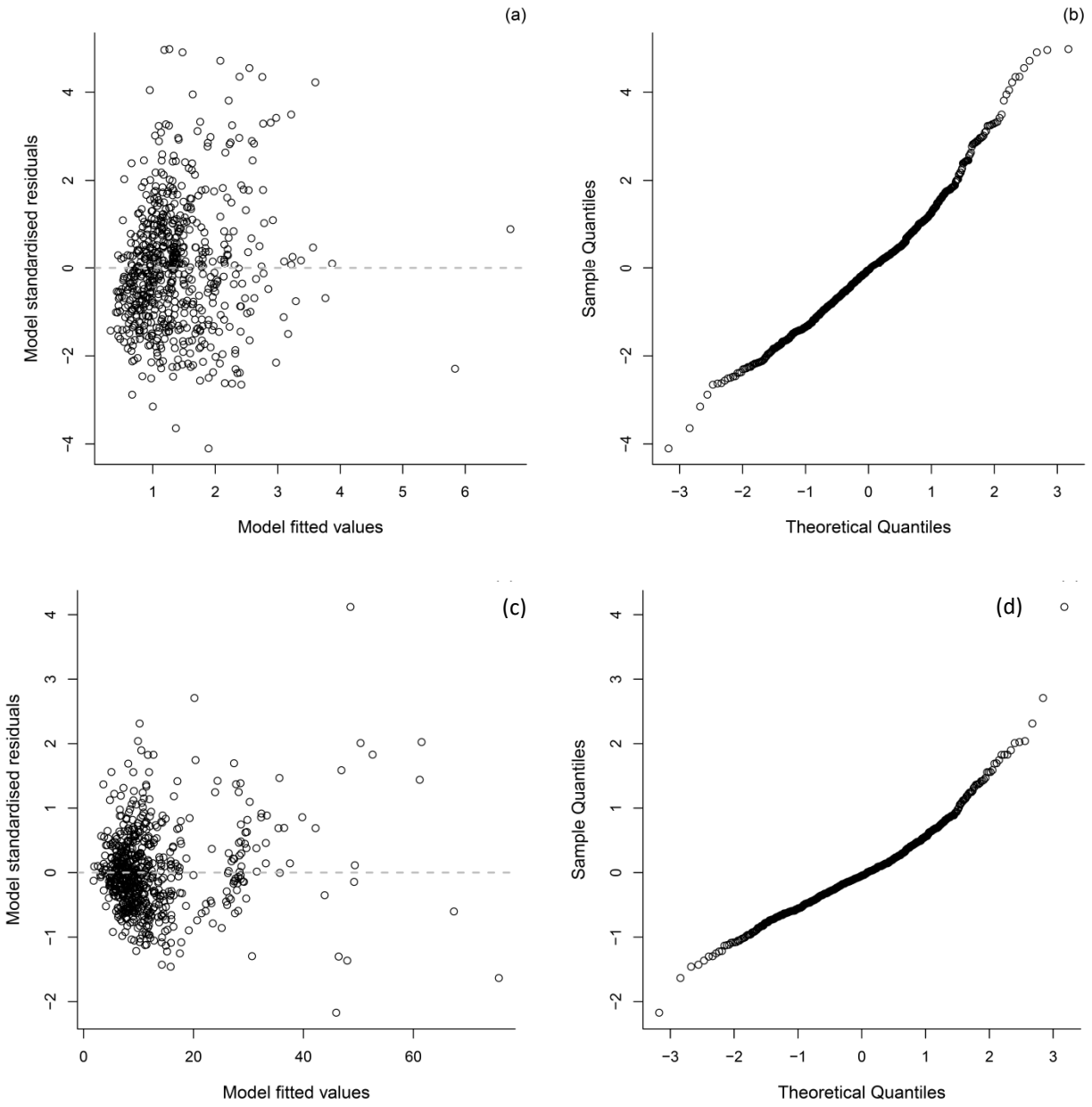

Figure S6. Model validation graphs for the area-based mixed effects model. Shown are standardised residuals plotted against fitted values for each of the continuous explanatory factors and variables used in the model's fixed components: (a) plant functional types (PFT) categorised according to *JULES* (BlT, broadleaved trees; C3H, C_3 herbs; NlT, needle-leaved trees; S, shrubs); (b) area-based rates of the V_{cmax} of Rubisco at 25ºC ($V_{cmax,\,a}{}^{25}$); (c) leaf nitrogen per unit leaf area ($[N]_a$); (d) leaf phosphorus per unit leaf area ($[P]_a$); and,(e) mean temperature of the warmest quarter at each site. See Table 5 in the main text for details on the models. Similar graphs were made for the mass-based model (data not shown). For (a), the central box in each plot shows the interquartile range; the median is shown as the bold line in each box; whiskers extend 1.5 times the interquartile range or the most extreme value, whichever is smaller; any points outside the values are shown as individual points.

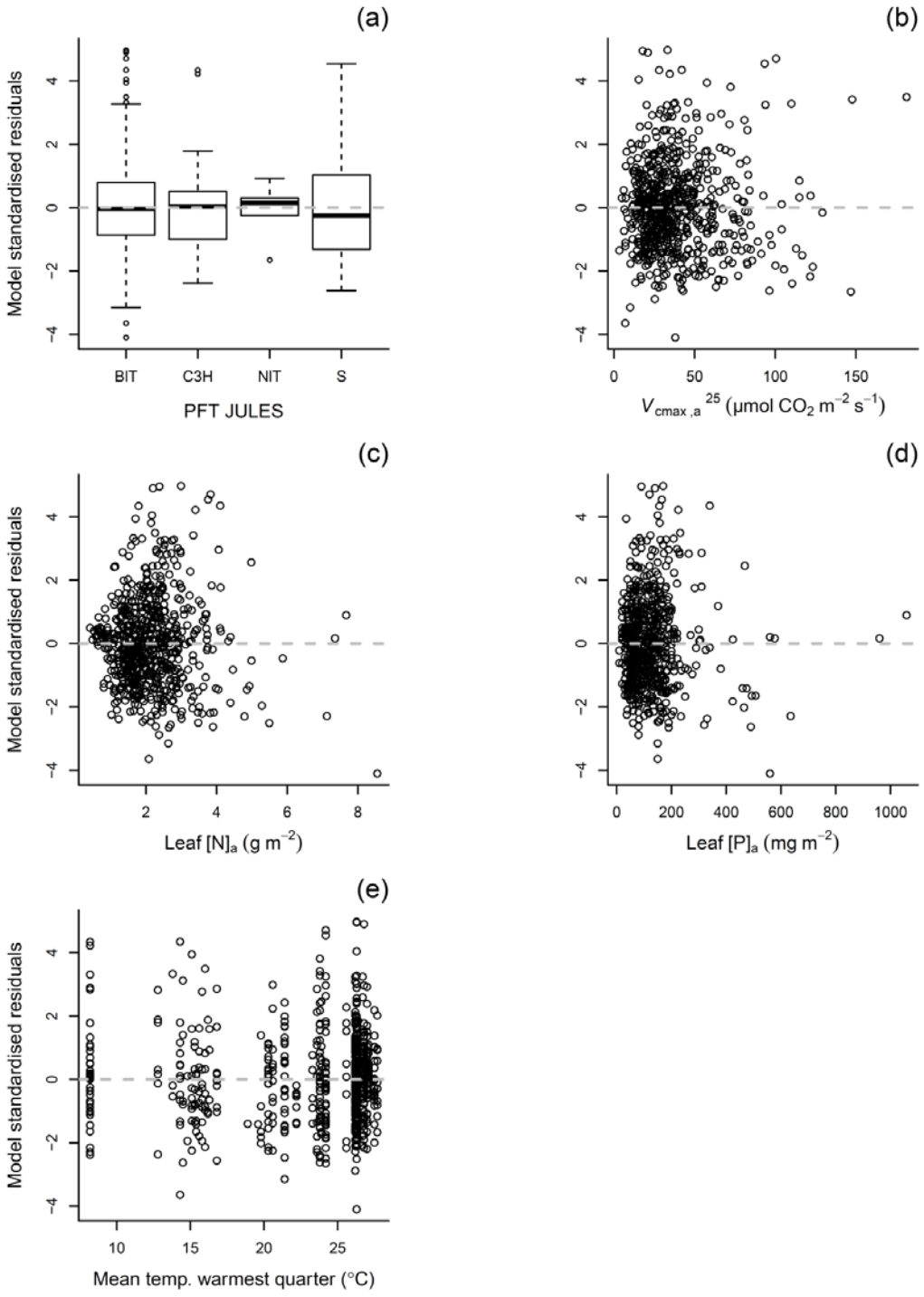

Figure S7. Standardised residuals plotted against fitted values for variables <u>not</u> used in the area-based model's fixed components. See Table 5 in the main text for details on the models. Similar graphs were made for the mass-based model (data not shown). Plots show residuals against (a) leaf mass per unit leaf area (M_a) categorised; (b) aridity index (ratio of mean annual precipitation to potential evapotranspiration); (c) precipitation of the warmest quarter at each site. See Table 5 in the main text for details on the models.

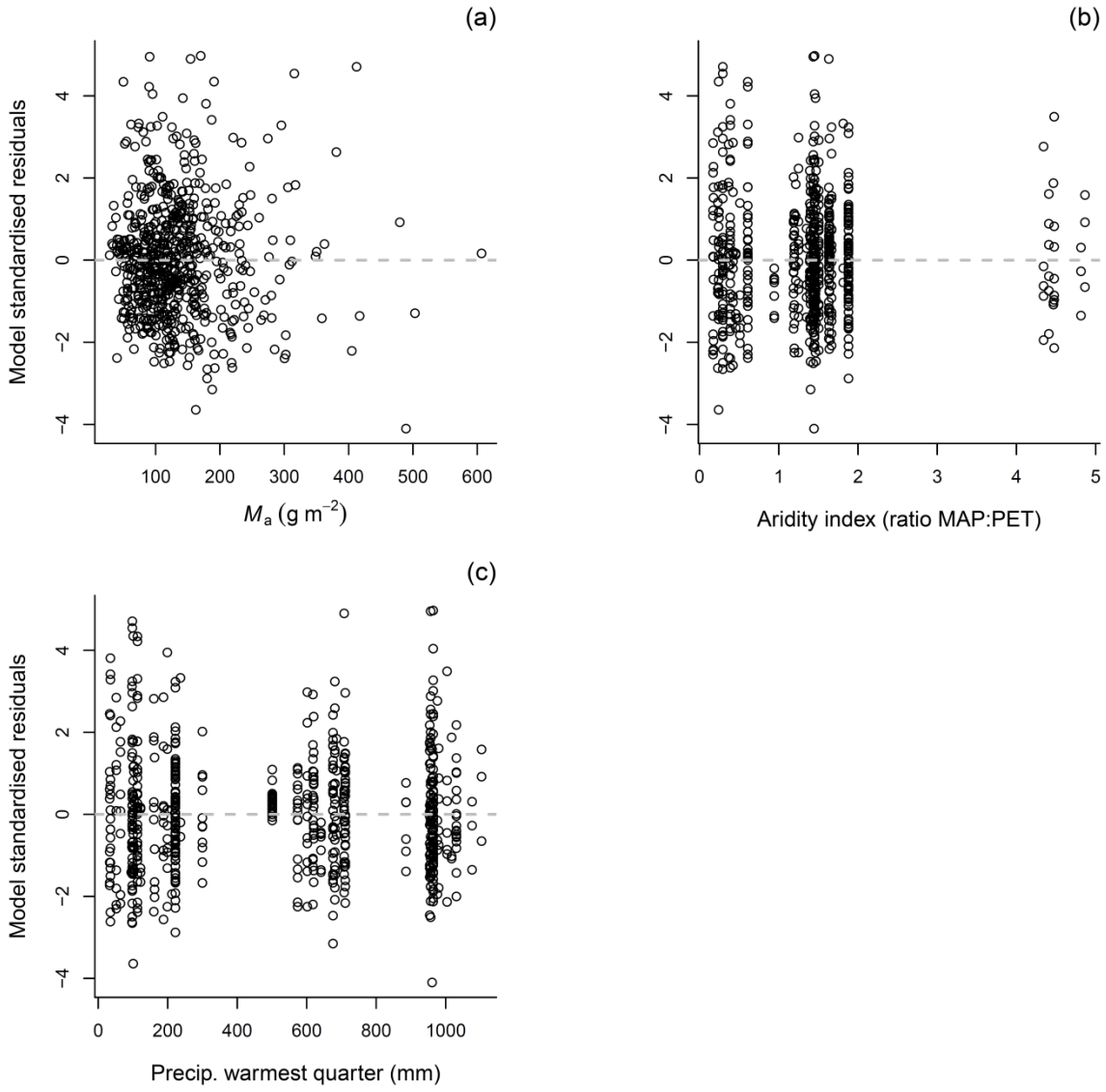

Figure S8. Dotchart of the area-based mixed model's random intercepts by Family. Points represent the difference (shown with 95% prediction intervals) for each family in the $R_{dark,a}^{25}$ response above or below the overall population mean after controlling for the model's fixed terms and site location (Figure S7). See Table 5 in the main text for details on the models. Similar graphs were made for the mass-based model (data not shown).

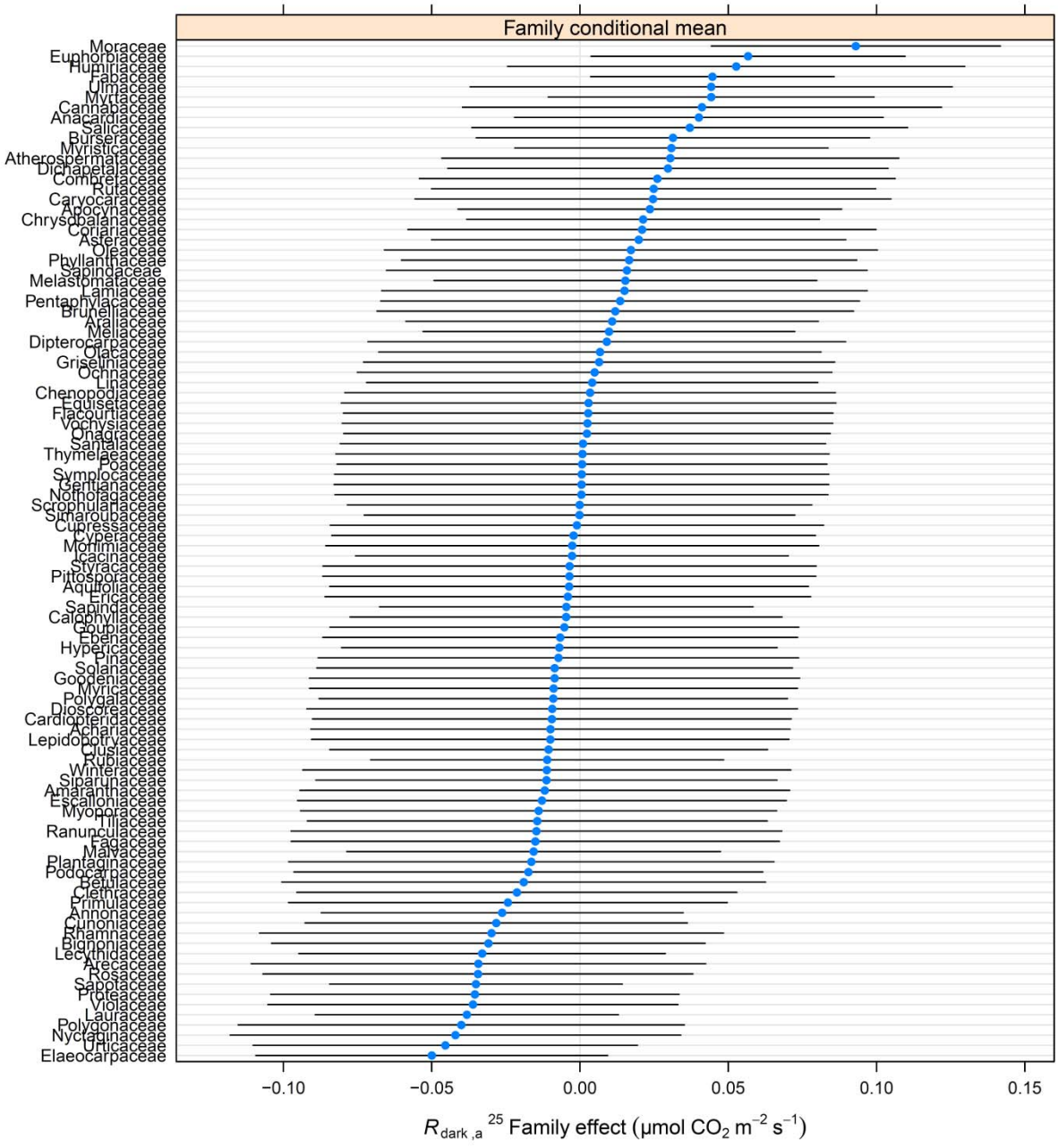

Figure S9. Dotchart of the area-based mixed model's random intercepts by site. Points represent the difference (shown with 95% prediction intervals) for each site in the $R_{dark,a}^{25}$ response above or below the overall population mean after controlling for the model's fixed terms and phylogenetic structure (Figure S6). See Table 5 in the main text for details on the models. Similar graphs were made for the mass-based model (data not shown)